Published by :
https://www.ijert.org/
An International Peer-Reviewed Journal

International Journal of Engineering Research & Technology (IJERT)
ISSN: 2278-0181
Vol. 15 Issue 05 , May - 2026

Design and Development of a Test Rig to Measure Performance Parameters of Aircraft Engine

Atharva Basarkar

Veermata Jijabai Technological Institute, Mumbai, Maharashtra

ABSTRACT

This thesis discusses the design and development of a test rig to measure the performance parameters of an aircraft IC engine for various loading conditions and at various throttle levels. The engine used for this application is an UL350i engine developed and manufactured by UL Power. The UL350i is a four-cylinder, four-stroke horizontally opposed spark ignition engine. The test setup developed is a generic test rig which can be used to test any aircraft IC engine of similar design.

Siemens NX is used for modelling of the components. These component models are then simulated for finite element analyses like static structural, modal and harmonic response in ANSYS 18.1. After studying the stress and deformation values in the initial designs, modifications were made to achieve a configuration whose stresses and deformations are under permissible values. All the analyses of the major components are well described in detail in this work.

Though there have been major advancements in the aviation engines in terms of power and fuel consumptions, IC engines still are a reliable and powerful source of power for lightweight aircrafts and UAVs. Their compact size and easy maintenance make them perfect for Reconnaissance Drones and Aircrafts and also for Training Aircraft. This report also presents the working and applications of Propeller IC Engine Propulsion system for the Unmanned Aerial Vehicle (UAV) and Single-Seater Lightweight Aircrafts IC engines.

International Journal of Engineering Research & Technology (IJERT)
ISSN: 2278-0181
Vol. 15 Issue 05 , May - 2026

CONTENTS

International Journal of Engineering Research & Technology (IJERT)
ISSN: 2278-0181
Vol. 15 Issue 05 , May - 2026

International Journal of Engineering Research & Technology (IJERT)
ISSN: 2278-0181
Vol. 15 Issue 05 , May - 2026

International Journal of Engineering Research & Technology (IJERT)
ISSN: 2278-0181
Vol. 15 Issue 05 , May - 2026

LIST OF TABLES

International Journal of Engineering Research & Technology (IJERT)
ISSN: 2278-0181
Vol. 15 Issue 05 , May - 2026

LIST OF FIGURES

International Journal of Engineering Research & Technology (IJERT)
ISSN: 2278-0181
Vol. 15 Issue 05 , May - 2026

International Journal of Engineering Research & Technology (IJERT)
ISSN: 2278-0181
Vol. 15 Issue 05 , May - 2026

International Journal of Engineering Research & Technology (IJERT)
ISSN: 2278-0181
Vol. 15 Issue 05 , May - 2026

International Journal of Engineering Research & Technology (IJERT)
ISSN: 2278-0181
Vol. 15 Issue 05 , May - 2026

International Journal of Engineering Research & Technology (IJERT)
ISSN: 2278-0181
Vol. 15 Issue 05 , May - 2026

Chapter – 1

Introduction

Four fundamental forces act on an aircraft during straight and level flight, and in order for the aircraft to stay in equilibrium, these forces must be balanced. The lift generated by the horizontal stabiliser and wing in the vertical direction balances the aircraft's weight. To maintain the forward flying speed, the aeroplane must overcome the drag force that is created as it travels through the air. The engine-propeller combination produces the thrust force, which acts as a counterbalance to drag.

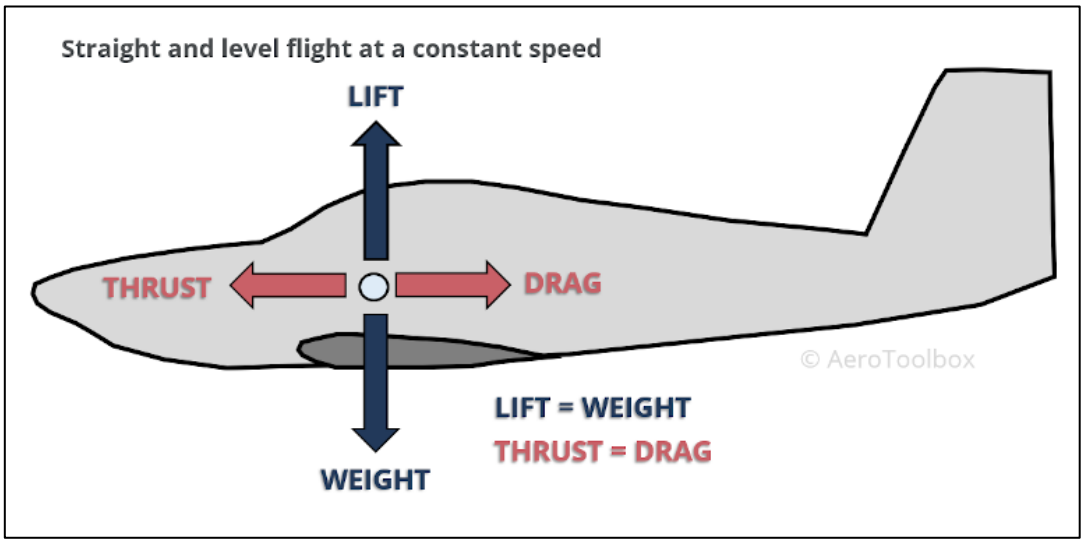

Fig. 1.1: The fundamental forces in flight {1}

The internal combustion engine operates based on the principle of generating rotational motion (crankshaft rotating) from reciprocating motion (piston movement up and down) for propeller drive. The combustion of a fuel and air mixture releases energy that is needed to move the pistons, causing them to move and doing useful work. Then, it is said that mechanical energy has been created from chemical energy (fuel).

1.1. Types of Aircraft Engines

The propulsion system of an airplane is called an aircraft engine, or aero engine. It is the central component, or heart, of aviation advancement. Aero engines need to be reliable, work in intense pressure, temperature, and speed conditions. They should be powerful, small and readily streamlined, lightweight, field repairable, fuel-efficient, and able to operate at an altitude that is appropriate for the aircraft and produce the least amount of emission and noise.

International Journal of Engineering Research & Technology (IJERT)
ISSN: 2278-0181
Vol. 15 Issue 05 , May - 2026

Based on their input power, aero engines can be divided into two primary groups: internal combustion engines and external combustion engines.

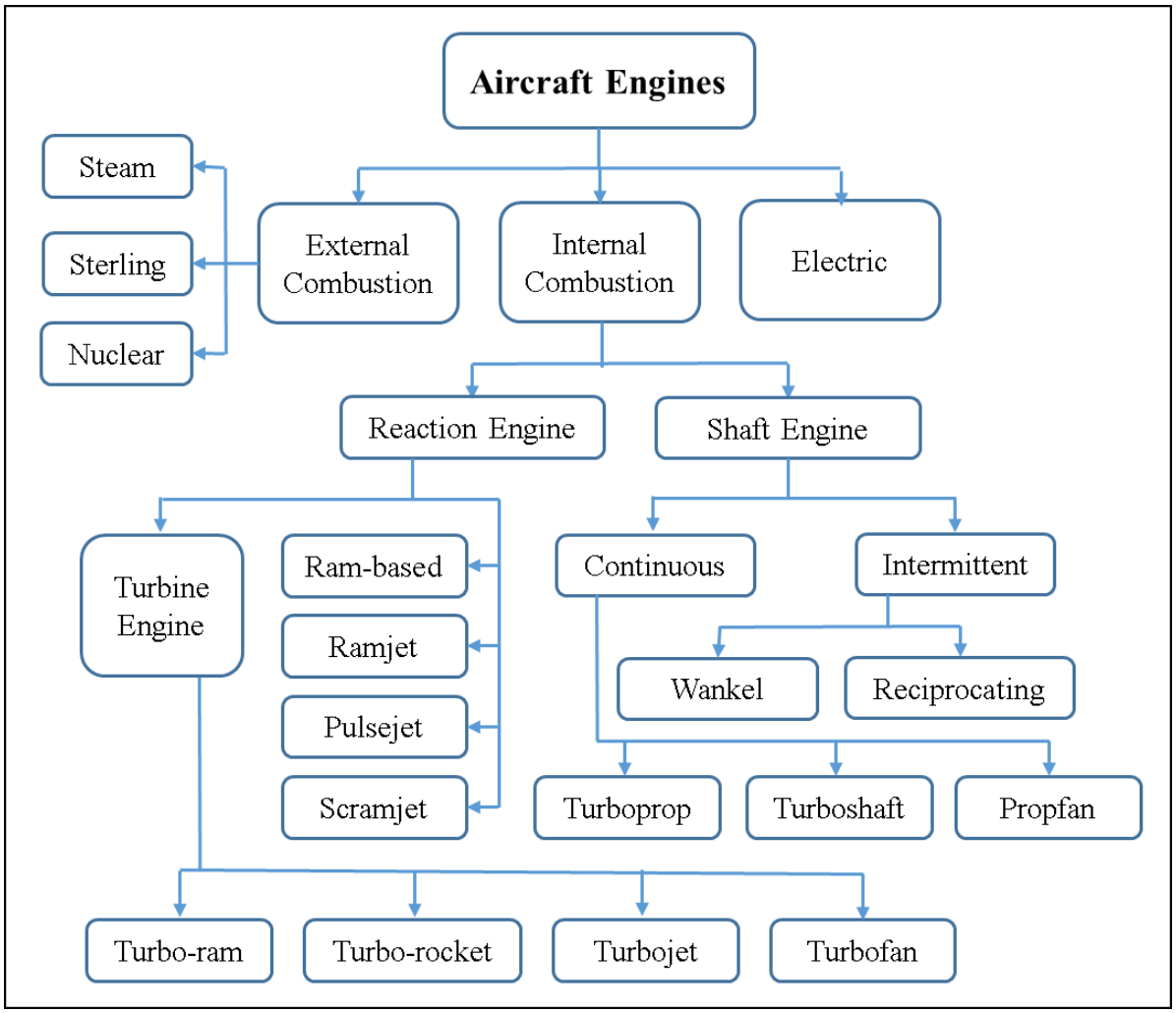

Fig. 1.2: Classification of Aircraft Engines

1.1.1. External Combustion Engines

An External Combustion engine is a heat engine where all heat transfer happens via the engine wall. This is not the case with an internal combustion engine, which obtains its heat from the combustion of fuel inside the working fluid body. Nuclear, Stirling, or steam engines are examples of external combustion engines. There are two types of EC engine: single-phase and dual-phase EC engine.

In single-phase engine the working fluid (any gas) is expanded by heating which causes motion. Stirling Engine is the example of single-phase EC engine.

International Journal of Engineering Research & Technology (IJERT)
ISSN: 2278-0181
Vol. 15 Issue 05 , May - 2026

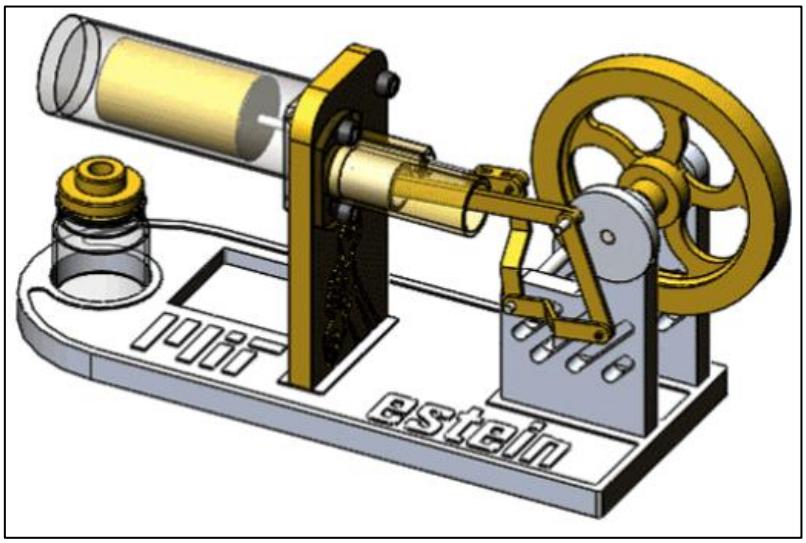

Fig. 1.3: Stirling Engine, an example of Single-Phase EC Engine {2}

The dual-phase engine uses phase transition of the working fluid to produce the work motion. Here, the working fluid (liquid) is heated to a temperature where it changes its phase (to gas) which expands and produces motion. These engines work on the different versions of Rankine cycle. Steam engine is an example of dual-phase EC engine.

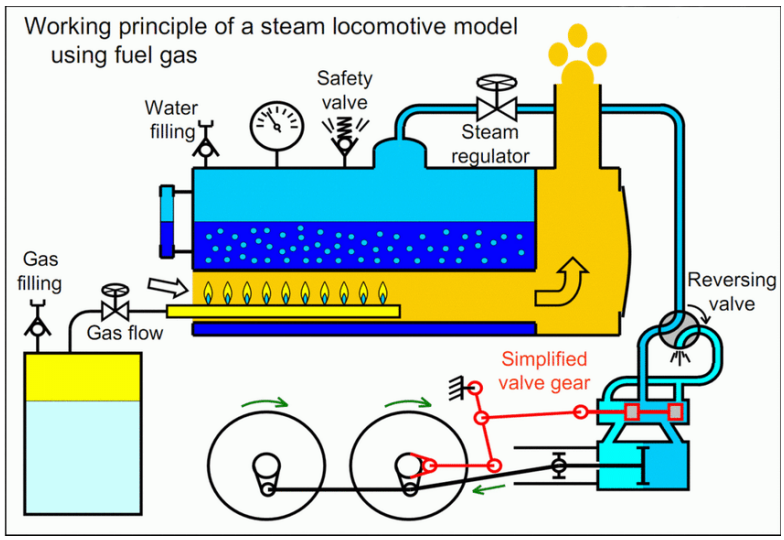

Fig. 1.4: A Schematic of Steam Engine, an example of Dual-Phase EC Engine {3}

International Journal of Engineering Research & Technology (IJERT)
ISSN: 2278-0181
Vol. 15 Issue 05 , May - 2026

1.1.2. Internal Combustion Engines

Shaft and reaction engines are the two main types of internal combustion engines. Both these engines are explained below:

a) There are two types of shaft engines: intermittent and continuous. There are two types of intermittent combustion engines (also called as piston engines): reciprocating and Wankel (rotary design). The next group of engines are continuous combustion engines also known as turbine shaft engines.is made up of turboprop, turboshaft, and propfan engines.

b) The reaction engine category consists of either turbine or athodyd (which stands for Aero Thermo Dynamic Duct) engines. Turbine engines include turbojet, turbofan, turbo ramjet, turbo rocket, and advanced ducted fan engines; athodyd category comprises scramjet, ramjet, and pulsejet engines.

1.2. Internal Combustion Engines

1.2.1. Piston Engines

An internal combustion engine that employs one or more reciprocating pistons to transform pressure into rotational motion is known as a piston engine, or reciprocating engine. The piston engines found in most cars and aircraft engines work on similar principles.

However, engines intended for aviation usage have undergone modifications such as the addition of dual ignition systems for increased safety and redundancy and air cooling for weight reduction. Piston engines can have their performance enhanced by the addition of superchargers or, less frequently, turbochargers. AVGAS is the fuel most frequently used in aviation piston engines; however, diesel fuel is increasingly seen, particularly in light aircraft.

Five categories can be used to group piston engines. They are opposing, radial, rotary, V-type, and inline. To enable forward flight, these engines are connected to a propeller.

1.2.2. Turboprop Engines

Both civil and military transport aircraft are powered by turboprop engines, which enable them to cruise at less than 450 mph (700 km/h). It is made up of a propeller and a gas generator, which includes a compressor, combustion chamber, and turbine. The compressor and propeller are both powered by the turbine. A turboprop has a gearbox to reduce the shaft's speed so that the propeller tips do not approach

International Journal of Engineering Research & Technology (IJERT)
ISSN: 2278-0181
Vol. 15 Issue 05 , May - 2026

supersonic speeds because gas turbines operate best at high speeds. An additional turbine is added as a substitute for the aforementioned turboprop engines, driving the propeller directly or through a gearbox.

Here, the compressor is the only engine driven by the first turbine. It is therefore free to revolve at its optimal speed—also known as a free- or power-turbine.

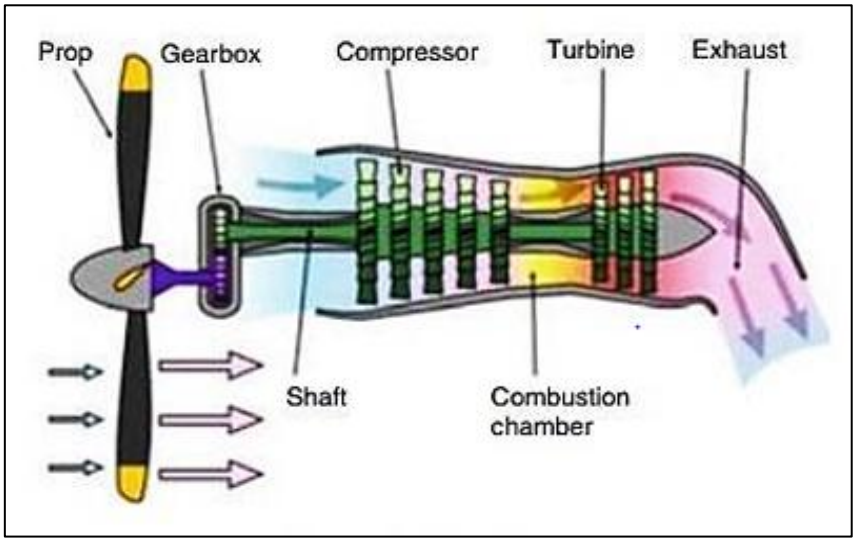

Fig. 1.5: Single Shaft Turboprop Engine [85]

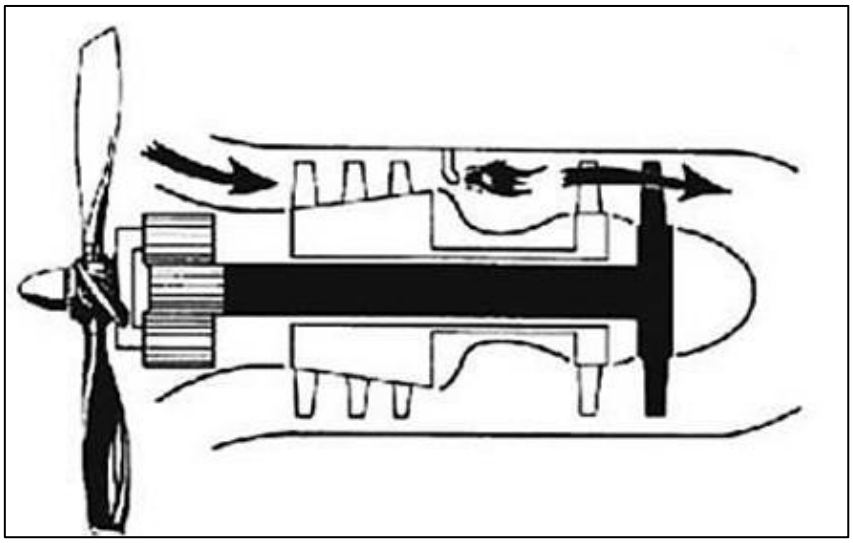

Fig. 1.6: Free Turbine Turboprop Engine [85]

The compressor-turbine is the name given to the other turbine. Modern turboprop engines use the exhaust jet stream and the propeller to produce thrust force. Only 10% to 20% of force is produced by the jet stream. As a result, some refer to turboprop engines as jet engines or response engines. Two turboprop engines are shown in Figure 1.5; the one on the left is a single-shafted engine with a propeller attached to the compressor-turbine shaft, and the one on the right is a free turbine.

International Journal of Engineering Research & Technology (IJERT)
ISSN: 2278-0181
Vol. 15 Issue 05 , May - 2026

1.2.3. Turboshaft Engines

Helicopters and auxiliary power units are the main applications for turboshaft engines. With one significant exception, a turboshaft engine and a turboprop are remarkably similar. In a turboprop, the engine, which is fastened to the aircraft, supports the propeller. The engine of a turboshaft does not physically support the helicopter's rotors directly.

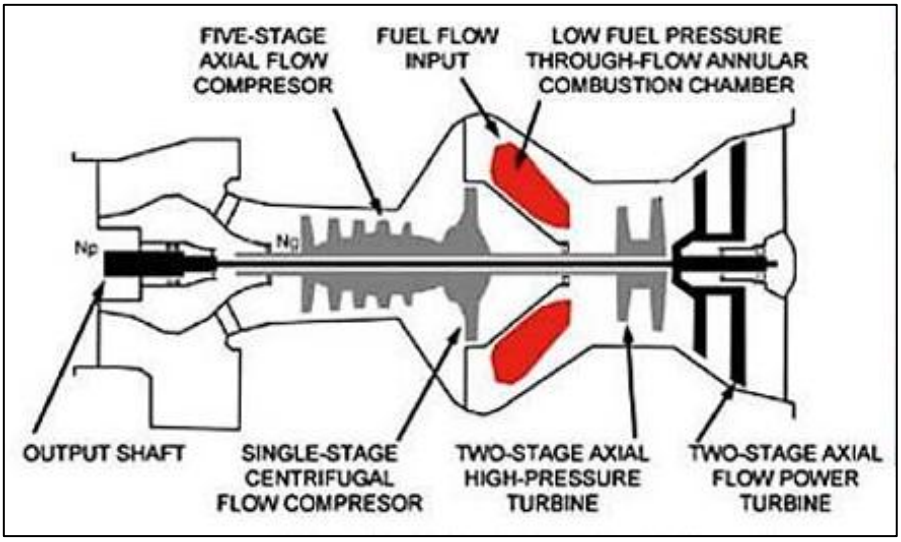

Fig. 1.7: GE T700 Turboshaft Engine [85]

The turboshaft engine only feeds the transmission through a spinning shaft after the rotor is attached to a gearbox that is fastened to the airframe. Several people consider the difference to be little because several aircraft manufacturers provide both turboprop and turboshaft engines based on the same design. The Seahawk helicopter is powered by a GE T700 turboshaft engine, as an example.

1.2.4. Propfan Engine

Propfans, also known as unducted fans or turboprop fans in the former Soviet Union, are modified turbofan engines in which the fan is positioned on the same axis as the compressor blades outside the engine nacelle.

Ultra-high bypass (UHB) engines and, more recently, open rotor jet engines are other names for propfans. The goal of the design is to combine the performance and speed of a turbofan with the fuel efficiency of a turboprop. The goal of the propfan concept was to outperform modern turbofans in terms of

International Journal of Engineering Research & Technology (IJERT)
ISSN: 2278-0181
Vol. 15 Issue 05 , May - 2026

fuel efficiency. This achievement comes with a noise penalty, though.

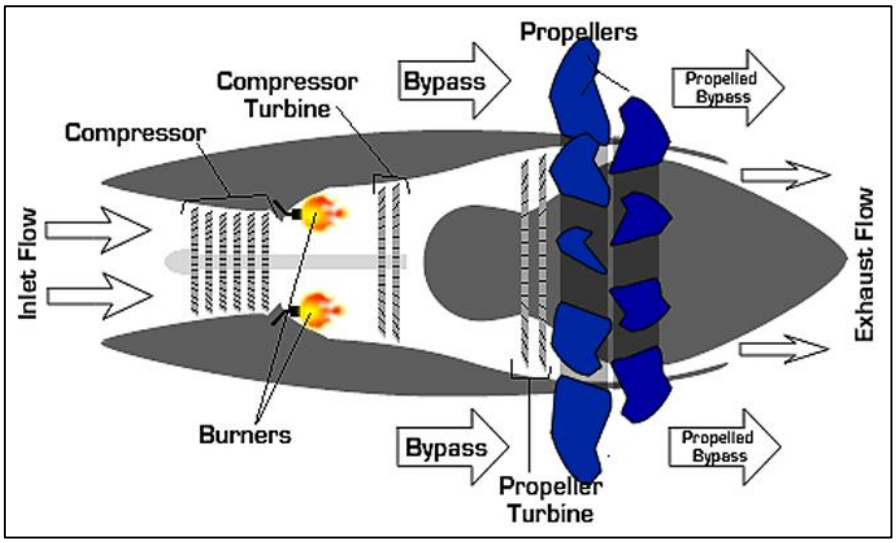

Fig. 1.8: Propeller Fan Engine [85]

1.2.5. Turbofan Engine

Turbofan engines are used in the majority of contemporary military aircraft, troop and freight transports, and airliners due to their strong thrust and good fuel efficiency. Similar to other gas turbines, it has a turbojet-like core engine that is encircled by a fan in front (or back, in the case of aft turbofan engines) and an extra turbine in the back. Similar to the turbine and core compressor, not all of the fan blades rotate with the shaft; some stay stationary.

The core shaft is traversed by the fan shaft. An engine with this configuration is referred to as a "two spool engine" (one "spool" for the fan and one for the core). Some advanced engines have additional spools for even higher efficiency. The engine inlet collects the entering air. A portion of the incoming air flows past the fan and into the core compressor and burner, where it is combined with fuel and burns.

Like in a basic turbojet, the hot exhaust travels through the fan turbines and core before exiting the nozzle. Similar to air passing via a propeller, the remaining incoming air travels through the fan and circumvents the engine. The airflow through the fan is moving at a velocity marginally higher than free stream. Thus, a turbofan's thrust is partially generated by the fan and partially by the core.

The bypass ratio is the proportion of air passing through the core to air passing around the engine. Low bypass ratio turbofans are the general name for engines having a bypass ratio of 1-2. The majority of modern transport aircraft have high bypass turbofans, whose bypass ratios are constantly rising and can approach 10 or more in certain turbofan engines. A turbofan produces additional thrust for almost the same quantity of fuel used by the core since the addition of the fan just slightly alters the fuel flow rate for the core. This indicates that the fuel efficiency of a turbofan is high.

International Journal of Engineering Research & Technology (IJERT)
ISSN: 2278-0181
Vol. 15 Issue 05 , May - 2026

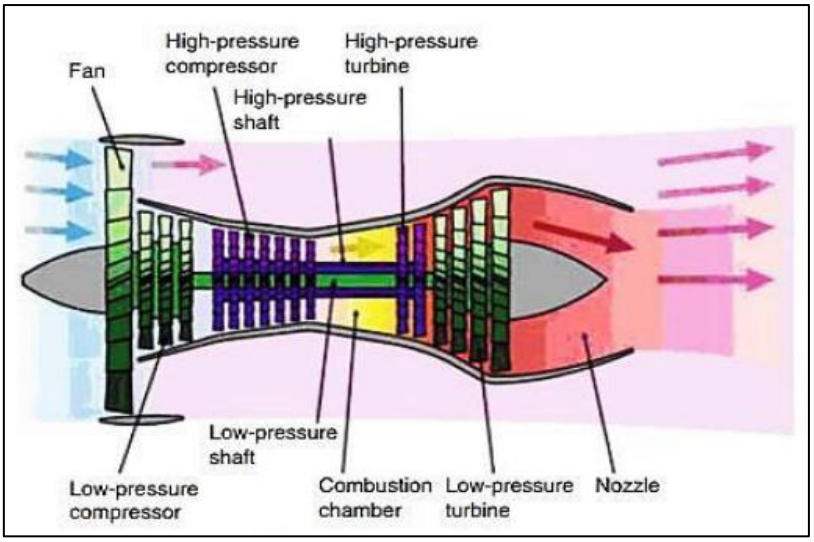

Fig. 1.9: High Bypass Ratio Turbofan Engines

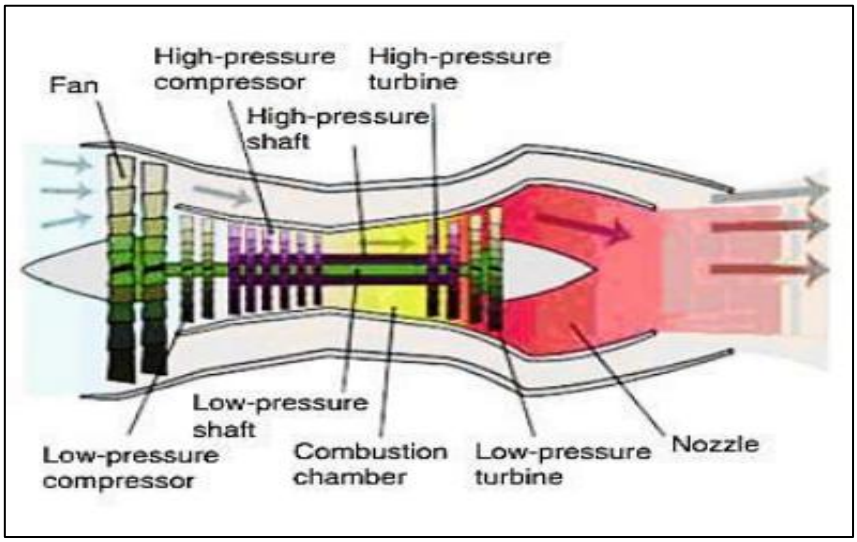

Fig. 1.10: Low bypass ratio Turbofan Engines [85]

Turbofans with a high bypass ratio are actually almost as fuel-efficient as turboprops. Because the fan is made up of many blades and is enclosed by the inlet, it may function more effectively at higher speeds than a standard propeller. For this reason, low-speed transports employ propellers, and high-speed transports use turbofans. Basic turbojets are not as fuel-efficient as low bypass ratio turbofans.

1.2.6. Turbojet Engine

A turbojet is a type of gas turbine engine that features one or more compressors to draw air in and compress it, a combustion section for adding fuel and lighting it, one or more turbines for drawing power from the expanding exhaust gases to power the compressor(s) and supply power to aircraft systems, and an exhaust nozzle for accelerating exhaust out the back of the engine to create thrust. A shaft connects each

International Journal of Engineering Research & Technology (IJERT)
ISSN: 2278-0181
Vol. 15 Issue 05 , May - 2026

compressor to a turbine.

More fuel is injected and burnt when the afterburner is activated, producing more thrust. As a result, more thrust is obtained but a lot more fuel is burned. With the afterburner disengaged, the engine runs more like a standard turbojet. Only fighter aircraft and the Concorde supersonic airliner have afterburners.

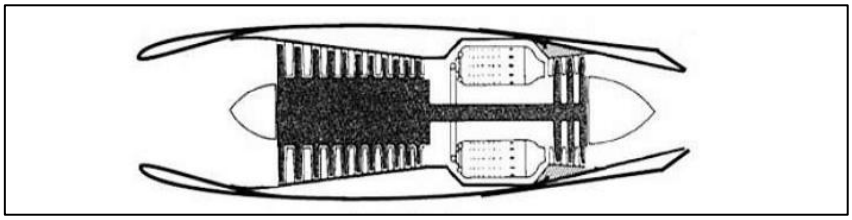

(a)

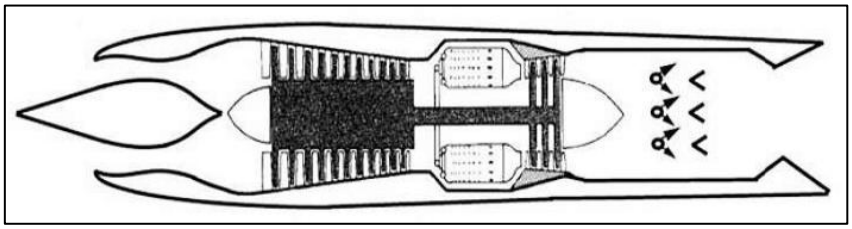

(b)

Fig. 1.11 (a) and (b): Subsonic and Supersonic Turbojet Engines respectively [85]

1.2.7. Ramjet Engine

A ramjet, also called a stovepipe jet, is a type of jet engine that admits and compresses incoming air without the need of a rotary compressor. It operates by exploiting the engine's forward momentum. An airplane cannot be moved from a stop by ramjets because they are unable to generate thrust at zero airspeed. The burner or combustor, the nozzle, and the input duct make up its three modules.

International Journal of Engineering Research & Technology (IJERT)
ISSN: 2278-0181
Vol. 15 Issue 05 , May - 2026

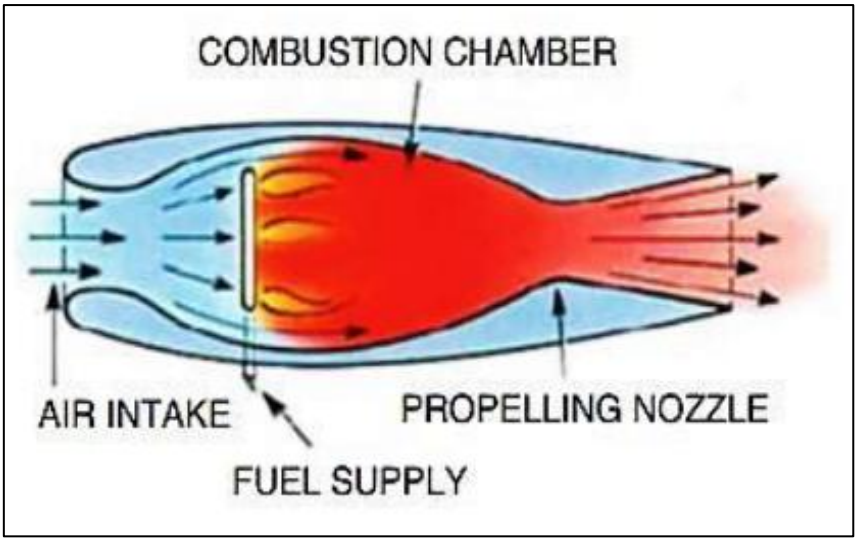

Fig. 1.12: Subsonic Ramjet Engine [85]

There are two varieties of it: liquid-fuel and solid-fuel ramjets. Ramjet engines can run at supersonic or subsonic speeds. Since the airflow is already subsonic and a simple hole is typically used, subsonic ramjets do not require a complex inlet.

Supersonic flow is slowed to subsonic speeds at the inlet of supersonic ramjets by one or more oblique shock waves, which are then followed by a powerful normal shock. Air thus reaches subsonic speeds near the combustion chamber's entry. By burning a fuel, the combustor increases the mass and heat of the compressed air. Flame holders in the combustion chamber prevent the flames from going out.

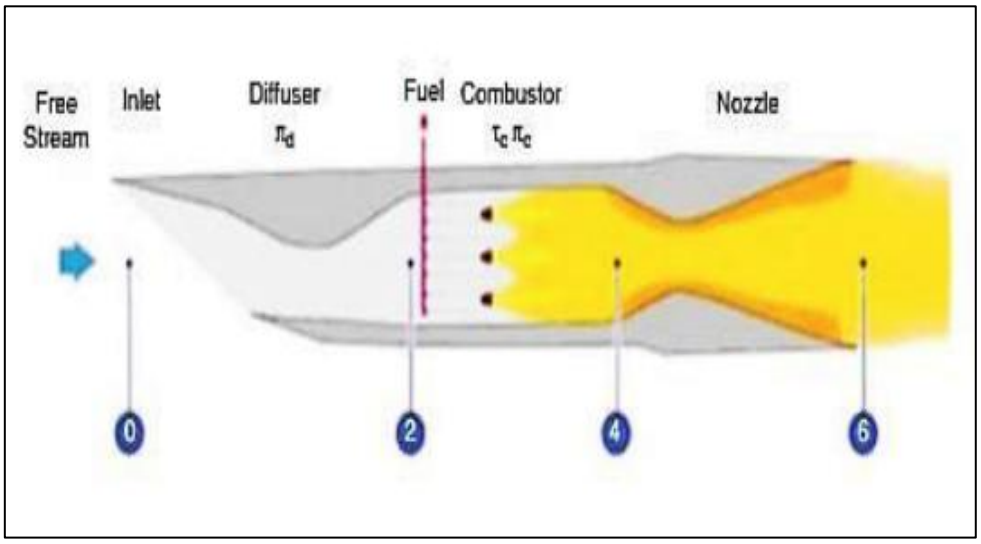

Fig. 1.13: Supersonic Ramjet Engine [85]

Stoichiometric fuel to air ratios allows for the safe operation of ramjet combustor, implying a combustor exit stagnation temperature of about 2400 K for kerosene. In order to generate thrust, combustion

International Journal of Engineering Research & Technology (IJERT)
ISSN: 2278-0181
Vol. 15 Issue 05 , May - 2026

products exiting the combustion chamber are reaccelerated through a nozzle and sent through a convergent-divergent nozzle at supersonic speeds. A converging nozzle accelerates exhaust flow for ramjets running at subsonic Mach numbers. Although they can reach at least Mach 5, supersonic ramjet engines function best at speeds close to Mach 3.

1.2.8. Scramjet Engine

Advancement over ramjets, the scramjet can run at far higher speeds than any other type of air-breathing engine. Supersonic Combustion Ramjet, as it is also known, is the abbreviation for the supersonic flow at which fuel and air burn relative to the engine. Scramjets have a potential maximum speed of Mach 17 and begin operating at a minimum speed of Mach 4.

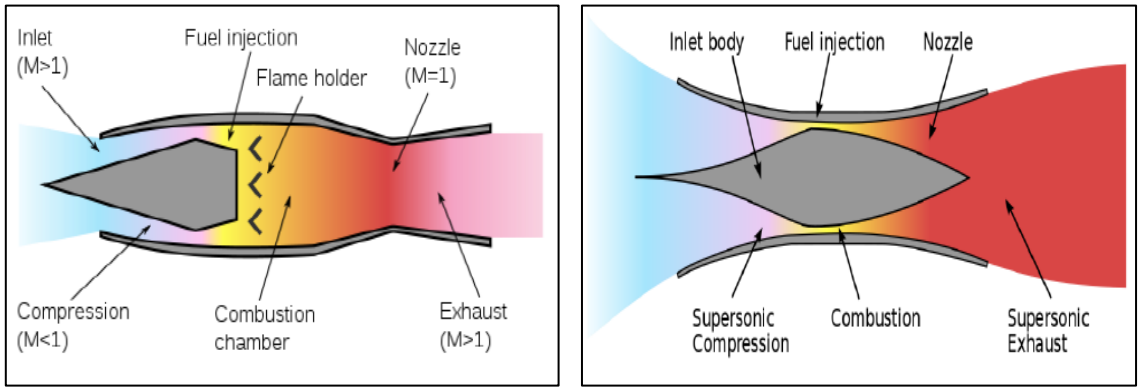

(a) Ramjet Engine (b) Scramjet Engine

Fig. 1.14 (a) and (b): Comparison between Ramjet Engine and Scramjet Engine [85]

1.2.9. Turboram (Turbo-Ramjet) Engine

Turbo ramjet is a combination engine that can operate as a turbojet or ramjet engine. This kind of jet engine is designed to fly at very high speeds. The turbo ramjet engine combines the high-speed, Mach 3-capable turbojet engine with the high-speed, high-Mach number ramjet engine.

A duct with a variable intake at the front and an afterburning jet pipe with a variable nozzle at the back surround the engine. The afterburner is turned on when the engine is taking off and accelerating like a regular turbojet; under other flying conditions, up to Mach 3, the afterburner is off.

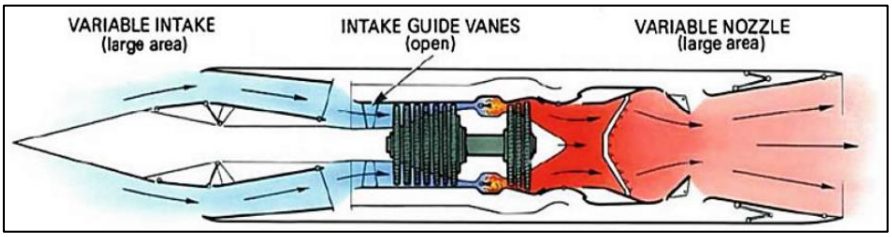

International Journal of Engineering Research & Technology (IJERT)
ISSN: 2278-0181
Vol. 15 Issue 05 , May - 2026

(a)

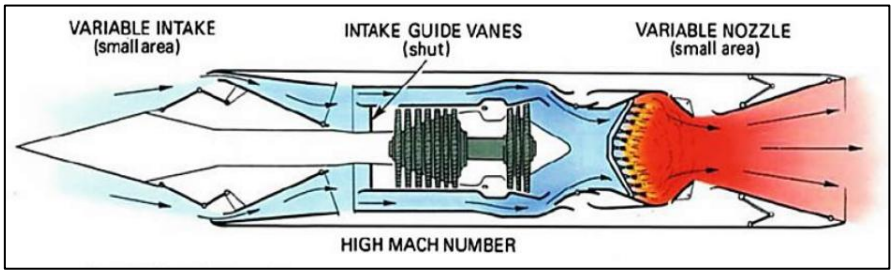

(b)

Fig. 1.15 (a) and (b): Low Mach No. and High Mach No. Aft Fan Turboram Engine respectively [85]

The turbojet shuts down as the aircraft reaches Mach 3, and guide vanes direct the intake air away from the compressor and into the afterburning jet pipe, creating a ramjet combustion chamber. When the engine runs in the ram jet mode, this engine is appropriate for an aircraft that has to cruise at a high speed for an extended period of time.

1.2.10. Turborocket Engine

The turbo-rocket engine, often referred to as the air turbo-rocket engine or simply the ATR, is a kind of air breathing engine that combines components of a jet engine and a rocket. The ATR is a member of the Turbine-Based Combined-Cycle, or TBCC, engine family, a broad category of propulsion engines. It might be regarded as a substitute engine for the turbo ramjet. Its primary distinction is that it carries its own oxygen, which allows for rapid combustion.

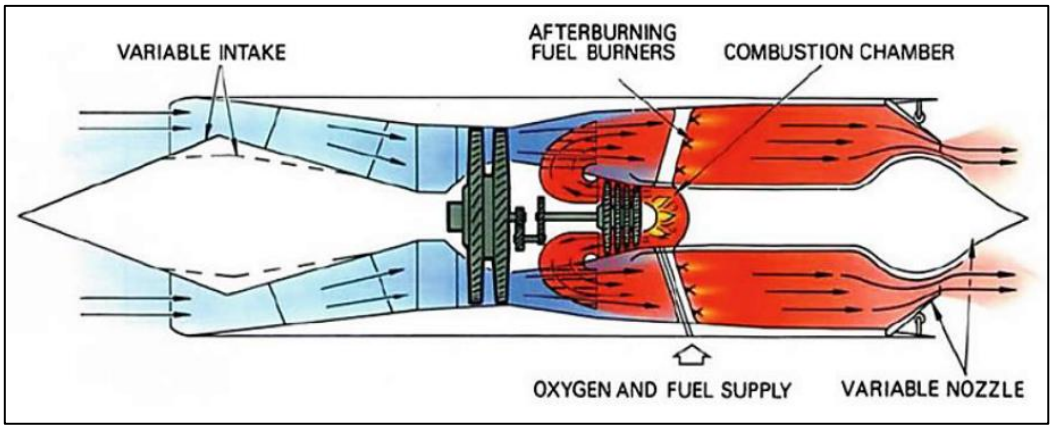

Fig. 1.16: Turborocket Engine [85]

Kerosene and liquid oxygen are burned in a combustion chamber akin to a rocket to provide the engine's multi-stage turbine, which powers a low-pressure compressor. Before the gas enters the turbine,

International Journal of Engineering Research & Technology (IJERT)
ISSN: 2278-0181
Vol. 15 Issue 05 , May - 2026

more fuel is sprayed into the combustion chamber for cooling purposes because the gas temperature will be approximately 3500 ºC

After adding compressor air to this fuel-rich combination (gas), the excess fuel is burned in a traditional afterburning system. Eventually, it exhausts through a propelling nozzle that is divergent and convergent. In certain ATRs, burning a solid propellant can generate hot gas. The engine uses more fuel even though it is lighter and smaller than the turbo ramjet. This tends to make it more appropriate for an aircraft type such as an interceptor or space launcher, which often has a short duration, all-acceleration flight plan, and demands high speed and high-altitude performance.

1.2.11. Advanced Ducted Fan Engine

Advanced ducted fans are essentially turbofans with big swept fan blades that are encased in ducts like turbofan engines. They have reduction gearing and pitch control just like propfans. The advanced ducted fan's bypass ratio ranges from 15:1 to 25:1. There are two basic types: one with counter-rotating blades and the other with a single propeller fan that is geared and has variable pitch.

The creation of these engines has involved a great deal of work at several aviation engine manufacturers, including Pratt & Whitney, MTU, and Fiat Avio. Such a high bypass ratio requires a thin-lip, slim-line nacelle.

1.3. Piston Engine Layouts

Light aircraft internal combustion engines typically follow one of several common layouts that are categorised based on how the cylinders are arranged in relation to the crankshaft. The most common layouts are discussed below in detail:

Installing an inverted inline engine (like the deHavilland Gipsy Major) on an aircraft with a nose-wheel may be difficult due to the placement of the cylinders. Because of this, these engines are usually found on aircraft with a tail wheel arrangement.

1.3.1. Horizontally Opposed (Flat) Engine

This is the most common cylinder arrangement for light general aviation aircraft. Two banks with an equal number of cylinders stacked horizontally are present in this instance. Every cylinder is connected to an equivalent cylinder on the opposite bank in order to lessen vibration. The crankshaft is positioned in the centre of the two banks of cylinders.

International Journal of Engineering Research & Technology (IJERT)
ISSN: 2278-0181
Vol. 15 Issue 05 , May - 2026

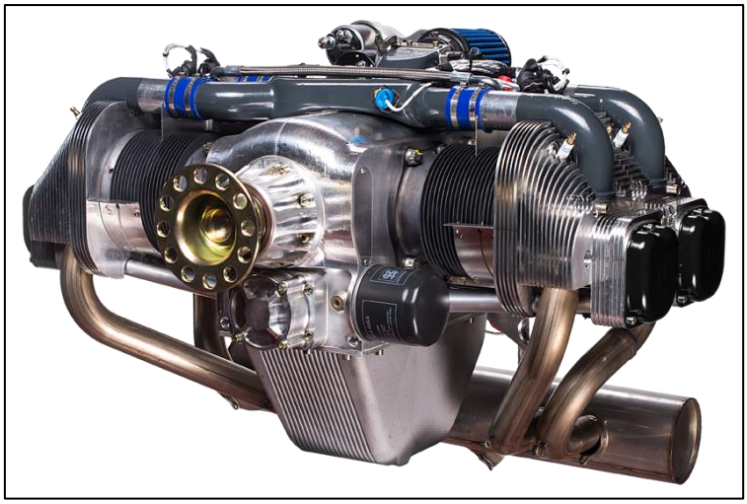

Fig. 1.17: UL Power 350i, an example of a Horizontally Opposed Engine {9}

Because the cylinders in a horizontally opposed engine are arranged in two banks rather than one, they can be made shorter than an identical inline engine. But this configuration makes the engine bigger and necessitates the use of two distinct cylinder heads rather than one.

Table 1.1: Aircrafts using Horizontally Opposed Engine {1}

Engine Name	Aircraft Examples	No. of Cylinder	Displace-ment	Power Output (HP)
Lycoming O-320 family	Cessna 172, Cessna 177, Piper PA-28 Cherokee, Piper PA-30 Twin Comanche, Robinson R22	4	5244 cc (5.24 L)	150 – 160
Lycoming O-540 family	Cessna 182, Cessna 206, Piper PA-32 Cherokee Six, Vans RV-10	6	8874 cc (8.87 L)	230 – 350
Continental IO-360 family	Cirrus SR20, Mooney M20, Piper PA-34 Seneca	6	5900 cc (5.9 L)	180 – 225
Rotax 912 family	Tecnam Echo, Diamond DA-20, CSA Sportcruiser	4	1212 cc (1.2 L)	80 – 100

1.3.2. Inline Engine

The distinguishing characteristic of inline engines is their vertical cylinder design, which is built in a single line along the crankcase. One advantage of this configuration is the engine's reduced frontal area that it presents to the incoming air. A low frontal area allows for a thinner engine cowling, reducing the aircraft's

International Journal of Engineering Research & Technology (IJERT)
ISSN: 2278-0181
Vol. 15 Issue 05 , May - 2026

drag signature. The challenge of cooling the rear cylinders in an inline arrangement usually places a restriction on the maximum number of cylinders that an engine can have.

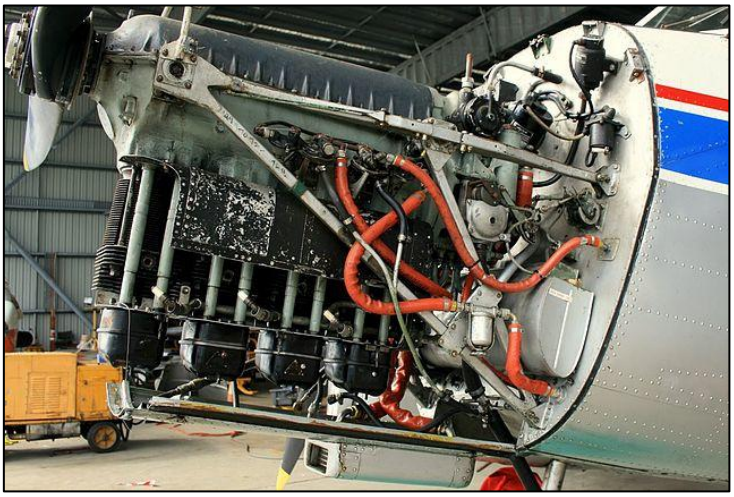

Fig. 1.18: DeHavilland Gipsy Major, an example of an Inline Engine {1}

1.3.3. Radial Engine

Similar to a wheel's spokes, radial engines are made up of a bank of cylinders arranged radially around a central crankshaft. Not every connecting rod can be fastened directly to the crankshaft since every cylinder in a bank is located in the same plane that is spaced apart radially from the crankshaft. Rather, a master-and-articulating-rod arrangement connects each piston to a ring on the master connecting rod, with one piston being directly attached to the crankshaft.

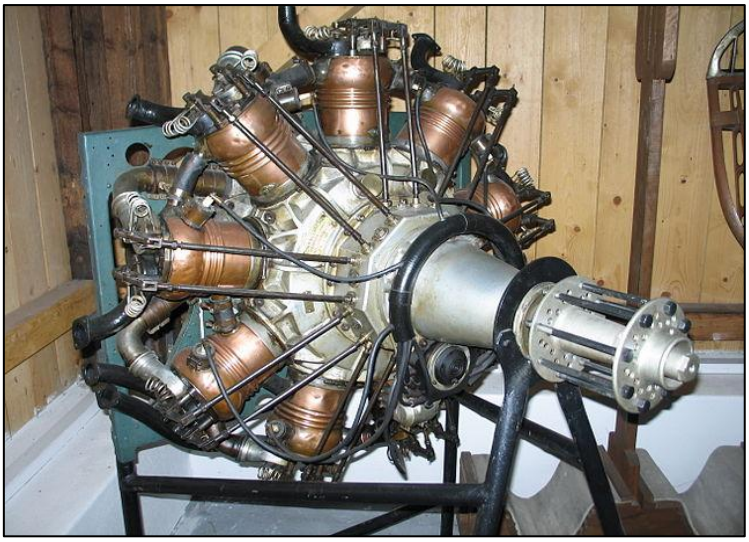

Fig. 1.19: Radial Engine {1}

International Journal of Engineering Research & Technology (IJERT)
ISSN: 2278-0181
Vol. 15 Issue 05 , May - 2026

Four-stroke radial piston engines are always built with an odd number of cylinders in order to accommodate the use of a reliable every-other firing order. This is done on the compression and combustion strokes to leave a one-piston gap between the pistons.

Larger aircraft, where it was possible to install many banks of pistons to create an engine with a high-power output while keeping the engine as compact as possible, were frequently equipped with radial engines. Radial engines were used in World War II-era aircraft like the Douglas C-47, Avro Lancaster, and Republic P-47 Thunderbolt. After World War II, jet engines and gas turbine engines were able to deliver more power more consistently with less total bulk, making huge radial engines virtually obsolete.

1.3.4. V-Type Engine

When viewed along the crankshaft's axis, the two banks of cylinders in a V-arrangement are what define V-type engines. When compared to a horizontally opposed layout, the engine's total dimensions can be decreased by placing the cylinders in a V-formation. The V-angle is the name given to the angle formed by the two banks of cylinders. Angles of 90°, 60°, and 45° are common.

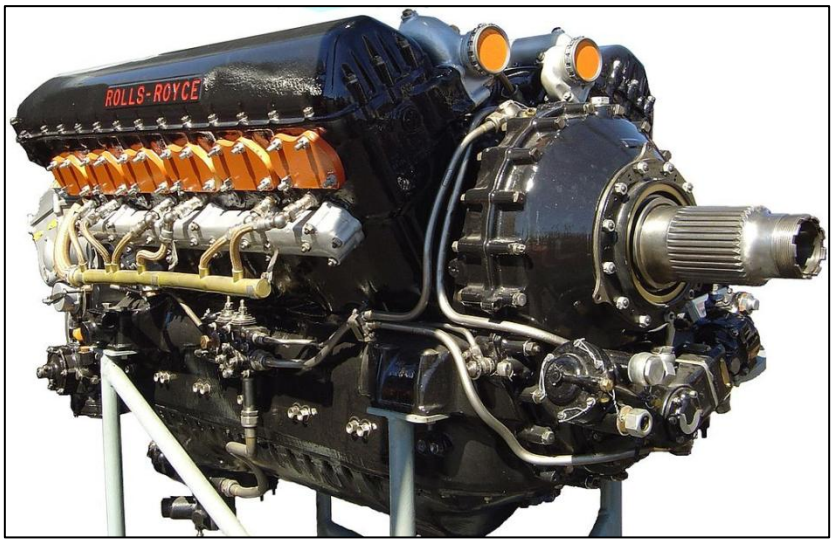

Fig. 1.20: Rolls-Royce V12 Merlin Engine, an example of V-Type Engine {1}

The Rolls-Royce V12 Merlin engine, which was one of the most well-known V-configuration engines ever made, propelled several World War II aircraft, such as the de Havilland Mosquito, Hawker Hurricane, and Supermarine Spitfire.

1.4. Applications of Piston Engines

IC engines are still a reliable source of power for light weight aircrafts and unmanned aerial vehicles

International Journal of Engineering Research & Technology (IJERT)
ISSN: 2278-0181
Vol. 15 Issue 05 , May - 2026

(UAVs). Many of the single seater aircrafts which are used by Indian Air Force and other country's air forces till date for training new recruits and quick on the go reconnaissance missions. Also, many of the UAVs use piston cylinder IC engine which fly at an altitude of 35,000 ft with speeds of 200 kmph and have range of around 350 kms. Some of the applications are mentioned below.

1.4.1. Garud (Pipistrel Virus SW80)

The Pipistrel Virus is a two-seat, single engine light aircraft. It is a high-wing, cantilever monoplane of pod-and-boom configuration with a T-tail and air brakes. The cabin has two seats side-by-side. Its fixed undercarriage can be provided in either tricycle or tailwheel configuration. It is powered by an 80 hp (60 kW) Rotax 912 engine.

The Rotax 912 is a horizontally-opposed four-cylinder, naturally-aspirated, four-stroke aircraft engine with a reduction gearbox. It features liquid-cooled cylinder heads and air-cooled cylinders.

The aircraft achieves a maximum speed of 283 km/h, cruise speed of 273 km/h at 75% power and a stall speed 79 km/h without flaps. Aircraft has a range of 1,450 km and endurance of 5.3 hours. Its service ceiling is 6,800 m (22,300 ft).

Fig. 1.21: Garud (Pipistrel Virus SW-80) {8}

1.4.2. DRDO Nishant

The DRDO's Aeronautical Development Establishment (ADE) is responsible for the development of the Nishant unmanned aerial vehicle (UAV). The Nishant UAV is primarily responsible for obtaining intelligence over enemy territory. It is also used for damage assessment, artillery firing correction, target

International Journal of Engineering Research & Technology (IJERT)
ISSN: 2278-0181
Vol. 15 Issue 05 , May - 2026

designation, reconnaissance, training, surveillance, ELINT, and SIGINT. The four hours and thirty minutes of endurance are plenty for the UAV. Nishant has finished the user trials and development phase.

The 380 kg Nishant UAV can be recovered using a parachute system and must be launched by rail using a hydro-pneumatic launcher. Launches with a speed of 45 m/s require 0.6 seconds and 100 kW of electricity; further launches can be spaced 20 minutes apart. The 14,000 kg Mobile Hydro-Pneumatic Launcher (MHPL) system on a Tatra truck has a 1000 launch life cycle before needing maintenance.

Figure 1.20: DRDO Nishant {9}

Nishant is one of the few UAVs in its weight class in the world that can be launched with a catapult and recovered with a parachute, doing away with the necessity for a runway required for traditional take-off and landing on wheels.

Nishant UAV is powered by an ALVIS AR-801 engine. This is a Wankel-type rotary, single rotor engine. It can produce 40 bhp at 6,000 engine rpm. Alternatively, the engine produces 51 bhp at 8,000 rpm (carburettor) or 60 bhp at 8,000 rpm (EFI). The aircraft is propelled by a 2-bladed fixed-pitch pusher propeller. The aircraft attains a maximum speed of 216 kmph and has a range of 100 km. It has an endurance limit of 4.5 hours and flies at 13,000 ft (3962 m) altitude.

1.4.3. DRDO Rustom - I

DRDO Rustom is medium altitude long endurance (MALE) UAV which is being developed by ADE, a unit of DRDO for all the three services of Indian Armed forces namely Indian Army, Air Force, and

International Journal of Engineering Research & Technology (IJERT)
ISSN: 2278-0181
Vol. 15 Issue 05 , May - 2026

Navy. Rustom is based on the Light Canard Research Aircraft (LCRA) NAL, developed by a team led by the late Professor Rustom Damania in the 1980s. The drone will have a modified design and new engines.

Figure 1.21: DRDO Rustom – I {8}

The Rustom-1 has a wing length of 7.9 m (26 ft). It weighs 720 kg (1,590 lb.) and is launched as a conventional projectile. Rustom can see enemy territory up to 250 kilometres (160 miles) and can carry multiple surveillance cameras and radars.

Rustom I is powered by a Lycoming O-320 engines four-cylinder air-cooled horizontally opposed engine. It can produce 112 kW (150 hp). The aircraft attains a maximum speed of 150 kmph and has a ferry range of 1000 km. It has an endurance limit of 12-15 hours and flies at 26,000 ft (7900 m) altitude.

1.4.4. IAI Searcher II

The IAI Searcher II is one of the most advanced UAVs in the world and was developed in Israel in the 1980s. More than 100 Searcher IIs are being operated by the Indian Air Force and the Indian Navy. It is powered by a piston-driven Limbach L550E.

The L550E is an air-cooled horizontally-opposed four-cylinder two-stroke petrol engine developing 37 kW (50 hp) at 7500 rpm which can drive a propeller either directly or geared. It employs a single magneto ignition, four carburettors, and is lubricated by oil mixture lubrication with a fuel to oil ratio of 25:1 for mineral oil or 50:1 for synthetic oil.

The UAV has maximum speed of 201 km/h and range of 350 km. It has an endurance limit of 20 hours. It can fly at service ceiling of 6,100 m (21,000 ft) with loiter speed of 110 to 150 km/h.

International Journal of Engineering Research & Technology (IJERT)
ISSN: 2278-0181
Vol. 15 Issue 05 , May - 2026

Figure 1.22: IAI Searcher II {9}

1.4.5. IAI Heron

The Israel Aerospace Industries' UAV division is responsible for developing the medium-altitude long-endurance unmanned aerial vehicle (UAV), known as the IAI Heron (Machatz-1). It can operate at up to 10.5 km (35,000 ft) for up to 52 hours during Medium Altitude Long Endurance (MALE) sorties. Although 52 hours of nonstop flight have been tested, the payload and flight profile indicate that a shorter effective operational maximum flying period is possible. It is powered by a Rotax 916 engine.

Rotax 916 is 4-cylinder air and water cooled horizontally-opposed piston engine that packs 160 kW (210 hp). The UAV reaches the maximum speed of 201 km/h and range of 350 km. It has an endurance limit of 20 hours. It can fly at service ceiling of 6,100 m (21,000 ft) with loiter speed of 110 to 150 km/h.

Figure 1.23: IAI Heron {8}

International Journal of Engineering Research & Technology (IJERT)
ISSN: 2278-0181
Vol. 15 Issue 05 , May - 2026

1.5. Problem Statement of the Project

Design and develop an engine test rig for a single-seater aircraft and UAVs to measure engine performance parameters and thrust produced.

1.6. Objectives of the Project

1. Design CAD model of the test rig by using adequate design approaches and calculations.
2. Perform finite element analysis of all the critical components in the FEA software.
3. Draft a Bill of Materials (BOM) of the Test Rig.

International Journal of Engineering Research & Technology (IJERT)
ISSN: 2278-0181
Vol. 15 Issue 05 , May - 2026

Chapter - 2

Literature Survey

This chapter presents a brief background to Propeller IC Engine Propulsion System and terms related to it. It also describes various test setups used in the IC engine propulsion system and gives relative information about the terms used in the testing of an IC Engine Propulsion Systems. This chapter looks at various research papers and texts related to development of test rig for and aircraft engine.

Ausserer J. K. et al (2013) [1] developed and validated a test setup to characterise the thermal losses of small internal combustion engines, optimize combustion phasing, and enable heavy fuel operations. The small ICEs (power <7.5 kW) have low thermal efficiencies due to high thermal losses. The literature says that efficiency and power of an ICE starts to drop as its area to volume ratio goes beyond 1.5 cm^2/cc. The test stand measures torque, brake power, rotational speed, mass flow rates up to 48 temperatures (including ambient, intake, cylinder head, fuel, and exhaust), 8 pressures (including ambient, intake, and exhaust), and throttle position. Tests were performed on three geometrically identical 3W 55i engines.

Arnold S. et al (2015) [2] developed two different test rigs, one for turbine engine and other for compressor. The use of additive manufacturing and novel test measurement techniques were incorporated in order to lower the cost of construction of the test setups. The instrumentation suite for the turbine engine included measurements of rotor speed, inlet pressure and temperature for compressor and combustor, and exit pressure and temperature for the turbine. Fuel and oil system pressures were also measured as part of the ECS. Vibration levels were measured using accelerometers.

Tripathi R. K. et al (2015) [3] developed a propeller test rig to measure the performance of a propeller used in a reciprocating or rotary engine aircraft. A 2-stroke SI engine is mounted over a beamed structure and a 2-blade fixed pitch propeller is attached to the engine. A Load cell and a transducer are attached to the beam to measure the thrust. The effect of thrust coefficient, speed power coefficient and power coefficient on propeller efficiency is studied. The thrust produced by the propeller was measured at various engine rpm and air flow rate across the propeller was measured using an anemometer. After performing all the tests, it was found that the thrust coefficient is inversely proportional to the advance ratio and hence at higher engine speeds the thrust produced increases. It was also found that the thrust is directly proportional to the advance ratio. Thus, the aircraft moves greater distance at higher thrust the thrust is directly proportional to the advance ratio. Therefore, the aircraft covers greater distance at higher thrust the propeller disk efficiency is directly proportional to the speed power coefficient and advance ratio. Hence the aircraft should fly at relatively higher speeds for low fuel consumption. Other conclusions drawn were

International Journal of Engineering Research & Technology (IJERT)
ISSN: 2278-0181
Vol. 15 Issue 05 , May - 2026

Advance ratio and speed power coefficient varies linearly and Power coefficient is inversely proportional to the advance ratio.

Rad I. O. et al (2021) [4] published a thesis on Test Rig Design for a Micro-Turbojet Engine. The objective of this thesis was to design and assemble a test rig to assess the on-ground performances and thermodynamic cycles of any micro-turbojet engine. An electronic system is also developed and implemented for sensor signal conditioning, data processing and to generate a database for complex post-processing applications

Pieper K. et al (2018) [5] designed a dynamically scaled, distributed electric propulsion aircraft test bed. The setup was developed to perform dynamic model validation of system identification flight testing in a scaled down model of an actual engine. The engine used was a 21% subscale model of a Cirrus SR22T. A new wing configuration integrated with series of electric ducted fans into the upper end of the wing trailing edge was designed to study the effectiveness of propulsive-based control and the effects of propulsion-airframe interactions. To validate performance specifications and capabilities, wind tunnel experiments were performed on propulsor combinations of motors, electronic speed controllers, and fans.

Wiegand A. et al (2012) [6] developed a test stand to evaluate a 2-stroke Micro IC Engine. The testing of micro engines demands high accuracy, high-speed and compact measurement systems since it involves compact dimensioning and high rotation speeds. The paper sheds the light on the component selections to fabricate a budget friendly and accurate test setup for a micro-IC engine. Fuel system calibration and combustion analysis are the main objectives achieved in this paper. The engine and the test setup were equipped with the various instruments viz. a low-speed pressure transducer to measure exhaust pressure, intake and exhaust thermocouples, an optical encoder to measure the crankshaft position, a hot-wire anemometer to measure air mass flow rate and a high-pressure transducer for cylinder.

Hartman J.A., et al (2014) [7] designed and developed an Airborne Subscale Transport Aircraft Research (AirSTAR) test-bed at NASA Langley Research Centre (LaRC). A Generic Transport Model (GTM) is used to provide an experimental flight test capability to conduct experiments pertaining to dynamics modelling and control beyond the normal flight conditions.

Pieper K. et al (2018) [8] published a thesis on Design, Development and Evaluation of a Distributed Propulsion Aircraft Test bed. The main objectives of this paper were to characterise the propulsion-airframe interactions experimentally for the Distributed Electric Propulsion (DEP) vehicles to ease the modelling and to perform vehicle-level flight control by exploring and validating the use of DEP. A Cirrus SR22-T was selected as the airframe and a 21& subscale radio-controlled model was fabricated with complete data

International Journal of Engineering Research & Technology (IJERT)
ISSN: 2278-0181
Vol. 15 Issue 05 , May - 2026

acquisition and flight control system instruments to capture the aircraft's state and performance during a flight. A total of eight ducted fans, four on each of the trailing edges of left and right wings were selected and were tested in the wind tunnel to validate the temperature and thrust performance.

Zhu D. et al (2006) [9] presented a thesis on the investigation, development, integration, calibration and instrumentations for Propulsion-Aerodynamic Test Rig (PATR) to measure the performance parameters like force, torque, pressure, and air flow. The main objective of the project was to aid in the study of aerodynamic super-circulation lift augmentation concept. For the remote operation of the PATR, a Graphic User Interface (GUI) was developed in MATLAB.

Ausserer J. K. et al (2012) [31] researched on validating, integrating, and testing of a hybrid-electric propulsion system for a small remotely piloted aircraft. The integration phase involved selection, testing, and assembly of components selected based on the already performed design simulations. The propulsion system was retro-fitted onto a glider airframe having a wingspan of 12 ft and 35 lbs. maximum take-off weight. The propulsion system is made capable of running on combustion only mode, electric only mode, dual (hybrid) mode and regenerative mode.

Borges M. et al (2015) [12] published a thesis titled 'Design of an Apparatus for Wind Tunnel Tests of Electric UAV Propulsion Systems.' In this work, an apparatus has been designed, developed and validated to test electric propulsion systems that can be used in an unmanned aerial vehicle. The test setup developed is capable for the testing of electric motors (upto 63 mm diameters) with propeller diameters limited to 27 inches.

Moulton N. et al (2007) [32] presented a paper on Performance Measurement and Simulation of a Small Internal Combustion Engine. A 3W Model Motoren's 100i-B2 engine was tested for its performance parameters like output power, torque, specific fuel consumption, exhaust and cylinder head temperatures and exhaust gas composition as a function of engine speed. Also, to identify the areas where the engine design could be modified in order to improve its performance, a numerical simulation was also carried out. The simulation suggested that engine's power output can be enhanced by reducing the exhaust port duration.

Fritz J. et al (2004) [39] published a research paper on Aeromobile regenerative super-circulation test stand. He developed a test stand that is able to measure the aerodynamic performances of non-conventional aerial vehicles like a flying car. The main aim of the research was to design and fabricate the test that can predominantly measure the lift and drag forces on the wings of an Aeromobile. The test stand is designed in such a way that tests can be performed both indoors and outdoors.

International Journal of Engineering Research & Technology (IJERT)
ISSN: 2278-0181
Vol. 15 Issue 05 , May - 2026

Braden T. Warwick et al (2017) [53] published a research paper on modal analysis of an engine mounted aircraft support frame, to determine its vibrational characteristics using computational methods. Computational and experimental results were compared by performing a pseudo-Orthogonality check. Structural modifications were made to reduce the modal density at engine blade pass frequency during cruising. The author recommended the use of topology optimisation methods to efficiently decrease the modal density of structurally critical components to minimize the mass and maintain their structural integrity.

Adkine A. S. et al (2017) [54] published a research paper on his work of performing a modal and static structural analysis on engine support bracket using FEA. In his work he compared the initial and modified designs of the support bracket based on the equivalent Von-Mises stress, total deformation and strain energy absorbed. Modal analysis was performed to check for self-excitation frequency of the support bracket, whether it is less than its natural frequency. The engine support bracket was analysed for four different materials, Gray Cast Iron, Aluminium Alloy, Magnesium Alloy and ERW-1 steel. The stress analysis results suggested that the ERW-1 material deformed and stressed less compared to others. Also, the self-excitation frequency of the modified design of the support bracket was nearly 4 % more than the natural frequency and hence was safe to use. Further analysis for different materials concluded that Aluminium has most deformation and less stiffness. The Magnesium alloy could be an alternative to ERW-1 steel but is more susceptible to corrosion.

Zhu J. et al (1989) [55] researched to study and predict the dynamic behaviour of chassis mountings for a diesel engine. It was found that while the addition of the bolt holes decreased the natural frequency of the overall structure, adding the C-section edges had an opposite effect. It was also found that the ribs influenced the dynamics of the structure based on their position, i.e., upper ribs increased whereas the lower ribs decreased the natural frequency of the mounting bracket. Harmonic response analysis was performed to determine the dynamic displacement of the supporting faces. All the results concluded the dynamic displacement varies linearly with the applied loads.

Wang M. et al (2017) [59] investigated on the vibration patters of a shaft and deformation of the support structure of an aero-engine’s fan-rotor system. The governing differential equations for the test setup are deduced using the Lagrangian approach with four degrees of freedom. The shaft contributes to the inertial factors whereas the flexible support structures are responsible for the stiffness items.

Nandhakumar S. et al (2021) [60] focused on optimising an existing electric chassis weight by replacing its steel members with Aluminium alloys in a way such that it will not compromise the strength

International Journal of Engineering Research & Technology (IJERT)
ISSN: 2278-0181
Vol. 15 Issue 05 , May - 2026

and safety and reduce the weight of the structure. The modified design was simulated for structural analysis in ANSYS 20.0 to ensure a safer design.

Magryta P. et al (2021) [64] researched on simulation of engine mount for an aircraft piston diesel engine for its strength. The mount is fixed on a stationary test stand consisting fixtures to hold the engine mount and engine at place. The mount is made of circular tubes of S235JR steel material. Three different versions of the mount have been analysed and simulated- initial mount design, modified design by rearranging the pipes and modified design by changing the pipe wall thickness. Boundary conditions for the all designed were kept same. The analysis simulation was carried out in CATIA V5 Generative Structure Analysis Module. For the simulation, the mount was loaded with engine weight of 1000 N, thrust of 5000 N and engine torque of 227 N-m. After the simulations it was found that the modifications made in the engine mount configuration resulted in reducing the maximum stresses and eliminate the areas where stress concentration may occur. Also, the results showed that the material used has strength far beyond the stresses generated in the mount structure.

Ramesh S. et al (2020) [65] published a paper on FEA analysis of an engine mount of a jet dragster car using ANSYS software. The simulation for Static Structural, Modal and Harmonic Response analyses were performed in order to determine the maximum Von-Mises stresses and the structure's frequency response. This is done to optimise the structure to reduce the overall weight of engine mount in such a way that its safety and structural integrity is not hampered. After performing the simulation, the original and modified design were compared and it was found that the modified design requires 17.9 % lighter and requires 18.6% less raw material than the original design. Also, total deformation of the modified design was 26.1% less than that of the original mount design.

Kim, J. J. et al (1997) [69] introduced a process that can automatically design an engine mount by using the parametric optimisation method. A code was developed and used along with a FEA program to perform the optimisation and determine the shape which could satisfy the strength and stiffness requirements of the engine mount. The experiment was conducted on a bush type engine mount model of a passenger car. The stiffness comparison of the optimised mount was done with the design specification of the existing mount along the principal direction.

Conti P. et al (1989) [78] researched on an alternative to determining the rigid body inertial properties of an object and its stiffness. Conventional method utilised a trifilar pendulum to determine the inertial properties. But the experiment results in large errors and can be tedious and unsafe for larger objects. As for the stiffness of mounts, individual components undergo static and dynamic tests. In the new developed method, the data to determine the inertial properties and stiffness is acquired from an artificial

International Journal of Engineering Research & Technology (IJERT)
ISSN: 2278-0181
Vol. 15 Issue 05 , May - 2026

excitation vibration test of an object which is mounted or supported on the ground. Transfer functions for three or more accelerometers are acquired to excite six rigid body modes. These modes are the input for a least square matrix algorithm to compare mass and centre of gravity location, mass moments and principal axes of inertia and tri-axial stiffness of each mount or support attachment.

Sebastian C. S. et al (2016) [81] published a paper on design and optimization of engine mount bracket. In this work the author designed an engine mount to analyse and study it for the displacements under the working loads. The mount model was designed in CATIA V5 and was simulated in ANSYS. Three materials were analysed for the engine mount structures, Aluminium alloy, Magnesium alloy and Titanium alloy. The initial design, when subjected to loading has a displacement of 20-30 mm which was unacceptable. Upon modifying the design, it was found that the Titanium alloy (Ti6Al4V) has the least displacement and stress values compared to Al-allow and Mg-alloy.

International Journal of Engineering Research & Technology (IJERT)
ISSN: 2278-0181
Vol. 15 Issue 05 , May - 2026

Chapter - 3

Methodology and Test Setup

This chapter consists of the details of the methodology used during the project work. This chapter also contains details of the different components being used in the setup and the simple analytical calculations done for them.

3.1. Approach for Project:

The following figure shows the methodology that is being used during the project which is as follows:

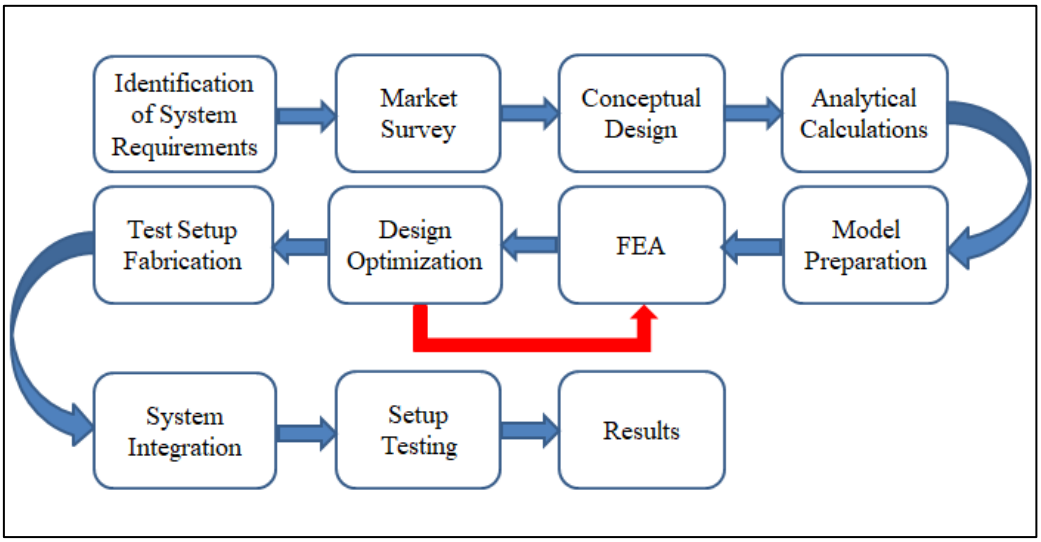

Fig. 3.1: Methodology Block Diagram

A thorough market survey was done for the existing methods being used for testing of the various configurations of the Propeller IC Engine propulsion system. After the market survey, a conceptual design was prepared by using an existing system for reference and certain modifications can be done after studying from the various literatures for different configurations.

A block diagram for the system to be designed is presented below. The diagram depicts the general layout of the test setup to be developed.

International Journal of Engineering Research & Technology (IJERT)
ISSN: 2278-0181
Vol. 15 Issue 05 , May - 2026

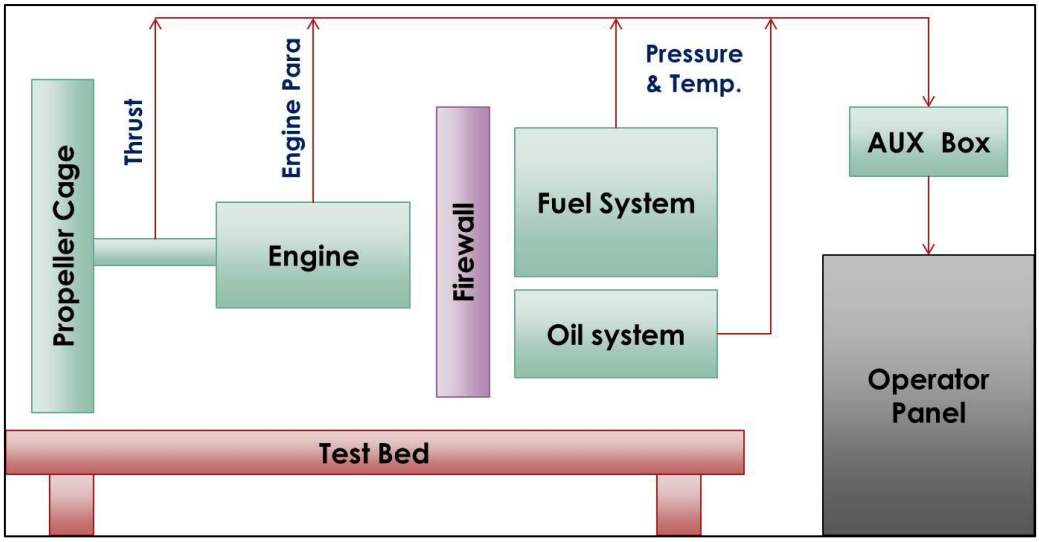

Fig. 3.2: Proposed Block Diagram for Test Setup

A model is being prepared on which the engine & propeller assembly can be mounted and clamped. A robust model of the stand is required to sustain the engine weight & thrust produced during the testing. After that FEM analysis will be done to predict the overall behavior of the stand structure on application of the various forces in ANSYS Workbench.

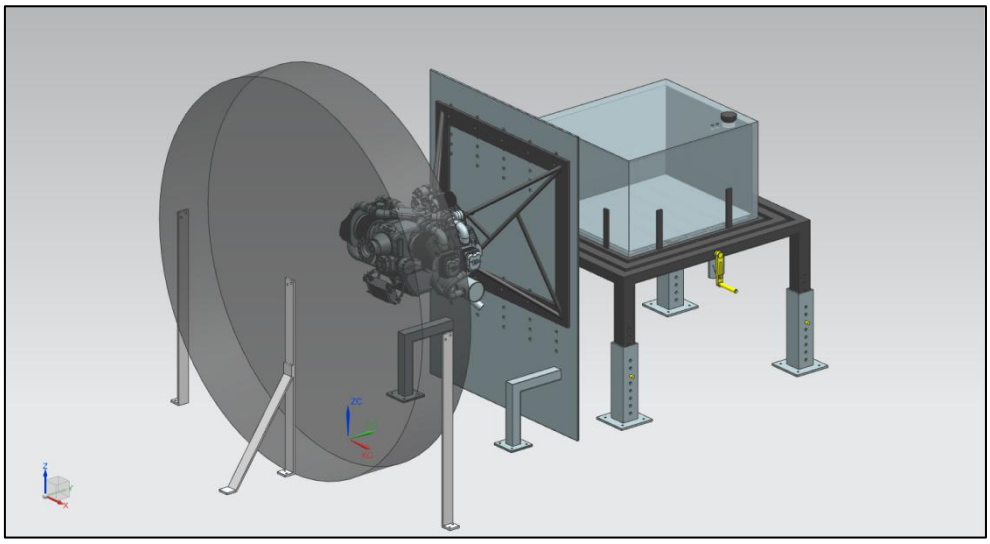

Fig. 3.3: Basic CAD of Proposed Test Rig modelled in NX 12.0

International Journal of Engineering Research & Technology (IJERT)
ISSN: 2278-0181
Vol. 15 Issue 05 , May - 2026

3.2. Project Timeline

Table 3.1: Timeline of the Project

Activity	Duration		Status
	Start	End	
Allotment of Project	Dec-23	Dec-23	Done
Characterisation and study of different engine test rigs	Dec-23	Jan-24	Done
Literature Survey	Dec-24	Feb-24	Done
Market Survey & Analysis	Jan-24	Feb-24	Done
Listing of Components for Test Setup	Dec-24	Feb-24	Done
Analytical Calculations and CAD Modelling	Mar-24		Done
FEA of critical components	Apr-24	May-24	Done
Report Generation	Feb-24	Aug-24	Done
Manufacturing of Setup & Integration			To be done
Testing & Evaluation of the system			To be done
Comparison of the results			To be done

International Journal of Engineering Research & Technology (IJERT)
ISSN: 2278-0181
Vol. 15 Issue 05 , May - 2026

3.3. System Requirements

A generic test rig has to be developed which can be used to test UL Power 350i and any engine similar it. In this thesis, a test rig has been designed with the following system requirements:

Table 3.2: Test Setup System Requirements

Propeller Diameter	64” (1.625 m) - 68” (1.727 m)
Thrust	1500 N
Torque	305 N-m
Fuel capacity	For engine running 6 hours
Roll and Pitch Bank Angles	35º

Following are the components that are designed considering the above constraints:

- A Propeller Safety Cage to accommodate the propeller of max size 68 inches.
- An Engine Mount Frame that can sustain 1500 N thrust, 305 N-m engine torque and 78 kg of engine weight and is also able to damp engine vibrations.
- A Fuel Tank of 210 litres capacity (considering additional 15% of fuel).
- A Firewall separating fuel tank and engine.
- An Attitude Table which can be banked in both roll and pitch axes.

In addition to the requirements mentioned in the table, a provision to adjust the distance between propeller safety cage and firewall and attitude table height levelling mechanism are also designed.

All the components, viz., propeller safety cage, engine mount frame, firewall, fuel tank, and attitude table have been designed in accordance with the above-mentioned requirements. The complete details of the UL350i engine and components along with their CAD models of are discussed in the upcoming chapters.

3.3.1. Calculating Fuel Tank Capacity

In the real-world scenario, the aircraft equipped with Ul350i engine runs at 2800 rpm for the maximum time during the flight. This speed is the cruise speed of the engine. Therefore, the fuel

International Journal of Engineering Research & Technology (IJERT)
ISSN: 2278-0181
Vol. 15 Issue 05 , May - 2026

requirement is calculated to run the engine at 2800 rpm for 6 hours of continuous testing. Additional fuel is also considered so that engine can run at speeds above 2800 rpm (maximum 3300 rpm).

In order to calculate the fuel tank capacity to meet the requirements of the test setup, the fuel consumption and specific fuel consumption of the UL350i engine were studied. From these characteristics, it was found that at 2800 rpm, fuel consumed is approximately 31 litres per hour. Therefore for 6 hours of running is-

$$Fuel\ consumption\ (fc) = 31\ lires\ x\ 6\ hrs$$

$$fc\ = 186\ lires$$

Additional 15% of fuel is considered, therefore-

$$Fuel\ consumption\ (fc) = 180 + (0.15\ x\ 180)\ litres$$

$$fc\ = 207\ lires \approx \mathbf{210\ litres}$$

Hence, a fuel tank of 210 litres capacity has been designed.

International Journal of Engineering Research & Technology (IJERT)
ISSN: 2278-0181
Vol. 15 Issue 05 , May - 2026

Chapter – 4

UL Power 350i Engine

4.1. Introduction

The UL Power 350i is a 4-stroke 4-cylinder horizontally opposed SI engine. It is a naturally aspirated engine with dual spark plugs with variable timings and pressure and temperature compensated electronic MPFI system. It is equipped with an Electronic RPM Limiter, integrated permanent magnet AC generator, electric starter, electric fuel pump and pressure regulator to eliminate vapor lock and facilitate starting even under adverse conditions and an external rectifier-regulator. The specifications of the engine have been listed in table below.

Table 4.1: UL Power 350i Engine Specifications

Displacement	3503 cc
Bore	105.6 mm
Stroke	100 m
Compression Ratio (each cylinder)	8 : 1
Firing Order	1-3-2-4
Direction of Rotation	Clockwise - seen from cockpit
Maximum Torque (ISA Conditions)	305 N-m @ 2400 rpm
Power Rating (ISA Conditions)	118 hp @ 3300 rpm / 116 hp @ 2400 rpm
Maximum Speed	3300 rpm
DC Output	30 Amp (+/- 15 Amp available above engine/fuel pump needs)
Oil Capacity	Min: 2.5 litres Max: 3.5 litres
Fuel	Regular unleaded automotive gasoline with min. 95 RON / 87 MON Oct (91 AKI) / AVGAS 100LL

International Journal of Engineering Research & Technology (IJERT)
ISSN: 2278-0181
Vol. 15 Issue 05 , May - 2026

4.2. Dimensions and Weight

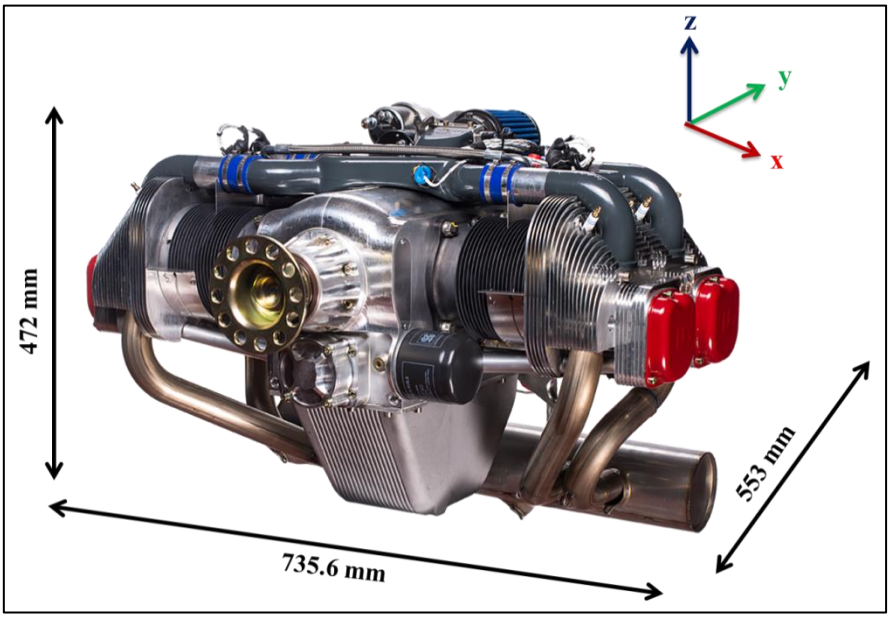

Fig. 4.1: UL Power 350i Engine Dimensions

- Maximum dimension in X direction (length) : 553.0 mm
- Maximum dimension in Y direction (width) : 735.6 mm
- Maximum dimension in Z direction (height) : 472.0 mm
- Dry weight of the basic standard engine: 66,1 kg
- Ready-to–fly weight: 78,4 kg

4.3. Performance

The performance of any engine can be determined by studying their Power-Torque characteristics, fuel consumption characteristics, etc. All the necessary curves about the engine performance are depicted below.

4.3.1. Power-Torque Curve

The power and torque curve of the engine has been established by performing repeated dynamometer tests. These tests were performed at both sea level and at weather conditions close to the ISA standard. The graph shows the real, available power and torque coming from the crankshaft of the UL Power 350i engine, corrected to the ISA conditions at sea level.

International Journal of Engineering Research & Technology (IJERT)
ISSN: 2278-0181
Vol. 15 Issue 05 , May - 2026

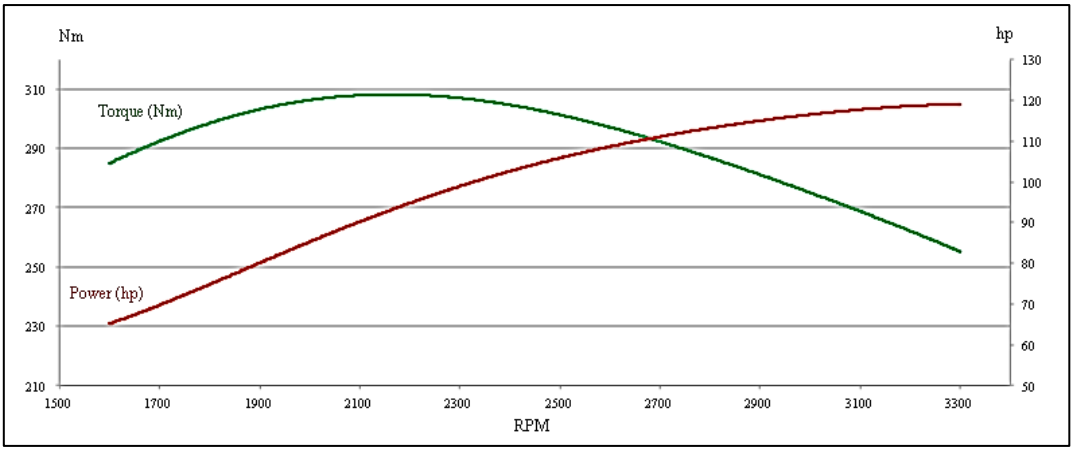

Fig. 4.2: UL350i Engine Power-Torque Characteristics

4.3.2. Power-Altitude Curve

The graph illustrates the engine's estimated available power for the UL350i at various RPM levels. Variable density altitude and wide-open throttle (WOT).

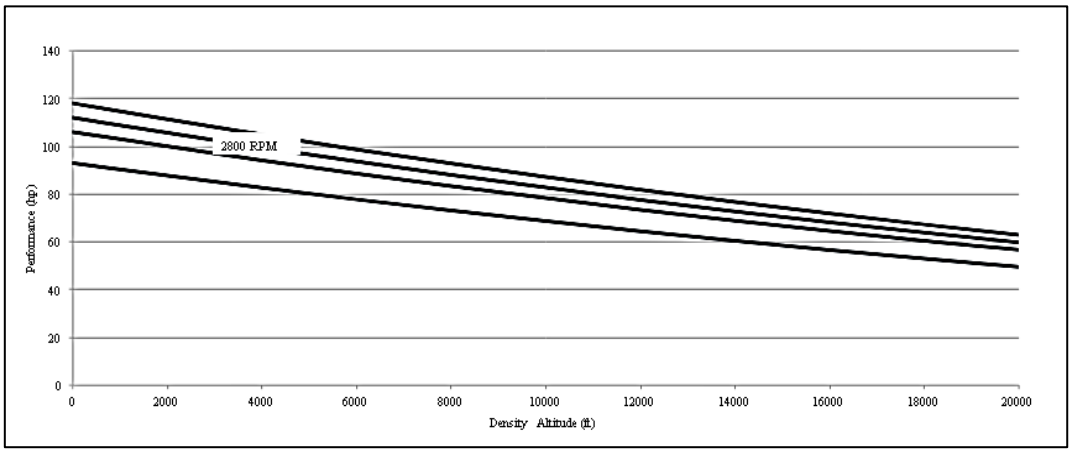

Fig. 4.3: UL350i Engine Power-Altitude Curve

4.3.3. Power-MAP Curve

International Journal of Engineering Research & Technology (IJERT)
ISSN: 2278-0181
Vol. 15 Issue 05 , May - 2026

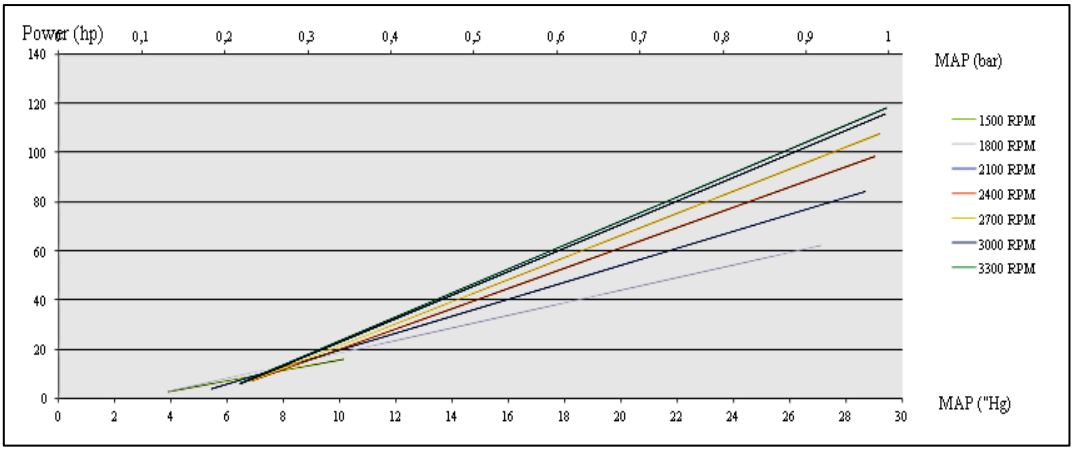

Fig. 4.4: UL350i Engine Power vs. MAP

4.3.4. Fuel Consumption Curve

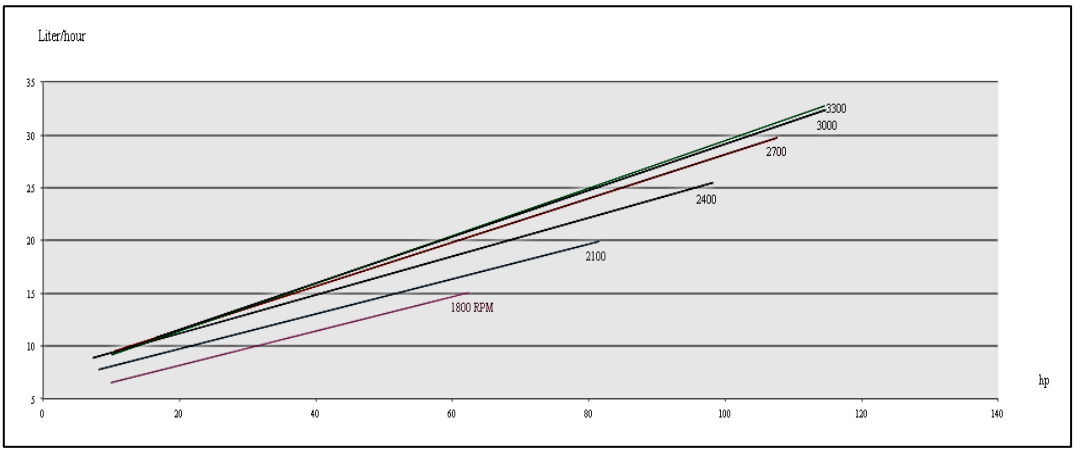

Fig. 4.5: UL350i Engine Fuel Consumption at various rpm

4.3.5. Specific Fuel Consumption (SFC) Curve

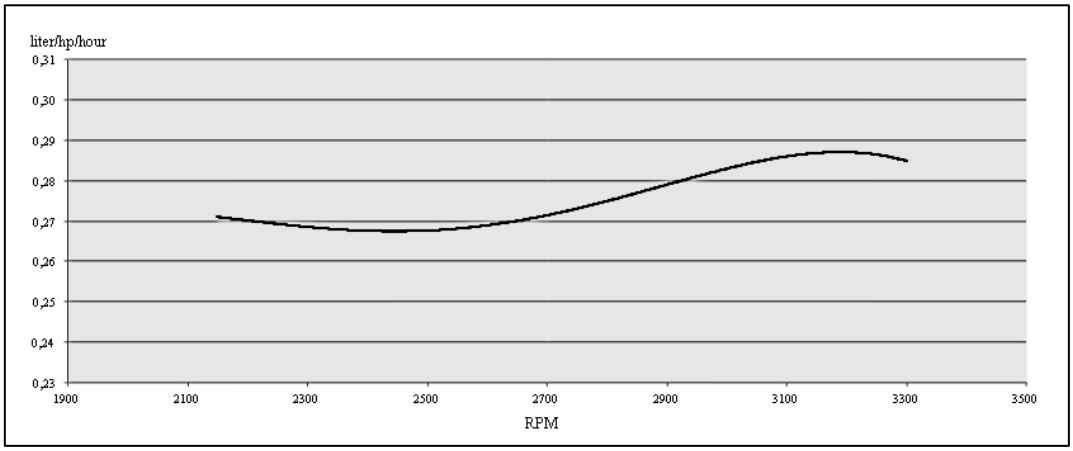

Fig. 4.6: UL350i Engine SFC at various rpm

International Journal of Engineering Research & Technology (IJERT)
ISSN: 2278-0181
Vol. 15 Issue 05 , May - 2026

Chapter - 5

Test Rig Components & CAD Models

This chapter consists of the final CAD model of all the components of the test rig and the details of various FEA analyses performed on them, to check whether the design of components is adequate and within the working stress limits.

5.1. Test Rig CAD Model

After much iteration, designs of all the components of the test rig were finalized. Below is the CAD Model of the complete test rig setup.

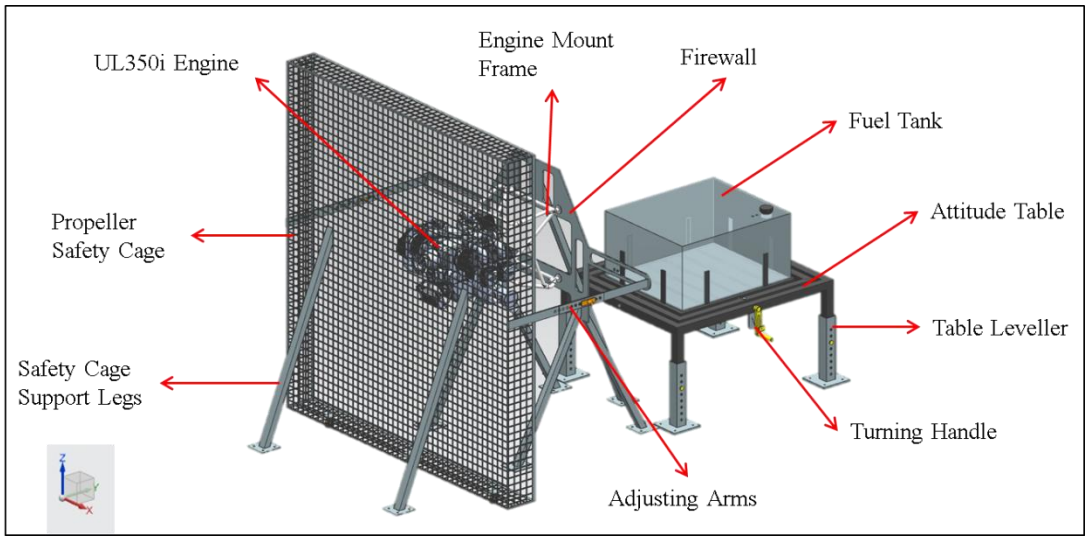

Fig. 5.1: Isometric View of the Test Rig Setup CAD Modelled in UGNX 12.0

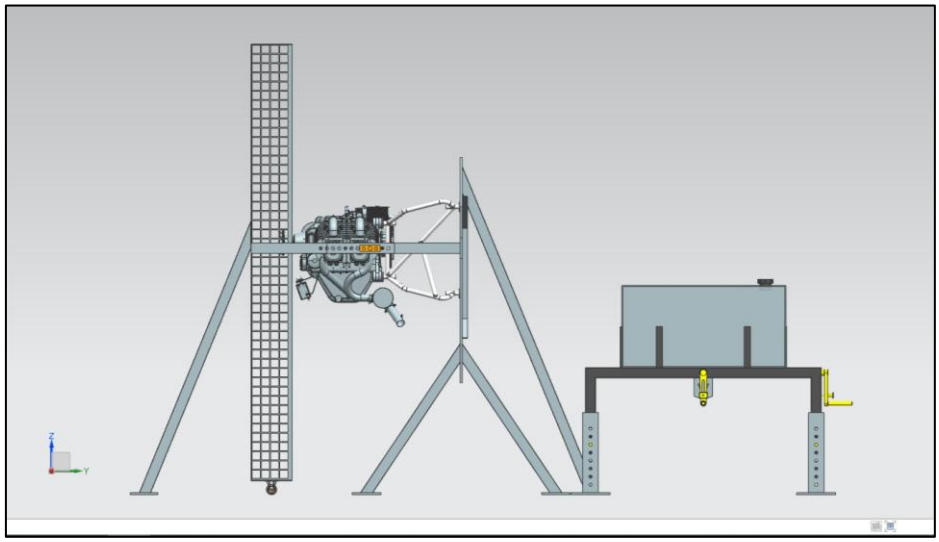

International Journal of Engineering Research & Technology (IJERT)
ISSN: 2278-0181
Vol. 15 Issue 05 , May - 2026

Fig. 5.2: Side View of the Test Rig Setup CAD Modelled in UGNX 12.0

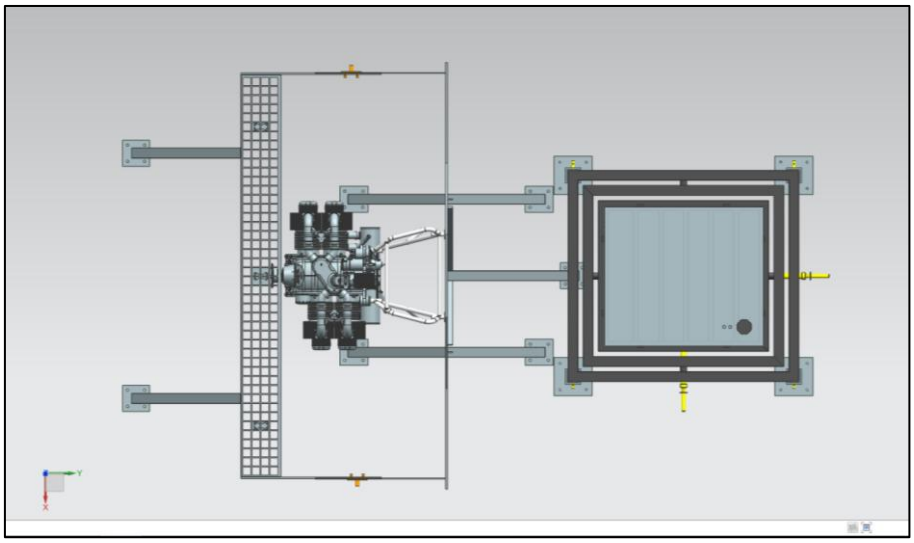

Fig. 5.3: Top View of the Test Rig Setup CAD Modelled in UGNX 12.0

The setup consists of following components:

- Propeller Safety Cage
- UL Power 350i Engine
- Engine Mount Frame
- Firewall with propeller cage distance adjustment links.
- Fuel Tank
- Attitude Table (to control roll and pitch)
  - Turning Handle with lock pin
  - Table height leveler

5.2. Components Description

5.2.1. Propeller Safety Cage

The propeller compatible for the UL350i engine can vary in diameter from 64 inch (1.625 m) to 68 inch (1.727 m). Keeping this and other constraints in mind, the propeller cage of dimension 2 m x 2.12 m x 200 mm has been designed. The mesh of dimension 40 mm x 40 mm made of Mild Steel rods of 5 mm diameter has been chosen since it is most used and readily available for this type of applications.

International Journal of Engineering Research & Technology (IJERT)
ISSN: 2278-0181
Vol. 15 Issue 05 , May - 2026

The cage is provided with the adjustment mechanism so that the distance from firewall can be adjusted to incorporate engines of various sizes. The materials for adjusting links are selected as EN8, a grade of mild steel, to allow easy machining and welding.

Two support legs are also provided to mount the cage to the test bed. They are mild steel hollow square pipes of dimension 38 mm x 38 mm and thickness 1 mm. These pipes are selected from the standard catalogue of JINDAL INDIA LIMITED.

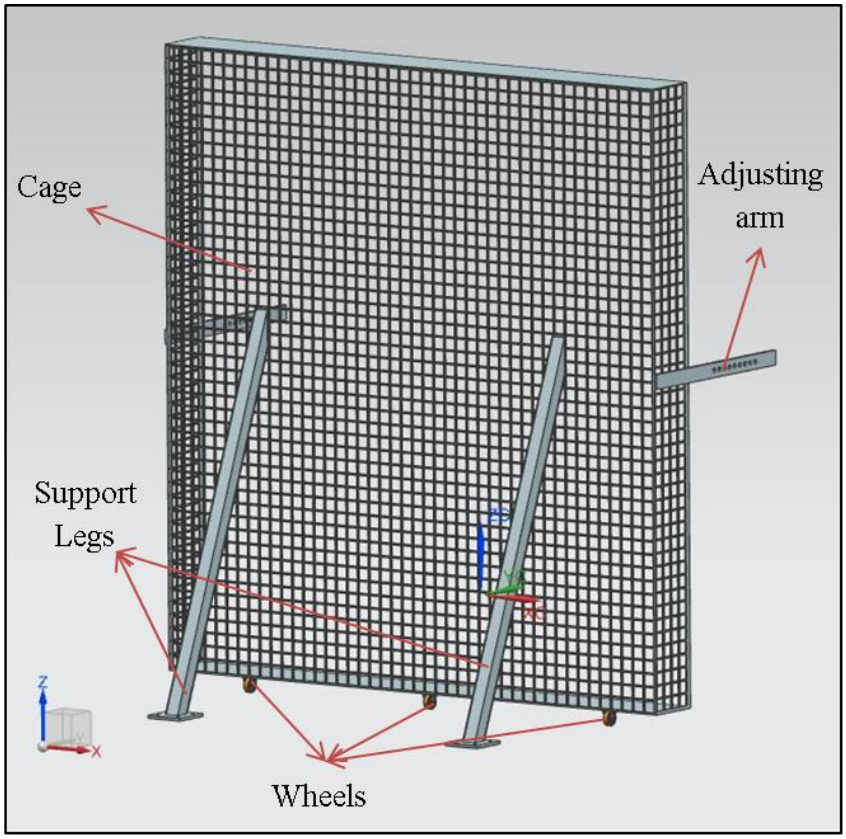

Fig. 5.4: Propeller Safety Cage CAD Modelled in UGNX 12.0

5.2.2. UL Power 350i Engine

All the details about the UL350i engine have been discussed in the previous chapter. Below is the CAD of the UL350i engine.

International Journal of Engineering Research & Technology (IJERT)
ISSN: 2278-0181
Vol. 15 Issue 05 , May - 2026

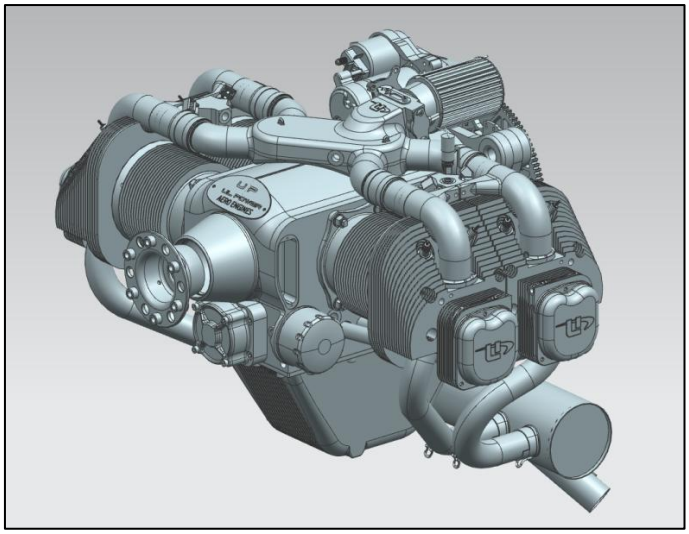

Fig. 5.5: UL Power 350i Engine CAD Model

5.2.3. Engine Mount Frame

The engine mount frame is structural member on which the engine will be fixed. This engine-frame assembly will be then mounted onto the firewall using standard bolts and nuts. The engine mount frame has to be designed in such a way that it can withstand all the loading conditions of the engine and propeller. The material for the frame is also to be selected which can damp the engine vibrations and has a long fatigue life.

For the mounting of the mount frame on the actual aircraft, the max size available for the firewall was 500 mm x 500 mm x 500 mm. The engine mount frame was necessary to design within these dimensions, as small as possible. Also, the mounting interfaces for the engine were 250 mm x 260 mm centre to centre. Keeping these constraints in mind, the engine mount frame shown below was developed.

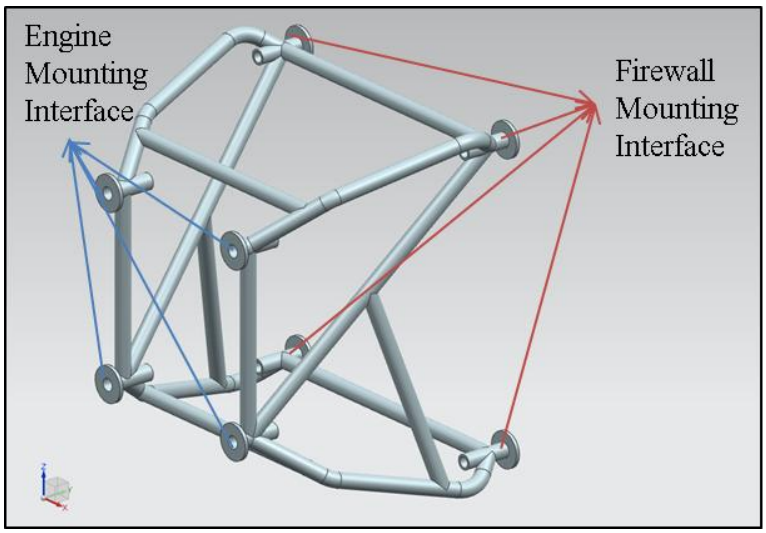

Fig. 5.6: Isometric View of the Engine Mount Frame CAD Modelled in UGNX 12.0

International Journal of Engineering Research & Technology (IJERT)
ISSN: 2278-0181
Vol. 15 Issue 05 , May - 2026

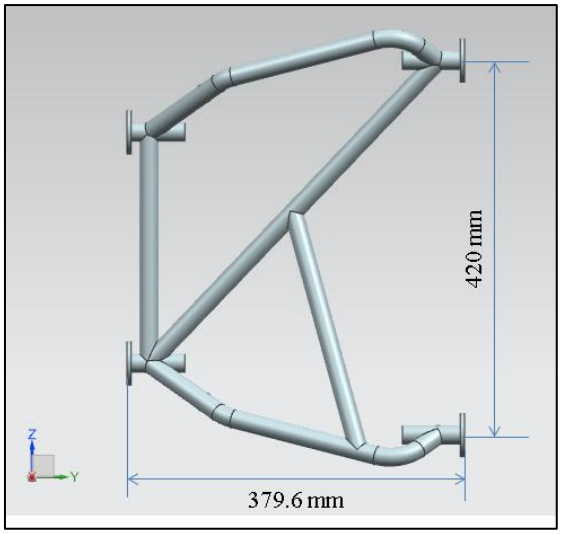

Fig. 5.7: Side View of the Engine Mount Frame CAD Modelled in UGNX 12.0

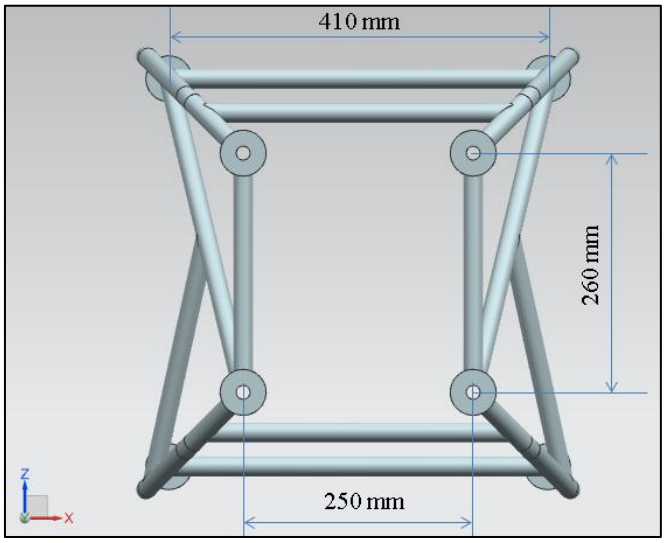

Fig. 5.8: Front View of the Engine Mount Frame CAD Modelled in UGNX 12.0

Material Selection for the Engine Mount Frame:

The material selection for the engine mount frame was done using weighted point method. The weighted point method is quantitative approach in which scores are assigned to the candidates based on different criteria. The criteria were vibration damping index, strength, density, availability of the material and cost per kilogram. The weights to these criteria were allotted by their importance to the application (engine mount frame) and are as follows:

Table 5.1: Weight table of different criteria

Criteria	Weights

International Journal of Engineering Research & Technology (IJERT)
ISSN: 2278-0181
Vol. 15 Issue 05 , May - 2026

Strength	0.30
Density	0.25
Vibration Damping Index	0.20
Availability	0.15
Cost	0.10
Total	**1**

The materials that were chosen to be evaluated were **Cast Iron, Al6061-T6 Aluminium Alloy** and **K1A Magnesium Alloy (Mg-Zr Alloy)**. The scores (out of 100) for the above-mentioned parameters for these three materials are provided in the table below.

Table 5.2: Score Table of different criteria for different materials

	Cast Iron	**Al6061-T6**	**K1A**
Strength	80	70	50
Density	60	75	90
Damping Index	50	70	80
Availability	95	85	65
Cost (per Kg)	80	65	40

The final score is calculated by multiplying the weights and the score and the candidate with highest total is selected.

$$WP = Weight * Score$$

Where, WP is the Weight Point for a material against a criterion.

Table 5.3: Weighted Point Table for Selection of Most Appropriate Material

International Journal of Engineering Research & Technology (IJERT)
ISSN: 2278-0181
Vol. 15 Issue 05 , May - 2026

	Cast Iron (CI)	AL6061-T6	K1A
Strength	24	21	15
Density	15	18.75	22.5
Damping Index	10	14	16
Availability	14.25	12.75	9.75
Cost	8	6.5	4
Total	**71.25**	**73.00**	**67.25**

Therefore, by using weighted point method of evaluation to select the material for engine mount frame, **Al 6061-T6** is deemed to be the most appropriate material. The table below shows the material properties of Al 6061-T6.

Table 5.4: AL 6061-T6 Material Properties

Properties	Value
Density (Kg/m3)	2703
Young's Modulus (GPa)	68.9
Bulk Modulus (GPa)	67.6
Shear Modulus (GPa)	25.8
Tensile Yield strength (MPa)	276
Tensile Ultimate Strength (MPa)	310
Poisson's Ratio	0.33
Coefficient of Thermal Expansion (/^{o}C)	2.36E-05

The engine mount frame is modeled using hollow circular pipes of dimension 21.1 mm x 3 mm. These are the standard available pipes selected from the JINDAL ALUMINIUM catalogue.

The interfaces where engine and firewall will be mounted are to be manufactured by machining (subtractive manufacturing) the Al 6061-T6 circular rods and are then welded to the pipes.

International Journal of Engineering Research & Technology (IJERT)
ISSN: 2278-0181
Vol. 15 Issue 05 , May - 2026

5.2.4. Firewall

The firewall plate acts both as protection to fuel tank and support to engine mount frame. Firewall has to be designed in such a way that it can withstand the engine loadings without much deformation, while keeping the overall weight as low as possible. Therefore, after numerous design iterations and FEA simulations, the final design is developed as shown in figure 5.9.

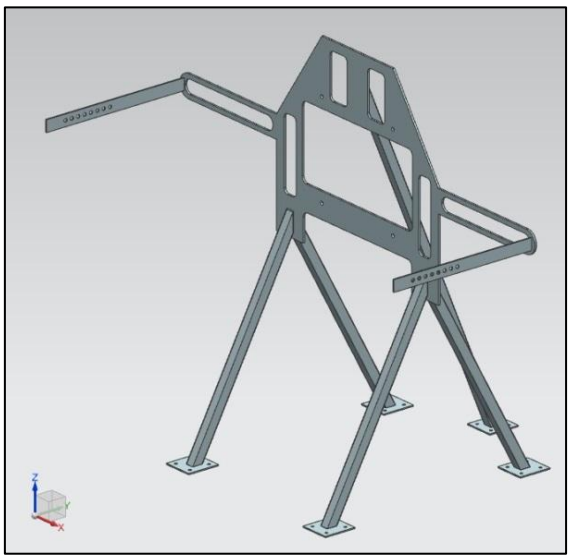

Fig. 5.9: Firewall CAD Modelled in UGNX 12.0

Material Selection for the Firewall:

The material selection for the firewall is done based on the experimental evidences and availability of the material in plate form. With extensive research and market survey, it was found that steel plates of grade EN 10025-2 S275 are widely used for such structures due to its high strength and good weldability. The material property of EN 10025-2 S275 is given in the table below.

Table 5.5: EN 10025-2 S275 Material Properties

Properties	Value
Density (Kg/m3)	7850
Young's Modulus (GPa)	210
Bulk Modulus (GPa)	175
Shear Modulus (GPa)	81
Tensile Yield strength (MPa)	275
Tensile Ultimate Strength (MPa)	430
Poisson's Ratio	0.3
Coefficient of Thermal Expansion (/K)	12E-06

International Journal of Engineering Research & Technology (IJERT)
ISSN: 2278-0181
Vol. 15 Issue 05 , May - 2026

Firewall is also equipped with the second half of the propeller safety cage distance adjustment arms. They are made of mild steel of EN8 grade. These arms are welded to the sides of the firewall plate.

The supporting legs welded to the main plate are used to mount the firewall to the test bed and transfer the loads to the test bed. There is a provision of bolting provided at the bottom of each leg. The dimension of the square pipes is 38 mm x 38 mm x 1.18 mm. This dimension is selected after performing static structural analysis of firewall in ANSYS 18.1 using legs of various dimensions. These legs are standard square hollow tubes of steel selected from the catalogue of JINDAL STEEL. IS 4913

5.2.5. Fuel Tank

The fuel tank is made by Aluminium plates of 5 mm thickness. Total fuel tank capacity is 210 litres. This is derived from studying the fuel consumption and Specific Fuel Consumption (SFC) curves. The fuel tank is provided with a seal cap to avoid the spillage of the fuel.

The overall dimensions of the fuel tank are 700 mm x 600 mm x 350 mm. Below is the CAD image of the Fuel Tank.

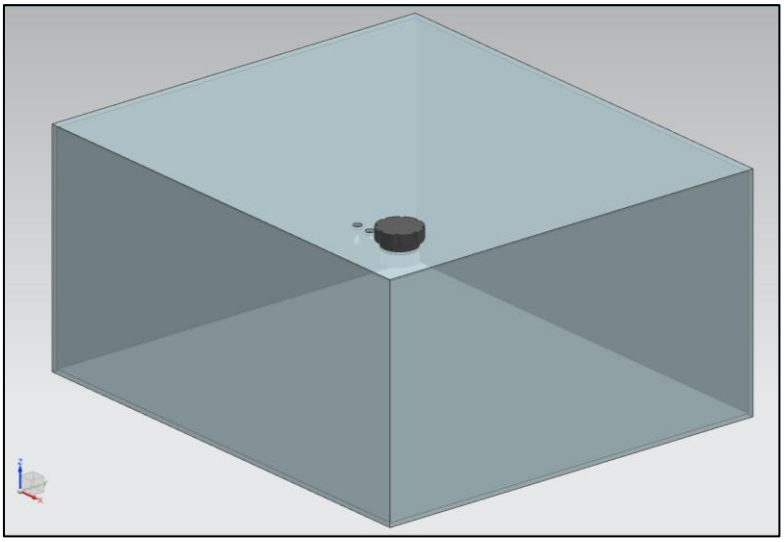

Fig. 5.10: Fuel Tank CAD Modelled in UGNX 12.0

5.2.6. Attitude Table

The attitude table is designed to test the fuel flow from the fuel tank at various roll and pitch angles. The UL Power 350i engine is designed to operate at maximum bank angles of 35º (roll and pitch).

The table is provided with a provision to manually rotate the fuel tank in both pitch and roll axes.

International Journal of Engineering Research & Technology (IJERT)
ISSN: 2278-0181
Vol. 15 Issue 05 , May - 2026

The table can be rotated using a turning handle in both pitch and roll axes from 0° to 35°. The handle includes a locking pin which can be inserted in the holes of an angle plate having the holes separated with an interval of 5°.

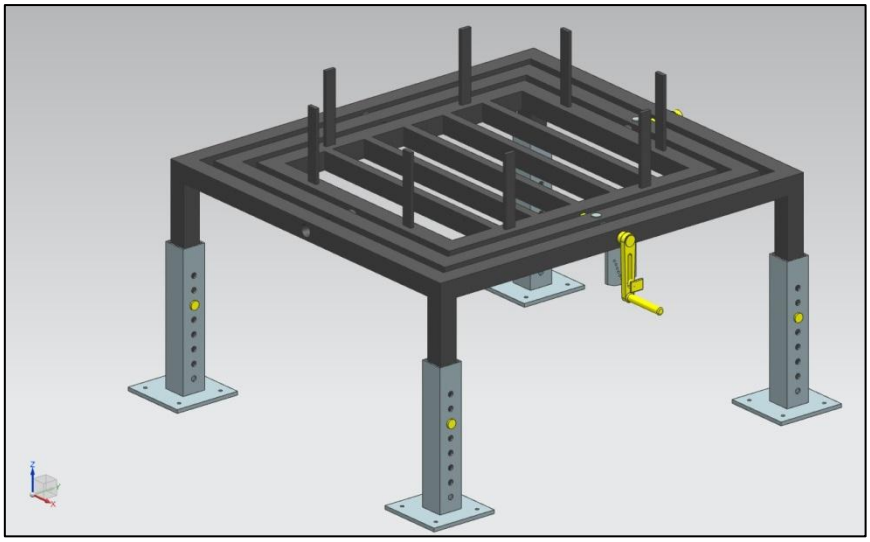

Fig. 5.11: Isometric View of Attitude Table CAD Modelled in UGNX 12.0

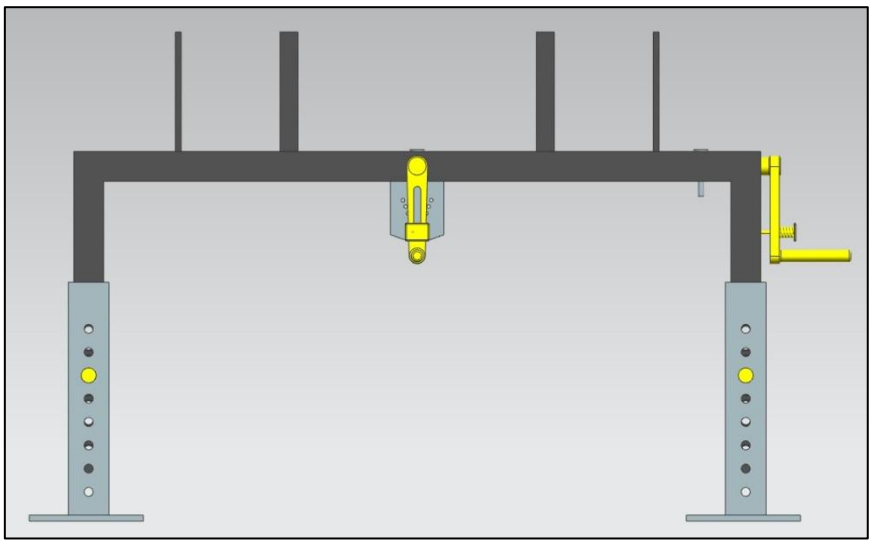

Fig. 5.12: Side View of Attitude Table CAD Modelled in UGNX 12.0

International Journal of Engineering Research & Technology (IJERT)
ISSN: 2278-0181
Vol. 15 Issue 05 , May - 2026

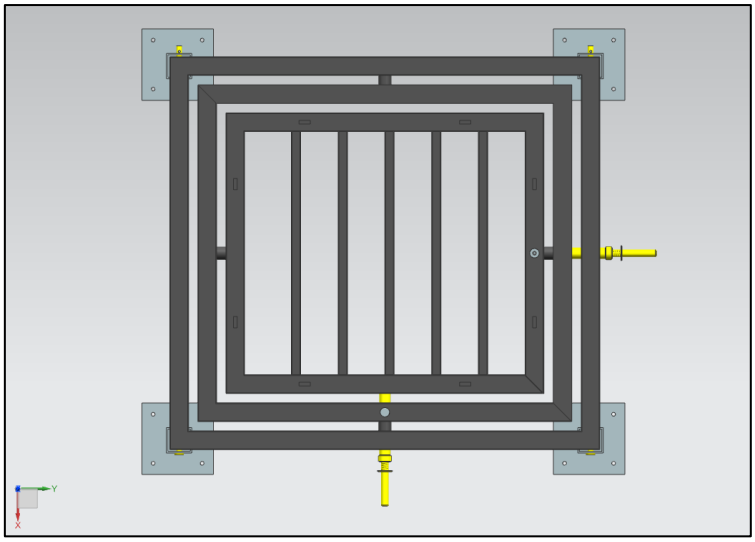

Fig. 5.13: Top View of Attitude Table CAD Modelled in UGNX 12.0

There are support rods that are provided to support the fuel tank and hold it in correct position while rolling or pitching. The legs of the table have holes which correspond to the holes of leveler legs. This mechanism is used to adjust the height of the fuel tank. It is incorporated to adapt to the height requirements, if needed, of different engines.

The pipes used in the table are of square cross-section of size is 50.8 mm x 50.8 mm and thickness of 2 mm. The pipe material selected is Al 6061–T6 since it has high weldability and low weight. All the pipes are selected from the standard catalogue of JINDAL ALUMINIUM.

Operating the Attitude Table:

There are three different motions than can be performed on the attitude table- height leveling, rolling and pitching. The rolling and pitching operations are performed in order to test whether the engine's fuel system is capable of running at the maximum bank angles (roll and pitch) as prescribed by the manufacturer.

The Height Leveling is done to keep the table in a level horizontal position at all times during the operation of the test rig. To do this, leveling legs, which are made from the hollow steel pipes of square cross-section having dimension 60 mm x 60 mm x 4 mm are designed. Holes of 15 mm diameter are provided on both leveling legs and attitude table legs at the same intervals. To keep the table at a desired level, holding pins or lock pins are inserted in the holes. These lock pins are made of mild steel.

International Journal of Engineering Research & Technology (IJERT)
ISSN: 2278-0181
Vol. 15 Issue 05 , May - 2026

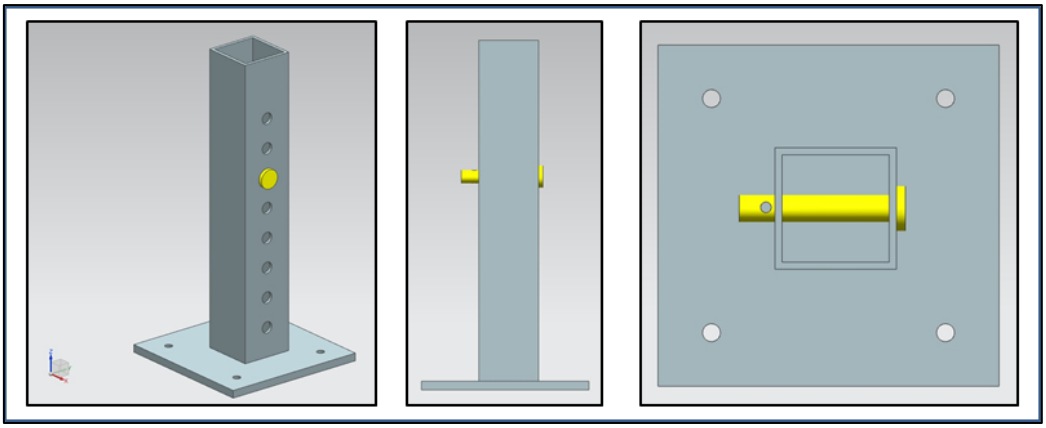

Fig. 5.14: Isometric View, Side View and Top View of Attitude Table Leveller

To bank the table in roll and pitch directions turning handles are provided. There is an angle plate on which holed are designed. These holes are present at 5° intervals. The spring-loaded lock pin of the turning handle is inserted in the hole of the angle plate to keep the attitude table at a fixed roll or pitch angle. The table can be banked upto 35°, which is the maximum rated banking by the engine manufacturer,

The attitude table is the assembly of three different parts: innermost structure where fuel tank is seated, middle structure and the outermost structure which has legs. These three parts are linked together in such a way that innermost structure (for rolling) turns independently while the middle structure (for pitching) turns along with the rolling structure. There is no relative banking between the innermost and middle structure while performing pitching motion. But to do the pitching motion, the turning handle of rolling must be pulled out.

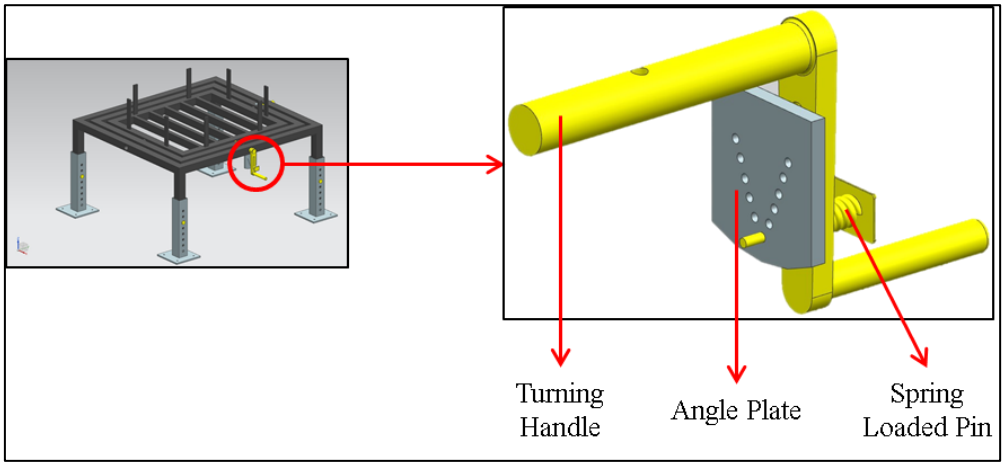

Fig. 5.15: Rolling and Pitching Mechanism

International Journal of Engineering Research & Technology (IJERT)
ISSN: 2278-0181
Vol. 15 Issue 05 , May - 2026

Chapter – 6

Finite Element Analyses

In this chapter, the results are all the analyses and their conclusions are discussed. These results are acquired after much iteration in the design of the respective components.

6.1. Static Structural Analysis (Engine Mount Frame)

The Engine Mount Frame is the most critical component on which majority of the engine and propeller forces are going to act. Therefore, it is extremely important to design its structure in such a way that it can withstand loading well beyond the permissible values.

6.1.1. Boundary Conditions

The Static Structural Analysis is carried in ANSYS R18.1. Following are the boundary conditions for Static Structural Analysis:

- Standard Earth Gravity (default option)
- Fixed support at engine mount frame and firewall interface.
- Max Thrust - 1500 N
- Max Torque - 305 N-m (CW when seen from the cockpit)
- Self-Weight - 1000 N

All the loads mentioned above are applied on the Centre of Gravity (CG) of the engine, which is at a distance of 273.5 from engine-engine mount frame interface as shown in the image below.

International Journal of Engineering Research & Technology (IJERT)
ISSN: 2278-0181
Vol. 15 Issue 05 , May - 2026

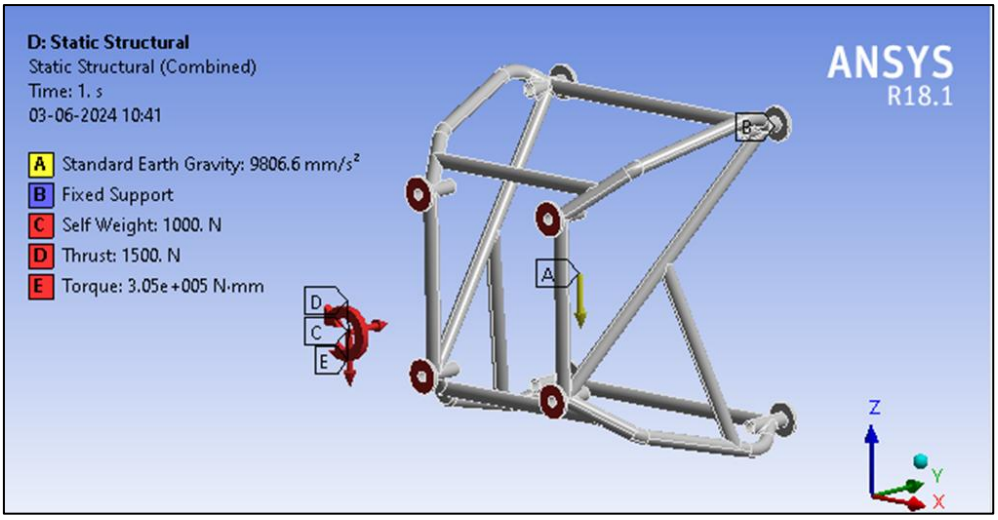

Fig. 6.1: Boundary Conditions for the Static Structural Analysis of Engine Mount Frame

6.1.2. Meshing

Meshing is an important step while doing the finite element analysis, where complex geometries are divided into simple elements that can be used as discrete local approximation of the large domain. The mesh has impact on accuracy, convergence and also the speed of solution.

ANSYS has various element types that can be used for different types of analyses. These element types are selected based on the geometry and type of analysis to be performed. The image below shows the types of elements available. ANSYS Structural includes all structural linear and nonlinear capabilities.

The following tables show elements listed by group label in numerical order, along with a description and graphical representation for each.

BEAM Elements	HF Elements	MESH Elements	SHELL Elements
CIRCU Elements	HSFLD Elements	MPC Elements	SOLID Elements
COMBIN Elements	INFIN Elements	PIPE Elements	SOLSH Elements
CONTAC Elements	INTER Elements	PLANE Elements	SOURC Elements
CPT Elements	LINK Elements	PRETS Elements	SURF Elements
FLUID Elements	MASS Elements	REINF Elements	TARGE Elements
FOLLW Elements	MATRIX Elements	ROM Elements	TRANS Elements

Fig. 6.2: Element Types in ANSYS 18.1

Since the engine mount frame is completely designed using tubes, therefore Structural Pipes has been selected. There are three types of structural pipe elements: PIPE288, PIPE 289 and ELBOW290. For the analysis, a combination of all three elements has been utilised.

International Journal of Engineering Research & Technology (IJERT)
ISSN: 2278-0181
Vol. 15 Issue 05 , May - 2026

Structural Pipe	3-D	PIPE288 2-Node Pipe	
		PIPE289 3-Node Pipe	
		ELBOW290 3-Node Elbow	

Fig. 6.3: Structural Pipe Types in ANSYS 18.1

All three element types mentioned above are suitable for the analysis of tubes which have radius to wall thickness ratio greater than 5. PIPE288 is a linear, quadratic, or cubic 2-node 3D pipe element, whereas PIPE289 and ELBOW290 are quadratic 3-node 3D pipe elements. All three pipe elements have six degrees of freedom at each node and are optimum to use for linear, large rotation, and/or large strain non-linear applications.

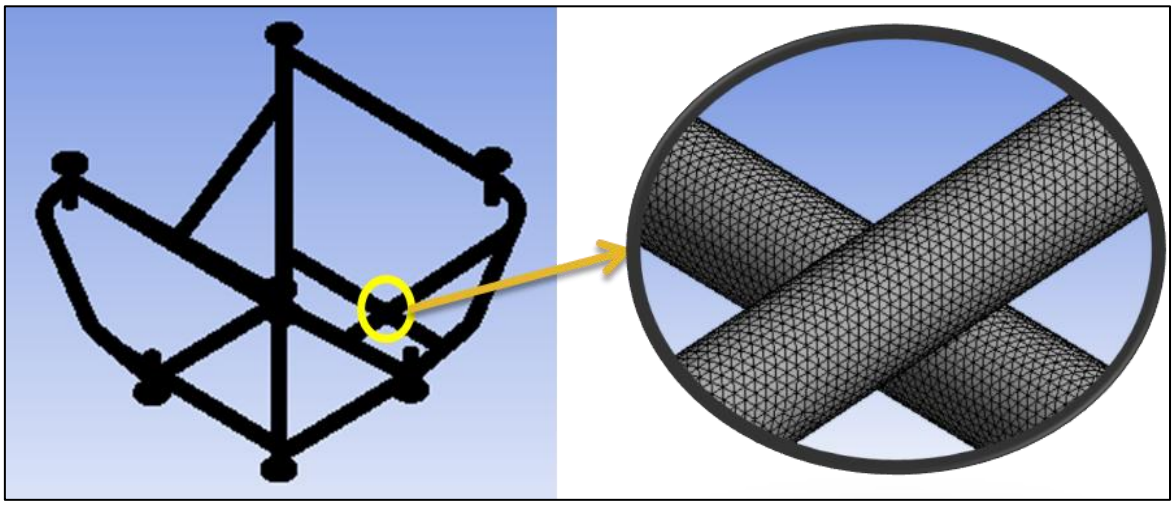

Fig. 6.4: Mesh generation of Engine Mount Frame in ANSYS 18.1

The mesh elements selected for the analysis are tetrahedrons elements. The method used is Patch Conforming Method. Image below gives the mesh details.

International Journal of Engineering Research & Technology (IJERT)
ISSN: 2278-0181
Vol. 15 Issue 05 , May - 2026

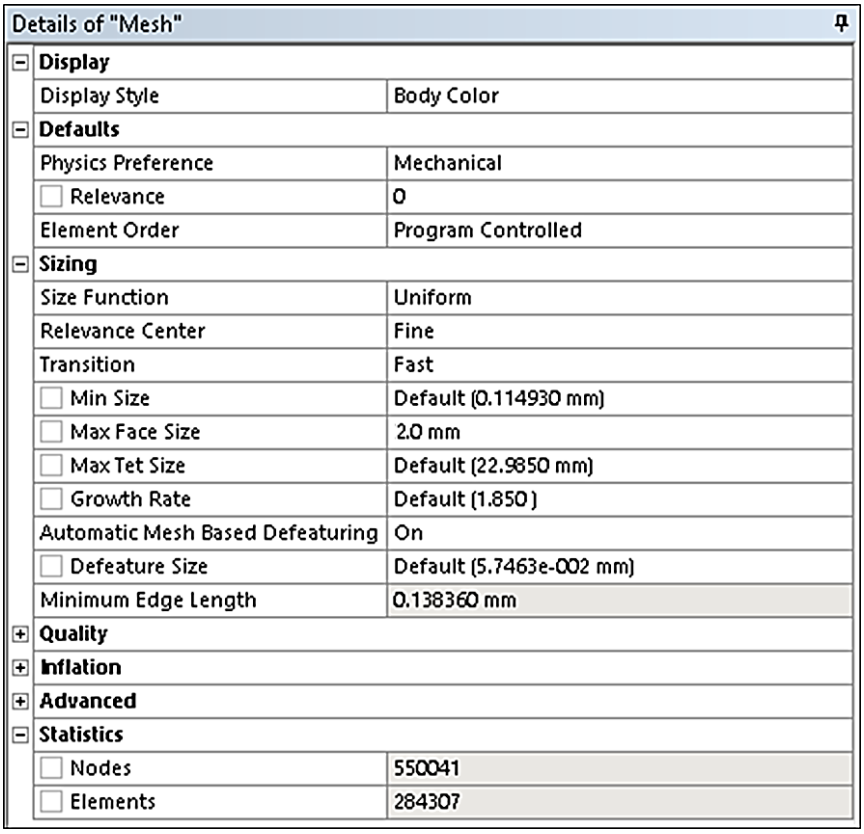

Details of "Mesh"	
Display	
Display Style	Body Color
Defaults	
Physics Preference	Mechanical
Relevance	0
Element Order	Program Controlled
Sizing	
Size Function	Uniform
Relevance Center	Fine
Transition	Fast
Min Size	Default (0.114930 mm)
Max Face Size	2.0 mm
Max Tet Size	Default (22.9850 mm)
Growth Rate	Default (1.850)
Automatic Mesh Based Defeaturing	On
Defeature Size	Default (5.7463e-002 mm)
Minimum Edge Length	0.138360 mm
Quality	
Inflation	
Advanced	
Statistics	
Nodes	550041
Elements	284307

Fig. 6.5: Mesh Details for the Analysis of Engine Mount Frame in ANSYS 18.1

Mesh Metric	Element Quality	Skewness	Orthogonal Quality
Min	1.0877E-02	1.81E-07	8.7709E-03
Max	1	0.93123	0.9975
Average	0.95755	0.2118	0.93478
Standard Deviation	9.1968E-02	0.12565	0.1211

Fig. 6.6: Mesh Metric (element size 2 mm) of Engine Mount Frame in ANSYS 18.1

The Mesh Metric describes the quality of the mesh generated. There are various parameters to check the mesh quality.

- Element Quality
- Aspect Ratio
- Jacobian Ratio
- Warping Factor
- Parallel Deviation
- Maximum Corner Angle

International Journal of Engineering Research & Technology (IJERT)
ISSN: 2278-0181
Vol. 15 Issue 05 , May - 2026

- Skewness
- Orthogonal Quality
- Characteristic Length

From the above list, the most used and simplest quality check is Skewness and Orthogonal Quality,

Skewness gives a measure of how distorted an element is from the Ideal element. There are two methods to calculate skewness:

a) Equilateral Volume Deviation- This method is used only for triangular and tetrahedron elements. It is calculated as:

$$skewness = \frac{Optimal\ Cell\ Size - Actual\ Cell\ Size}{Optimal\ Cell\ Size}$$

b) Normalised Angle Deviation- It is calculated as:

$$skewness = max\left(\frac{\theta_{max} - \theta_e}{180 - \theta_e}, \frac{\theta_e - \theta_{min}}{\theta_e}\right)$$

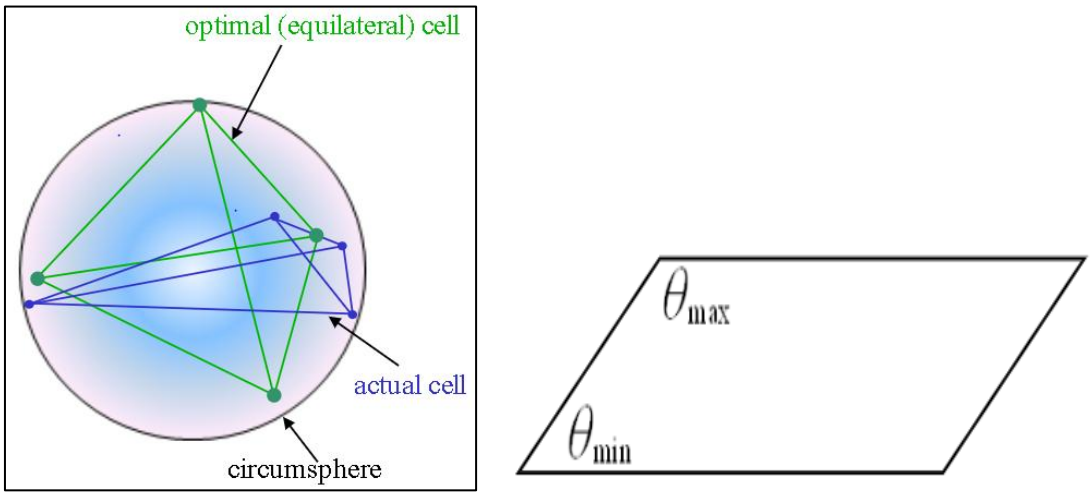

(a) (b)

Fig. 6.7 (a) & (b): Equilateral Volume Deviation and Normalised Angle Deviation Methods to measure the Skewness of the Mesh Element

Orthogonal Quality or Orthogonality of a cell is computed using the vector from the centroid of the cell to each of cell's faces, face area vector and vector from centroid of the cell to the centroid of the adjacent cells.

Orthogonal Quality is calculated using the equation:

International Journal of Engineering Research & Technology (IJERT)
ISSN: 2278-0181
Vol. 15 Issue 05 , May - 2026

$$OQ = min\left(\frac{\bar{A}_i.\bar{C}_i}{|\bar{A}_i||\bar{C}_i|}, \frac{\bar{A}_i.\bar{f}_i}{|\bar{A}_i||\bar{f}_i|}\right)$$

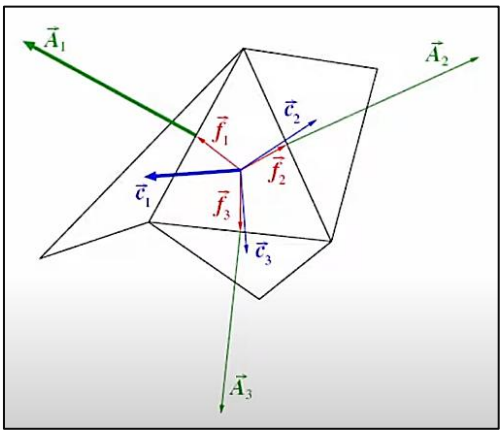

Fig. 6.8: Vectors in a mesh element to calculate Orthogonal Quality

6.2. Static Structural Analysis (Frame-Firewall Assembly)

The engine mount frame will be bolted to the firewall. Hence, the firewall will also experience all the forces and moments produced by the engine and the propeller. Therefore, in this section, the static structural analysis of engine mount frame-firewall assembly is discussed.

6.2.1. Boundary Conditions

The Static Structural Analysis is carried in ANSYS R18.1. Following are the boundary conditions for Static Structural Analysis:

- Standard Earth Gravity (default option)
- Fixed support at the bolting points of support legs of the firewall
- Max Thrust - 1500 N
- Max Torque - 305 N-m (CW when seen from the cockpit)
- Self-Weight - 1000 N

International Journal of Engineering Research & Technology (IJERT)
ISSN: 2278-0181
Vol. 15 Issue 05 , May - 2026

- Cylindrical support at the cage adjusting link which is radially fixed and axially and tangentially free.

All the loads mentioned above are applied on the Centre of Gravity (CG) of the engine, which is at a distance of 273.5 from the extreme left (as per the image below) of the engine-engine mount frame interface.

The connection between the engine mount frame and the firewall has been considered as default, since computation of user-defined connection would be beyond the system capabilities.

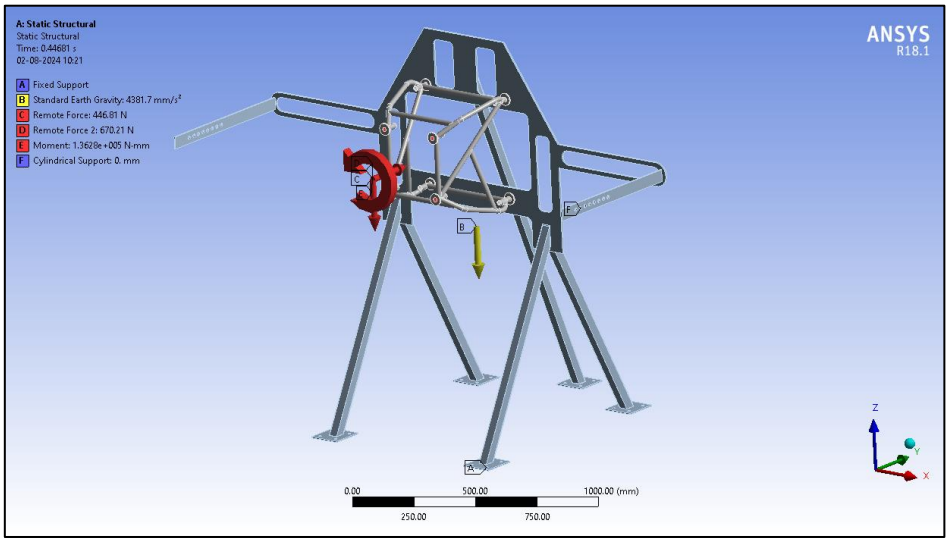

Fig. 6.9: Boundary Conditions for the Static Structural Analysis of Frame-Firewall Assembly

6.2.2. Meshing

Discretisation of complete geometry into small no of finite elements is known as meshing. For the analyses, both engine mount frame and the firewall have been discretised using different element sizes. This is done since the firewall has large dimensions as compared to the engine mount frame. If the firewall is meshed in the same element size as that of the engine mount frame, the computation will become quite tedious and will be beyond the capacity of the system.

Details of "Patch Conforming Method" - Method	
Scope	
Scoping Method	Geometry Selection
Geometry	2 Bodies
Definition	
Suppressed	No
Method	Tetrahedrons
Algorithm	Patch Conforming
Element Order	Use Global Setting

Fig. 6.10: Tetrahedron Mesh details of Frame-Firewall Assembly Analysis in ANSYS 18.1

International Journal of Engineering Research & Technology (IJERT)
ISSN: 2278-0181
Vol. 15 Issue 05 , May - 2026

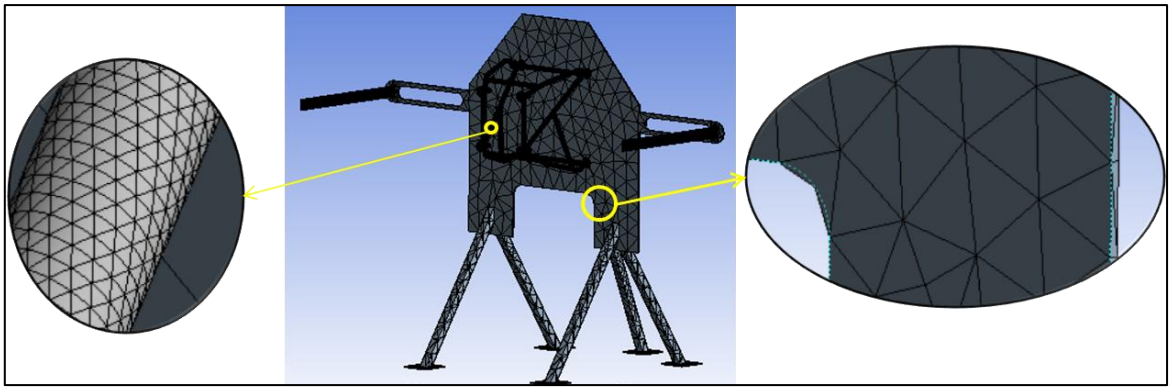

Fig. 6.11: Mesh Elements of Frame-Firewall Assembly Analysis in ANSYS 18.1

Details of "Body Sizing" - Sizing

Scope	
Scoping Method	Geometry Selection
Geometry	1 Body
Definition	
Suppressed	No
Type	Element Size
Element Size	75. mm
Advanced	
Defeature Size	Default (0.21938 mm)
Size Function	Uniform
Behavior	Soft
Growth Rate	Default (1.850)

Fig. 6.12: Mesh details of Firewall for Frame-Firewall Assembly Analysis in ANSYS 18.1

International Journal of Engineering Research & Technology (IJERT)
ISSN: 2278-0181
Vol. 15 Issue 05 , May - 2026

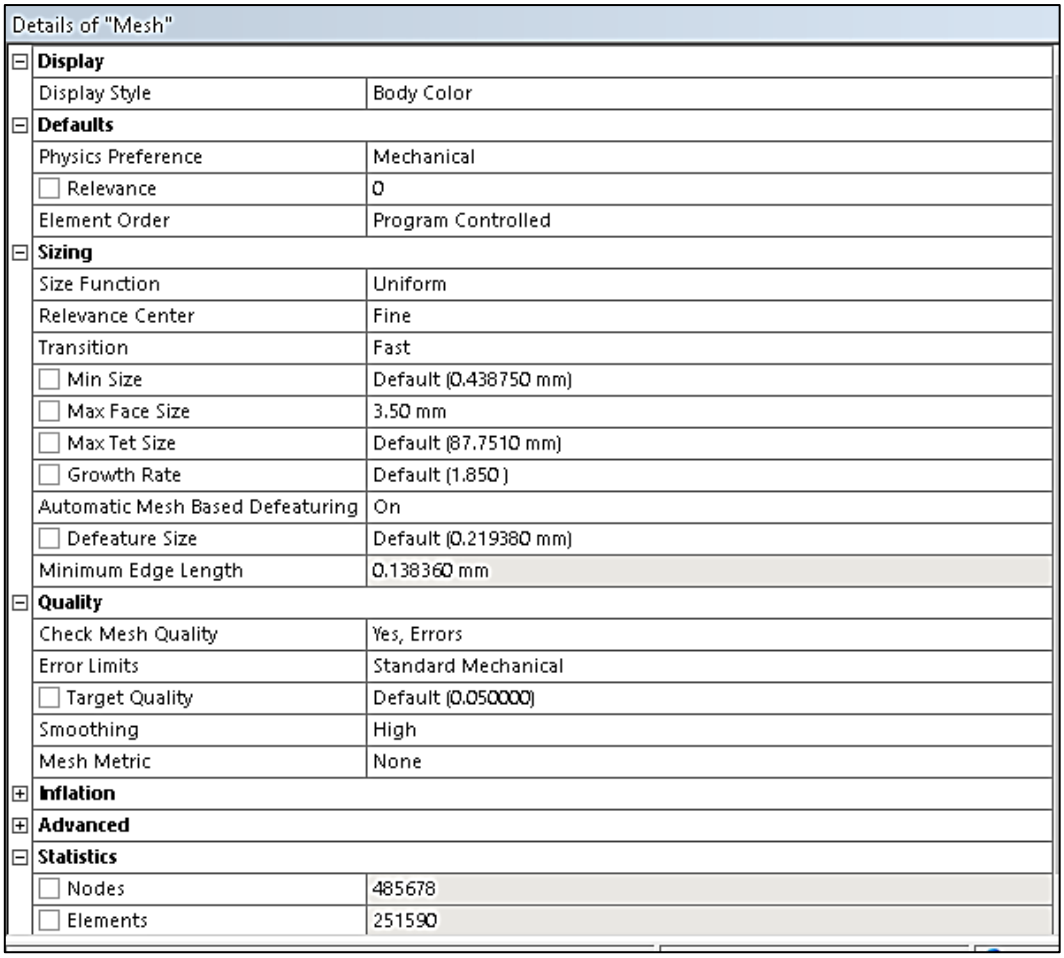

Details of "Mesh"	
Display	
Display Style	Body Color
Defaults	
Physics Preference	Mechanical
Relevance	0
Element Order	Program Controlled
Sizing	
Size Function	Uniform
Relevance Center	Fine
Transition	Fast
Min Size	Default (0.438750 mm)
Max Face Size	3.50 mm
Max Tet Size	Default (87.7510 mm)
Growth Rate	Default (1.850)
Automatic Mesh Based Defeaturing	On
Defeature Size	Default (0.219380 mm)
Minimum Edge Length	0.138360 mm
Quality	
Check Mesh Quality	Yes, Errors
Error Limits	Standard Mechanical
Target Quality	Default (0.050000)
Smoothing	High
Mesh Metric	None
Inflation	
Advanced	
Statistics	
Nodes	485678
Elements	251590

Fig. 6.13: Mesh details of Engine mount fame for Frame-Firewall Assembly Analysis in ANSYS 18.1

Fig. 6.9 gives the mesh details of engine mount frame. But as stated earlier, the firewall, due to its large dimensions, has been discretized using the tetrahedron elements of **75 mm** size as shown in Fig 6.10. This is done using the Body Sizing under the Mesh.

6.3. Modal Analysis of Engine Mount Frame

In structural engineering and dynamics, modal analysis is a key technique used to examine the dynamic properties of mechanical systems. It offers important insights into the natural modes of vibration, related modes shape, and frequencies of these systems.

Understanding and optimizing the behaviour of structure exposed to outside forces or disturbances require the use of an analytical methodology. Finding the resonant frequency at which a structure naturally vibrates and the associated motion patterns, or mode shape, are the main goal of modal analysis. These features are essential for understanding how a structure responds to dynamic loads, which enables engineers

International Journal of Engineering Research & Technology (IJERT)
ISSN: 2278-0181
Vol. 15 Issue 05 , May - 2026

to identify possible weak points, adjust design parameters, and put specific fixes in place for improved performances.

6.3.1. Boundary Conditions

The Modal Analysis is performed in ANSYS 18.1. In modal analysis, unless the component is rotary, only fixed supports are defined as the boundary condition for analysis. The image below shows the fixed support provided at engine mount frame-firewall interface.

For rotary components, a rotational velocity needs to be provided as the boundary condition along with fixed supports.

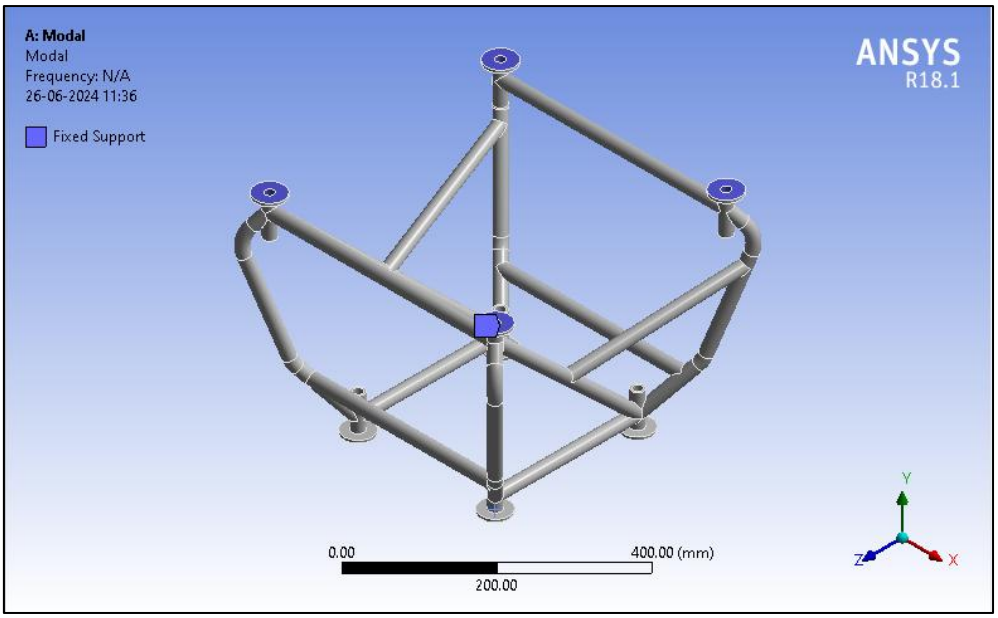

Fig. 6.14: Boundary Conditions for the Modal Analysis of Engine Mount Frame

6.3.2. Meshing

The same meshing condition has been used here as that has been used in Static Structural Analysis mentioned in Section 5.3.2.

6.3.3. Obtaining Results

For getting results of modal analysis, Mechanical APDL solver is used. Now, a Structure or in our case, Engine Mount Frame can have infinite number of frequency modes, but only a few significant numbers of modes contribute to the response of interest. To validate if we have taken enough number of modes which contribute the most, we will check it through Participation Factor table in Solution information. The

International Journal of Engineering Research & Technology (IJERT)
ISSN: 2278-0181
Vol. 15 Issue 05 , May - 2026

Participation factor is a measure of how much a mode contributes to the response at a particular point of interest.

The Participation factor will help us to know which modes are most significant for a particular analysis and whether additional modes need to be considered to accurately capture the dynamic behaviour of system. If the Participation factor of a mode is low, it indicates that those modes have minimal influence on the response and can be neglected in further analysis.

If enough number of modes is not taken into consideration, we have to include additional modes to capture the full dynamic behaviour of the engine mount frame

MODE	FREQUENCY	PERIOD	PARTIC.FACTOR	RATIO	EFFECTIVE MASS	CUMULATIVE MASS FRACTION	RATIO EFF.MASS TO TOTAL MASS
1	137.222	0.72874E-02	0.65576E-01	1.000000	0.430015E-02	0.895446	0.561415
2	213.029	0.46942E-02	0.26796E-02	0.040863	0.718024E-05	0.896941	0.937429E-03
3	302.989	0.33005E-02	-0.49655E-04	0.000757	0.246559E-08	0.896942	0.321899E-06
4	384.047	0.26038E-02	0.18291E-03	0.002789	0.334570E-07	0.896949	0.436804E-05
5	412.424	0.24247E-02	0.22121E-01	0.337332	0.489328E-03	0.998845	0.638851E-01
6	451.626	0.22142E-02	-0.23556E-02	0.035921	0.554870E-05	1.00000	0.724421E-03
sum					0.480225E-02		0.626966

Fig. 6.15: Participation Factor calculation in x-direction

MODE	FREQUENCY	PERIOD	PARTIC.FACTOR	RATIO	EFFECTIVE MASS	CUMULATIVE MASS FRACTION	RATIO EFF.MASS TO TOTAL MASS
1	137.222	0.72874E-02	-0.39935E-05	0.000113	0.159480E-10	0.126662E-07	0.208212E-08
2	213.029	0.46942E-02	0.32029E-05	0.000090	0.102583E-10	0.208136E-07	0.133930E-08
3	302.989	0.33005E-02	0.35411E-01	1.000000	0.125391E-02	0.995883	0.163707
4	384.047	0.26038E-02	-0.22767E-02	0.064293	0.518321E-05	0.999999	0.676703E-03
5	412.424	0.24247E-02	0.29255E-04	0.000826	0.855829E-09	1.00000	0.111734E-06
6	451.626	0.22142E-02	-0.10981E-04	0.000310	0.120573E-09	1.00000	0.157417E-07
sum					0.125909E-02		0.164383

Fig. 6.16: Participation Factor calculation in y-direction

International Journal of Engineering Research & Technology (IJERT)
ISSN: 2278-0181
Vol. 15 Issue 05 , May - 2026

MODE	FREQUENCY	PERIOD	PARTIC.FACTOR	RATIO	EFFECTIVE MASS	CUMULATIVE MASS FRACTION	RATIO EFF.MASS TO TOTAL MASS
1	137.222	0.72874E-02	0.16214E-04	0.000513	0.262888E-09	0.170163E-06	0.343218E-07
2	213.029	0.46942E-02	-0.20186E-04	0.000638	0.407465E-09	0.433909E-06	0.531974E-07
3	302.989	0.33005E-02	-0.31615E-01	1.000000	0.999479E-03	0.646948	0.130489
4	384.047	0.26038E-02	0.23331E-01	0.737999	0.544359E-03	0.999304	0.710698E-01
5	412.424	0.24247E-02	-0.77148E-04	0.002440	0.595188E-08	0.999308	0.777058E-06
6	451.626	0.22142E-02	-0.10343E-02	0.032715	0.106969E-05	1.00000	0.139655E-03
sum					0.154491E-02		0.201699

Fig. 6.17: Participation Factor calculation in z-direction

MODE	FREQUENCY	PERIOD	PARTIC.FACTOR	RATIO	EFFECTIVE MASS	CUMULATIVE MASS FRACTION	RATIO EFF.MASS TO TOTAL MASS
1	137.222	0.72874E-02	0.50622E-03	0.000349	0.256257E-06	0.628926E-07	0.346197E-09
2	213.029	0.46942E-02	-0.66158E-03	0.000456	0.437688E-06	0.170313E-06	0.591304E-09
3	302.989	0.33005E-02	1.4022	0.966361	1.96615	0.482548	0.265621E-02
4	384.047	0.26038E-02	1.4510	1.000000	2.10541	0.999274	0.284436E-02
5	412.424	0.24247E-02	-0.92565E-02	0.006379	0.856832E-04	0.999295	0.115756E-06
6	451.626	0.22142E-02	-0.53586E-01	0.036931	0.287150E-02	1.00000	0.387933E-05
sum					4.07452		0.550457E-02

Fig. 6.18: Participation Factor calculation in Rotational X-direction

MODE	FREQUENCY	PERIOD	PARTIC.FACTOR	RATIO	EFFECTIVE MASS	CUMULATIVE MASS FRACTION	RATIO EFF.MASS TO TOTAL MASS
1	137.222	0.72874E-02	-10.270	1.000000	105.473	0.436913	0.155856
2	213.029	0.46942E-02	9.1819	0.894044	84.3066	0.786144	0.124578
3	302.989	0.33005E-02	-3.9609	0.385677	15.6889	0.851133	0.231831E-01
4	384.047	0.26038E-02	2.9605	0.288266	8.76458	0.887440	0.129512E-01
5	412.424	0.24247E-02	3.4063	0.331672	11.6028	0.935503	0.171451E-01
6	451.626	0.22142E-02	-3.9459	0.384213	15.5700	1.00000	0.230073E-01
sum					241.406		0.356720

Fig. 6.19: Participation Factor calculation in Rotational Y-direction

MODE	FREQUENCY	PERIOD	PARTIC.FACTOR	RATIO	EFFECTIVE MASS	CUMULATIVE MASS FRACTION	RATIO EFF.MASS TO TOTAL MASS
1	137.222	0.72874E-02	-8.1052	1.000000	65.6949	0.500362	0.920822E-01
2	213.029	0.46942E-02	0.60523	0.074672	0.366306	0.503152	0.513438E-03
3	302.989	0.33005E-02	-4.4302	0.546584	19.6267	0.652637	0.275100E-01
4	384.047	0.26038E-02	0.26093	0.032192	0.680830E-01	0.653156	0.954295E-04
5	412.424	0.24247E-02	-4.4849	0.553333	20.1143	0.806355	0.281935E-01
6	451.626	0.22142E-02	-5.0423	0.622101	25.4246	1.00000	0.356368E-01
sum					131.295		0.184031

Fig. 6.20: Participation Factor calculation in Rotational Z-direction

International Journal of Engineering Research & Technology (IJERT)
ISSN: 2278-0181
Vol. 15 Issue 05 , May - 2026

From the figures 5.21 we get to know that Mode 1 is the most critical in X -direction, Rotational Y-direction and Rotational Z-direction. Similarly, Mode 3 is the most critical in both Y and Z-directions and Mode 4 is most critical in Rotational X-direction. These will be responsible for the maximum deformation of engine mount frame.

6.4. HARMONIC ANALYSIS

Harmonic analysis is a type of dynamic response analysis in which when subjected to periodic loads, behaviour of solid structures is simulated for its steady-state behaviour and provides frequency-dependent results. In other words, it studies the behaviour of linear structures under a load varying sinusoidally with time.

The harmonic analysis enables to simulate the steady-state structural response of solids applied with periodical loads. This is similar to a transient dynamic analysis where inertial effects are taken into consideration and the results are frequency-dependent unlike a transient analysis, where they are time-dependent. This makes it possible to compute the response of a structure over a frequency spectrum when subjected to vibrating forces or displacements.

Since this is a linear simulation, only linear elastic materials can be used. However, damping effects can be analysed. All linear boundary conditions are available for this simulation type. The results of a harmonic simulation are complex numbers and can be exported either as Magnitude and Phase or as Real and Imaginary parts.

6.4.1. Boundary Conditions

For the harmonic analyses, the same mesh has been used as that of the modal analysis. Also, the forces and moments and the fixed supports are same as used in the static structural analysis of the engine mount frame.

The frequency modes that are generated by modal analysis are the inputs for the harmonic response analysis. All the deformation will be calculated at these generated frequency modes only.

International Journal of Engineering Research & Technology (IJERT)
ISSN: 2278-0181
Vol. 15 Issue 05 , May - 2026

Chapter – 7

Results

In this chapter, the results are all the analyses mentioned in the previous chapter are discussed. The results shown below are of the final design of the components which are acquired after much iteration.

7.1. Static Structural Analysis (Engine Mount Frame)

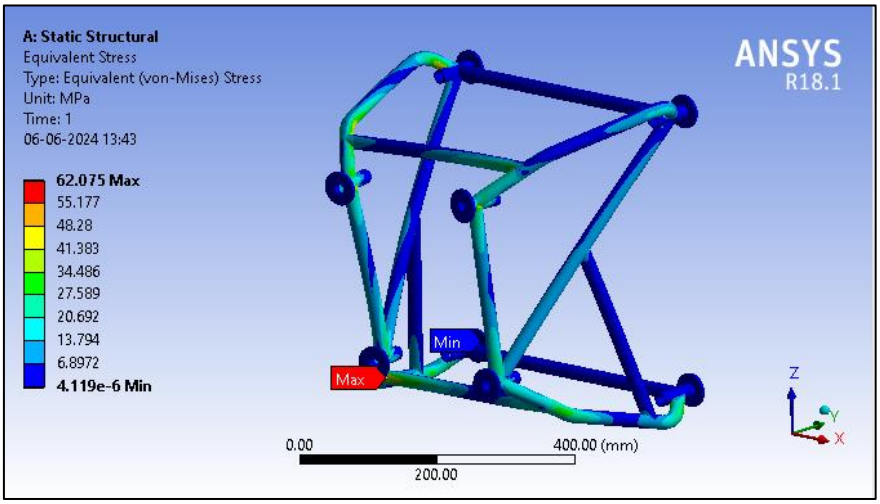

Fig. 7.1: Equivalent Von-Mises Stress

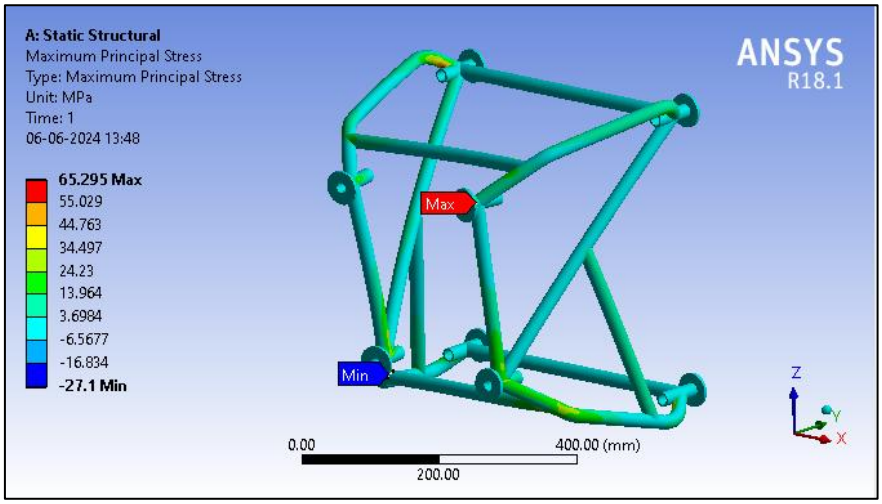

Fig. 7.2: Maximum Principal Stress

International Journal of Engineering Research & Technology (IJERT)
ISSN: 2278-0181
Vol. 15 Issue 05 , May - 2026

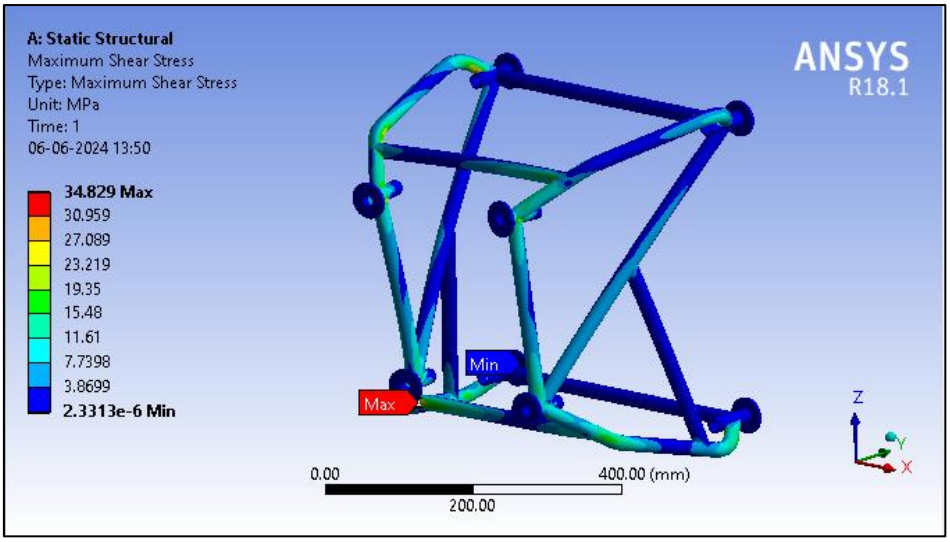

Fig. 7.3: Maximum Shear Stress

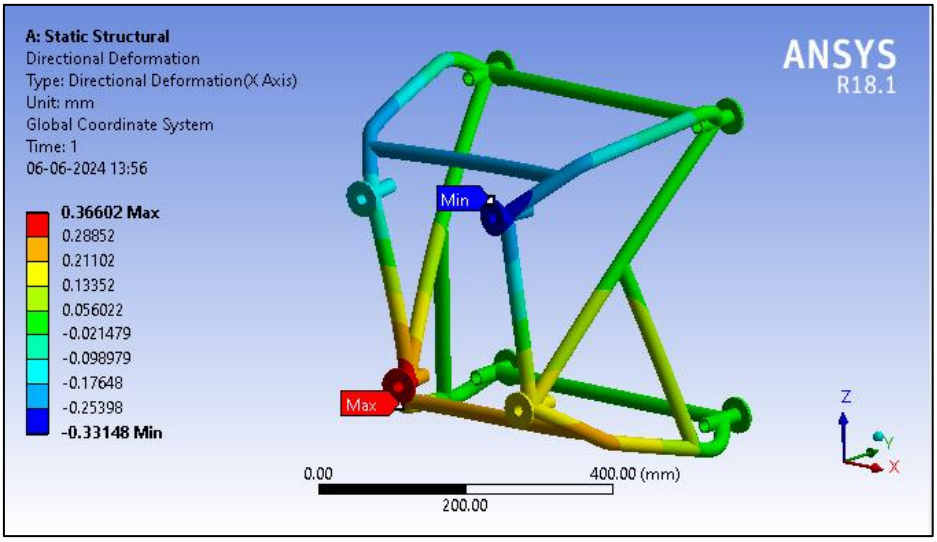

Fig. 7.4: Directional Deformation (X-axis)

International Journal of Engineering Research & Technology (IJERT)
ISSN: 2278-0181
Vol. 15 Issue 05 , May - 2026

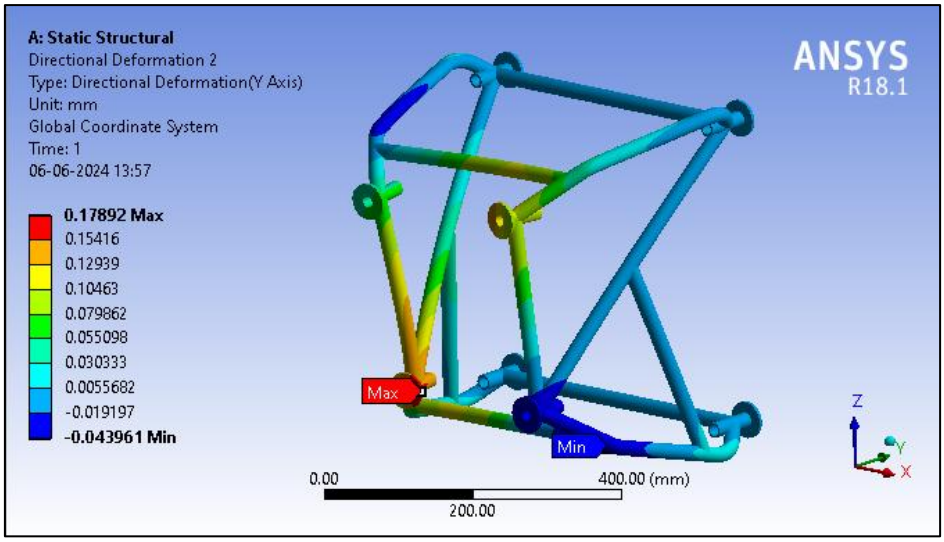

Fig. 7.5: Directional Deformation (Y-axis)

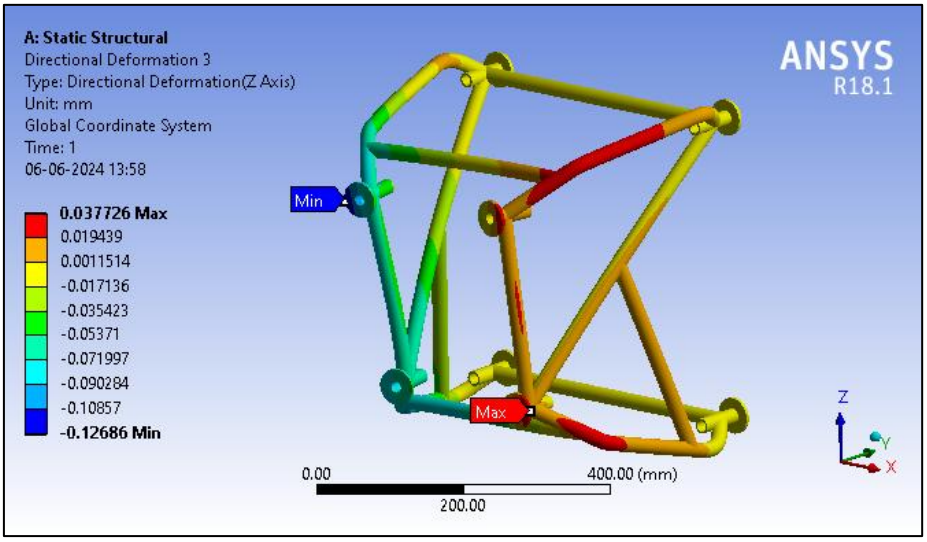

Fig. 7.6: Directional Deformation (Z-axis)

International Journal of Engineering Research & Technology (IJERT)
ISSN: 2278-0181
Vol. 15 Issue 05 , May - 2026

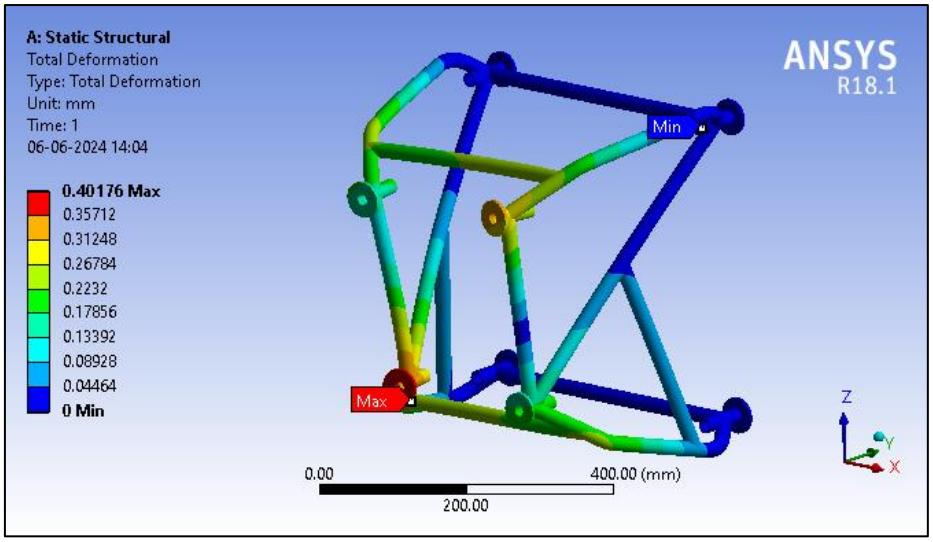

Fig. 7.7: Total Deformation

International Journal of Engineering Research & Technology (IJERT)
ISSN: 2278-0181
Vol. 15 Issue 05 , May - 2026

7.2. Static Structural Analysis (Firewall)

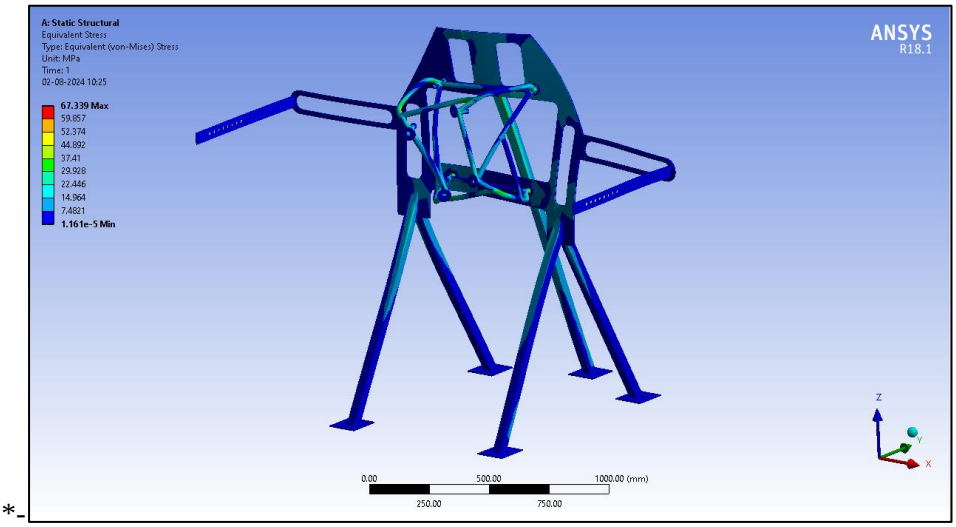

Fig. 7.8: Equivalent Von-Mises Stress

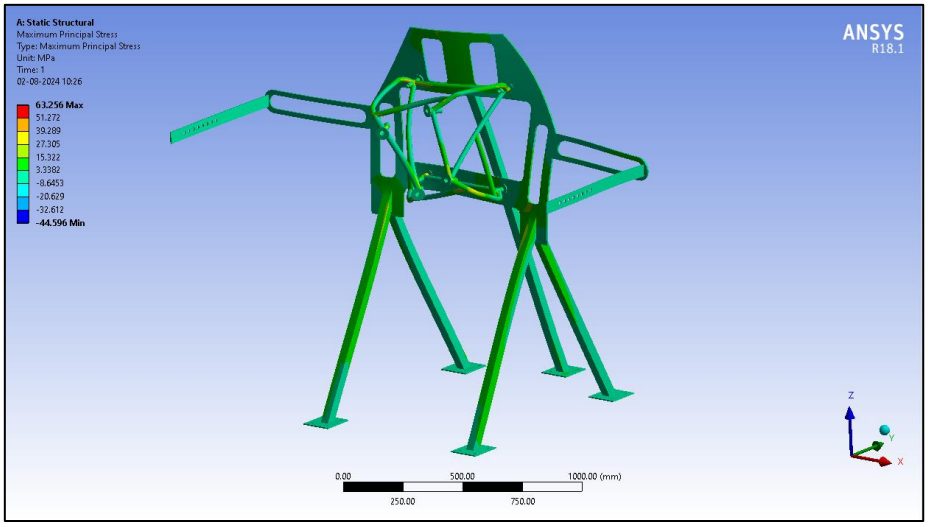

Fig. 7.9: Maximum Principal Stress

International Journal of Engineering Research & Technology (IJERT)
ISSN: 2278-0181
Vol. 15 Issue 05 , May - 2026

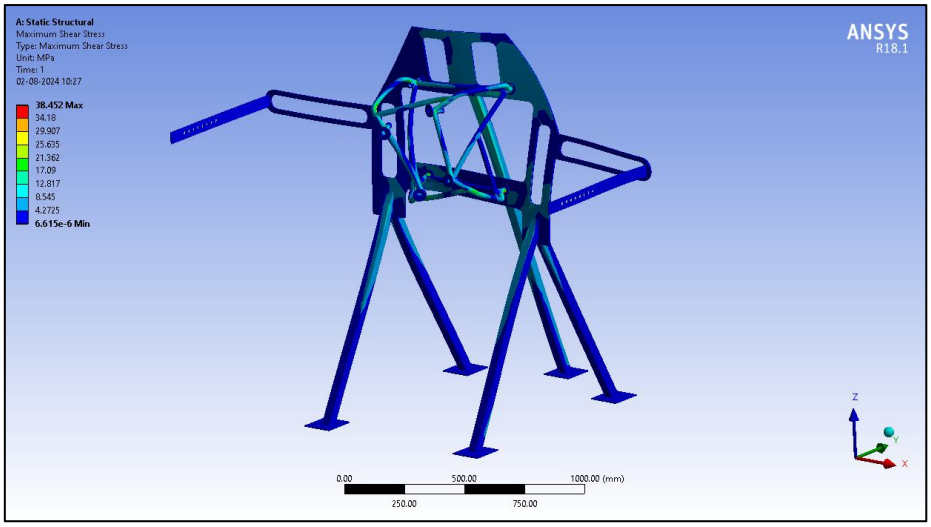

Fig. 7.10: Maximum Shear Stress

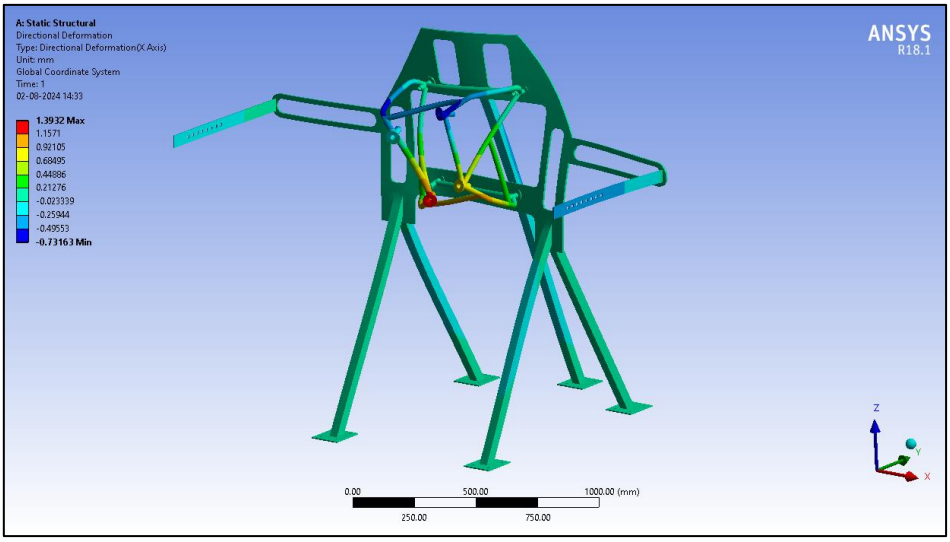

Fig. 7.11: Directional Deformation (X-axis)

International Journal of Engineering Research & Technology (IJERT)
ISSN: 2278-0181
Vol. 15 Issue 05 , May - 2026

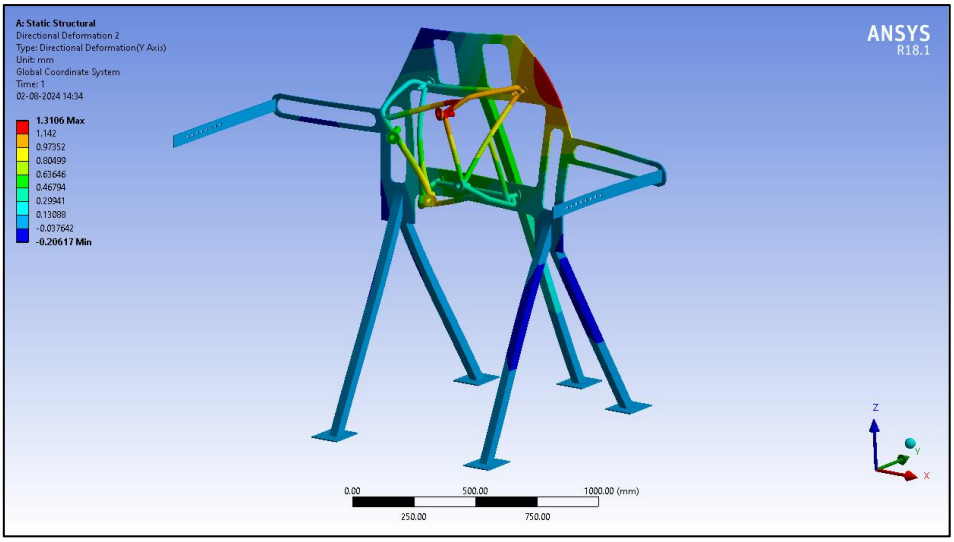

Fig. 7.12: Directional Deformation (Y-axis)

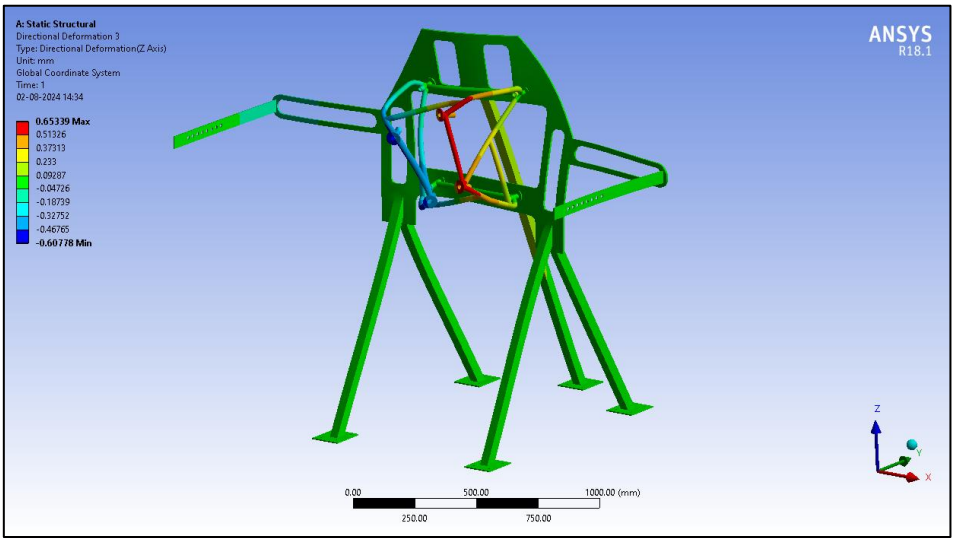

Fig. 7.13: Directional Deformation (Z-axis)

International Journal of Engineering Research & Technology (IJERT)
ISSN: 2278-0181
Vol. 15 Issue 05 , May - 2026

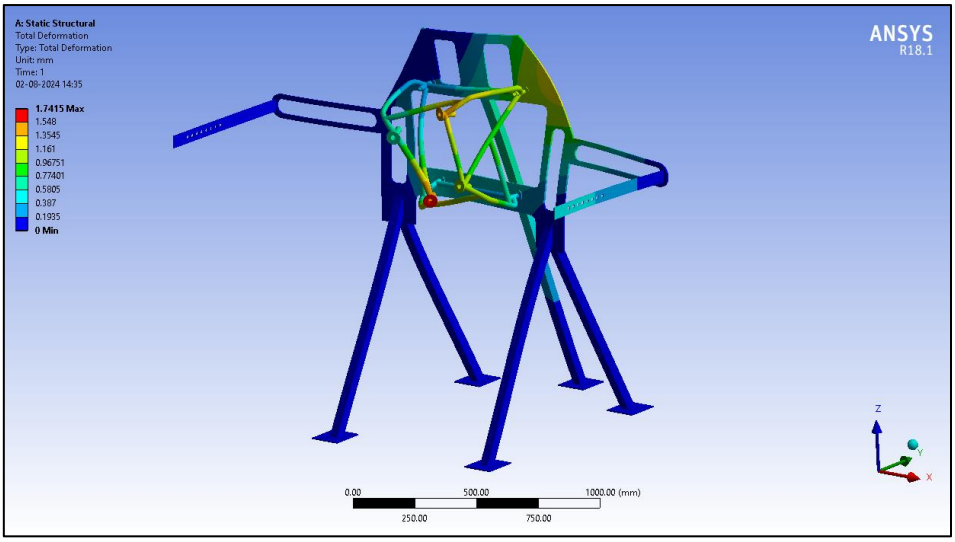

Fig. 7.14: Total Deformation

7.3. Modal Analysis of Engine Mount Frame

As discussed in the previous chapter, Mode 1, Mode 3 and Mode 4 are the most critical modes in the natural frequency band of engine mount frame. Therefore, Modal Analysis results at these modes are discussed in this section.

	Mode	Frequency [Hz]
1	1.	137.22
2	2.	213.03
3	3.	302.99
4	4.	384.05
5	5.	412.42
6	6.	451.63
7	7.	464.05
8	8.	520.15
9	9.	561.73
10	10.	570.26

Fig. 7.15: 10 Modes of Natural Frequency of Engine Mount Frame

International Journal of Engineering Research & Technology (IJERT)
ISSN: 2278-0181
Vol. 15 Issue 05 , May - 2026

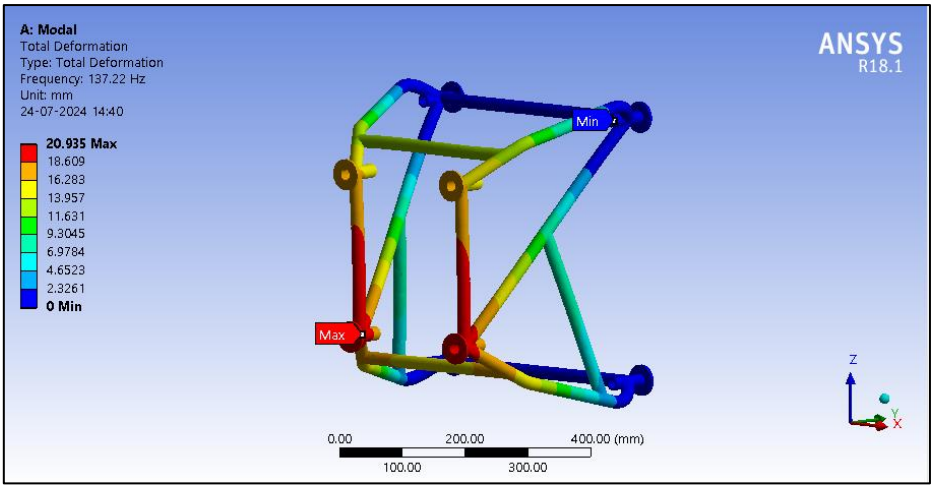

Fig. 7.16: Total Deformation of Engine Mount Frame due to Resonance at Critical Mode 1

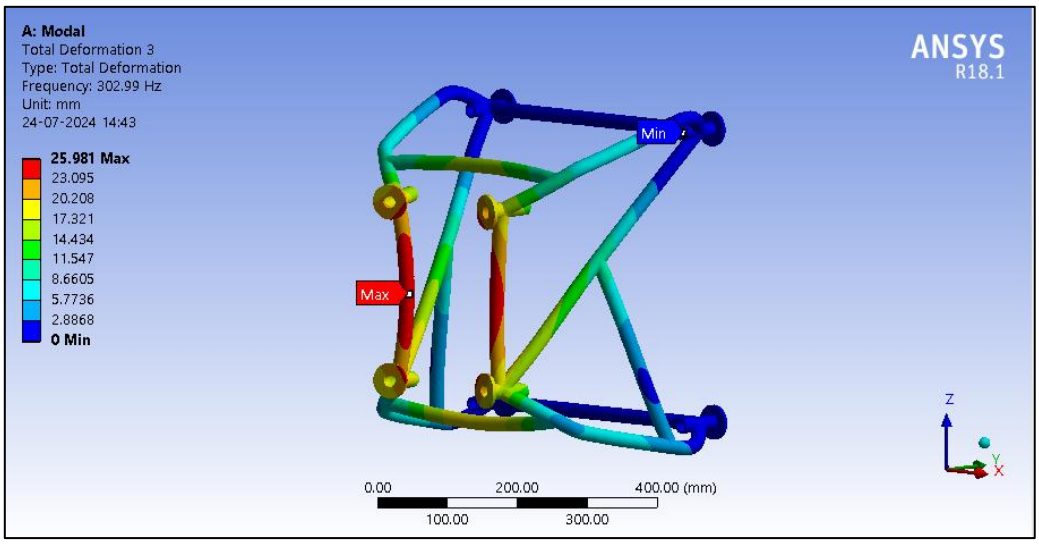

Fig. 7.17: Total Deformation of Engine Mount Frame due to Resonance at Critical Mode 3

International Journal of Engineering Research & Technology (IJERT)
ISSN: 2278-0181
Vol. 15 Issue 05 , May - 2026

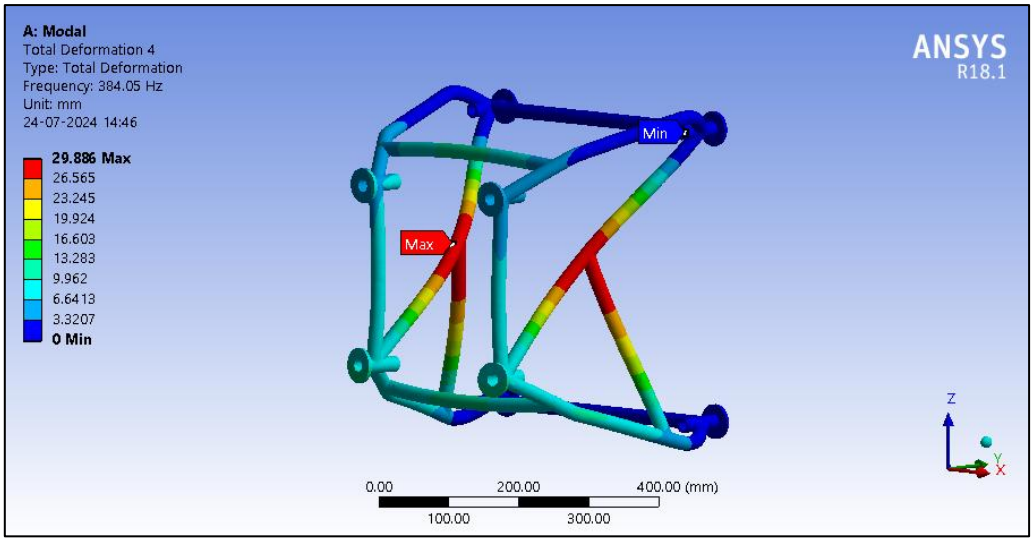

Fig. 7.18: Total Deformation of Engine Mount Frame due to Resonance at Critical Mode 4

International Journal of Engineering Research & Technology (IJERT)
ISSN: 2278-0181
Vol. 15 Issue 05 , May - 2026

7.4. Harmonic Response Analysis of Engine Mount Frame

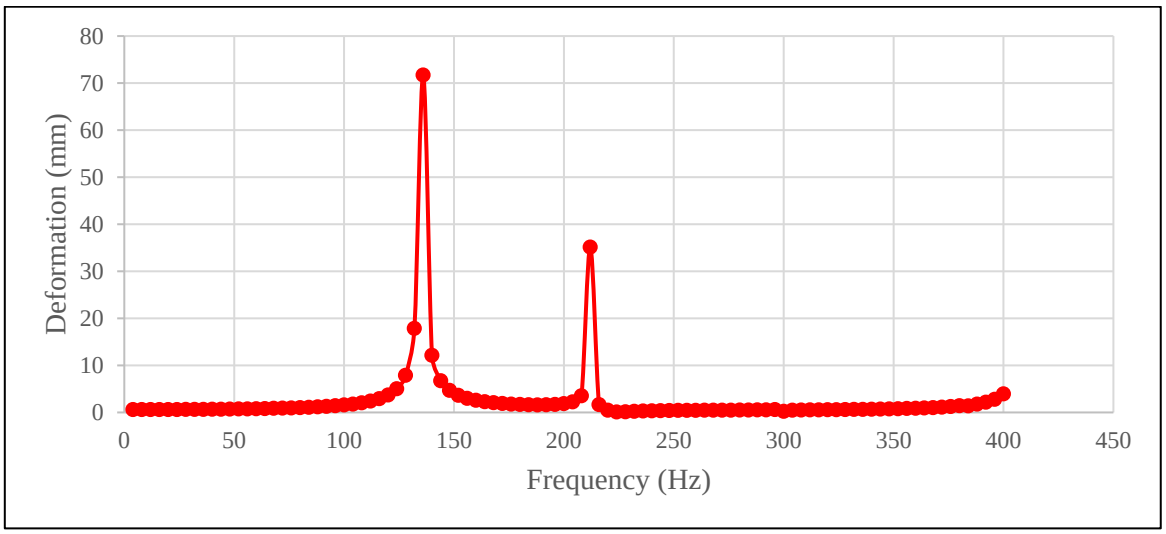

Fig. 7.19: Deformation vs. Frequency Curve of Engine Mount Frame in X-direction

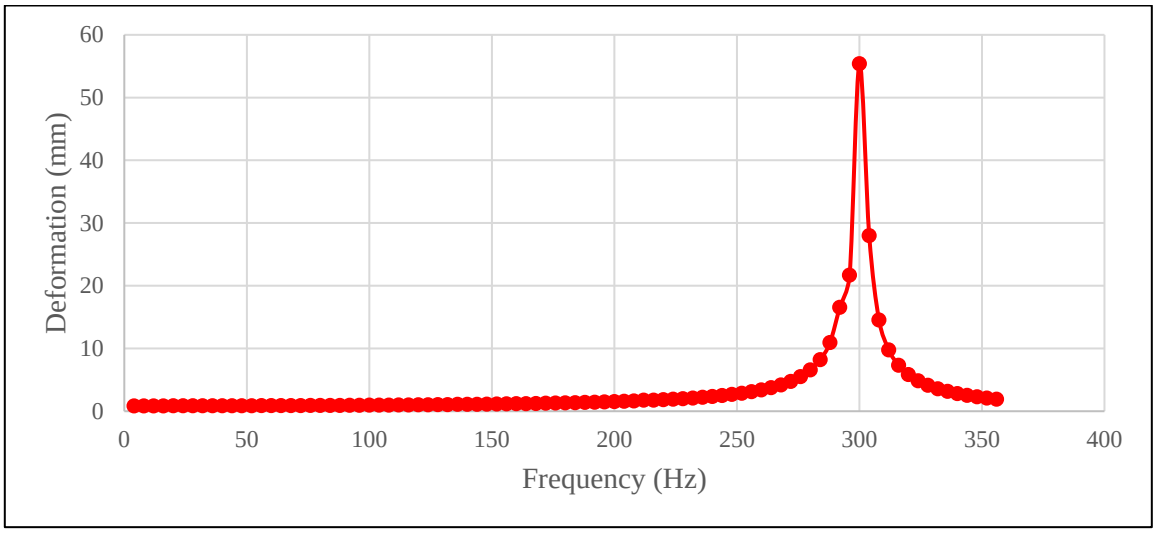

Fig. 7.20: Deformation vs. Frequency Curve of Engine Mount Frame in Y-direction

International Journal of Engineering Research & Technology (IJERT)
ISSN: 2278-0181
Vol. 15 Issue 05 , May - 2026

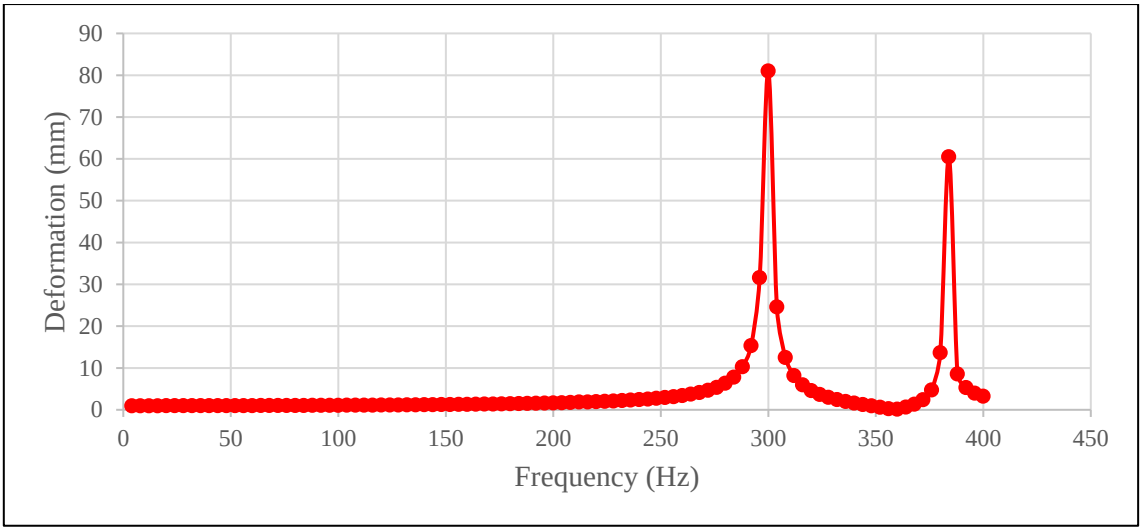

Fig. 7.21: Deformation vs. Frequency Curve of Engine Mount Frame in Z-direction

7.5. Bill of Materials (BOM)

Table 7.1: Bill of Material of Test Rig

S. No.	Components	Qty.	Material/Type	Weight Per Unit (kg)
1	**Structural Members**			
1.1	Propeller Safety 40 x 40 mm Mesh Cage	1	EN8	42.91
1.2	Engine Mount Frame	1	AL 6061 - T6	2.64
1.3	Engine Firewall	1	AISI 4340	37.45
1.4	Fuel Tank	1	AL 6061 - T6	13.75
1.5	Attitude Table (Pitch and Roll)	1	AL 6061 - T6	27.44
1.6	Turning Handle	2	EN8	1.30
1.7	Attitude Table Leveller	4	EN8	5.87
1.8	Angle Plate	2	EN8	0.65
1.9	Cage - Firewall Lock Pin	2	EN8	0.25
1.1	Attitude Table Leveller Lock Pin	4	EN8	0.017

International Journal of Engineering Research & Technology (IJERT)
ISSN: 2278-0181
Vol. 15 Issue 05 , May - 2026

1.11	Bolts - Propeller Safety Cage to Test Bed (M12)	8	OEM	
1.12	Bolts - Firewall to Test Bed (M12)	20	OEM	
1.13	Bolts - Engine Mount Frame to Firewall (M15)	4	OEM	
1.15	Bolts - Attitude Table Leveller to Test Bed (M10)	16	OEM	
2	**Propulsion System**			
2.1	UL Power 350i Engine	1	OEM	78.4
2.2	Bolts - Engine to Engine Mount Frame (M18)	4	OEM	
2.4	Coarse Filter	1	OEM	
2.5	Fine Filter	1	OEM	
2.6	Fuel Pump	2	OEM	
2.7	Engine ECU	1	OEM	
2.8	Alternator	1	OEM	
2.9	IC Engine Battery	1	OEM	
2.10	Forward Flight Propeller	1	CRPF	
2.11	Auxiliary Box (AUX BOX)	1	OEM	

International Journal of Engineering Research & Technology (IJERT)
ISSN: 2278-0181
Vol. 15 Issue 05 , May - 2026

Chapter – 8

Summary and Conclusion

8.1. Summary

This thesis discusses in detail the design and analysis and of a complete setup of a test rig for a Propeller Reciprocating IC Engine. The design of all the components to be used is discussed in detail along with the material selection process for the critical components of the test setup.

Also, finite element analysis of the critical components: engine mount frame and firewall, are also stated with complete description. Static Structural Analysis of both engine mount frame and firewall are discussed and Modal Analysis and Harmonic Analysis of engine mount frame is discussed in detail. Mesh Metric settings and element type selection is also mentioned for better understanding of the all the FEA simulations,

The summary of the results of Static Structural Analysis of Engine Mount Frame is as follows:

- Equivalent Von-Mises Stress : 62.075 MPa
- Max Principal Stress : 65.295 MPa
- Max Shear Stress : 34.829 MPa
- Max Deformation in x-axis : 0.366 mm
- Max Deformation in y-axis : 0.178 mm
- Max Deformation in z-axis : 0.038 mm
- Max Total Deformation : 0.402 mm

The summary of the results of Static Structural Analysis of Firewall is as follows:

- Equivalent Von-Mises Stress : 63.202 MPa
- Max Principal Stress : 70.499 MPa
- Max Shear Stress : 36.033 MPa
- Max Deformation in x-axis : 1.362 mm
- Max Deformation in y-axis : 1.162 mm
- Max Deformation in z-axis : 0.337 mm
- Max Total Deformation : 2.502 mm

International Journal of Engineering Research & Technology (IJERT)
ISSN: 2278-0181
Vol. 15 Issue 05 , May - 2026

The summary of the results of the Modal Analysis of Engine Mount Frame is as follows:

- Critical Natural Frequency Mode 1 : 137.22 Hz
- Critical Natural Frequency Mode 3 : 302.99 Hz
- Critical Natural Frequency Mode 4 : 384.05 Hz
- Max Total Deformation at Mode 1 : 20.935 mm
- Max Total Deformation at Mode 3 : 25.981 mm
- Max Total Deformation at Mode 4 : 29.886 mm

These deformations of engine mount frame at various critical modes are caused only by excitation frequency resonating with the natural frequency modes. The accurate deformation is determined by the Harmonic Response analysis in which working loads are also applied on the engine mount frame. The deformation vs. frequency graphs are depicted in the previous chapter. Those are the results of the harmonic response analysis.

The summary of the results of the Harmonic Response Analysis of Engine Mount Frame is as follows:

- Deformation in X-direction at 136 Hz : 71.684 mm
- Deformation in X-direction at 212 Hz : 35.128 mm
- Deformation in Y-direction at 300 Hz : 65.386 mm
- Deformation in Z-direction at 300 Hz : 80.990 mm
- Deformation in Z-direction at 384 Hz : 60.493 mm

As seen, these deformations occur at frequencies which are very close to the natural frequency modes (critical modes) of the engine mount frame as shown in Fig. 7.15.

8.2. Conclusion

The design and development of a generic test rig for propeller reciprocating IC engine has been discussed in this work. Any aircraft piston engine with similar design as UL350i engine can be tested on this test rig by designing and manufacturing an engine mount frame as per the firewall and engine bolting constraints. The test rig components are designed after much iteration in such a way that they are easy to move to different location and can be adjusted according to the needs.

Like, a provision to adjust Propeller Safety Cage distance is provided so that different engines and propellers can be easily mounted. Also, wheels are also provided so that Cage can be moved from one place

International Journal of Engineering Research & Technology (IJERT)
ISSN: 2278-0181
Vol. 15 Issue 05 , May - 2026

to another. All the components are optimised to best possible design to keep their weights as low as possible without compromising the strength.

The static structural analysis of the critical components, i.e., engine mount frame and firewall show that all the stresses and deformations are well within the permissible values. Modal analysis of engine mount frame tells that first mode of natural frequency spectrum (137.2 Hz) is well above the maximum engine frequency (3300 rpm = 55 Hz).

Hence it can be concluded that all the system and design requirements are met. The modularity desired, i.e., cage adjustment and attitude table banking and levelling are also achieved. Also, all the components are sufficiently strong to work under the described loading conditions and even more than that to certain extend.

International Journal of Engineering Research & Technology (IJERT)
ISSN: 2278-0181
Vol. 15 Issue 05 , May - 2026

References

[1] Ausserer, J. K., Litke, P. J., Rowton, A., Polanka, M., & Grinstead, K. Development of test bench and characterization of performance in small internal combustion engines. SAE Technical Paper. 2013.

[2] Arnold, S., Anusonti-Inthra, P., Cox, J. R., & Hartman, J. (2015). Development of a Turbine Engine and Compressor Test Rigs for Graduate Level Education and Research. In 51st AIAA/SAE/ASEE Joint Propulsion Conference (p. 3813).

[3] Tripathi, R. K., Tiwari, M. V., Khunger, I., & Berwal, P. (2015). Development of propeller test rig and evaluation of propeller performance.

[4] Rad, I. O. (2021). Test rig design for a micro jet engine (Bachelor's thesis, Universitat Politècnica de Cataluña).

[5] Pieper, K., Perry, A., Ansell, P., & Bretl, T. (2018, July). Design and development of a dynamically, scaled distributed electric propulsion aircraft testbed. In 2018 AIAA/IEEE Electric Aircraft Technologies Symposium (EATS) (pp. 1-2). IEEE.

[6] Wiegand, A., Miers, S., Blough, J., Kowalski, D., & Biske, A. (2012). Development of a micro-engine testing system (No. 2012-32-0105). SAE Technical Paper.

[7] Hartman, J. A. (2014). Design and Fabrication of a Low-Cost Turbine Engine Component Testbed (TECT).

[8] Pieper, K. C. (2018). Design, development and evaluation of a distributed electric propulsion testbed aircraft (Doctoral dissertation, University of Illinois at Urbana-Champaign).

[9] Zhu, D. (2006). Supercirculation Aerodynamic-Propulsion Test Rig Instrumentation Development (Master's thesis, Ohio University).

[10] Hattenberger, G., Drouin, A., & Bronz, M. (2016, October). Electric propulsion system characterization through experiments. In IMAV 2016, International Micro Air Vehicle Conference and Competition.

[11] Rajendran, P., & Smith, H. (2018). Experimental assessment of various batteries and propellers for small solar-powered unmanned aerial vehicle. Bandung Institute of Technology.

[12] Borges, M. (2015). Design of an apparatus for wind tunnel tests of electric UAV propulsion systems. Instituto Superior Técnico.

[13] Yazid, Y., Ez-Zazi, I., Guerrero-Gonzalez, A., El Oualkadi, A., & Arioua, M. (2021). UAV-enabled mobile edge-computing for IoT based on AI: A comprehensive review. Drones, 5(4), 148.

[14] Manoharan, D., Chandramohan, S., Chakkath, S., & MAURYA, S. (2017). Design, Development & Testing of Test Rig Setup for UAV Propulsion System (No. 2017-01-2064). SAE Technical Paper.

[15] Kotarski, D., Krznar, M., Piljek, P., & Simunic, N. (2017, July). Experimental identification and characterization of multirotor UAV propulsion. In Journal of Physics: Conference Series (Vol. 870, No. 1, p. 012003). IOP Publishing.

[16] Borges, M. (2015). Design of an apparatus for wind tunnel tests of electric UAV propulsion systems. Instituto Superior Técnico.

[17] Samuel, A., & Lin, Y. (2015). Airvolt Aircraft Electric Propulsion Test Stand. In 51st AIAA/SAE/ASEE Joint Propulsion Conference (p. 4108).

[18] Mayer, R., Kubicki, B., Rodriguez, B., Harris, A., & Caudle, D. (2011). Electric Aircraft Propulsion Test Rig Design & Fabrication.

[19] Morelli, G. (2022). Designing a test rig for an electrical multi-propeller system.

[20] Savvaris, A., Xie, Y., Wang, L., Wang, S., & Tsourdos, A. (2018). Control and optimisation of hybrid electric propulsion system for light aircraft. The Journal of Engineering, 2018(13), 478-483.

[21] Bester, J. E., Mpanda, A., Polfliet, N., van den Keybus, J., & Hazemeyer, G. M. (2013, September). Design of an electrical distribution test rig for validation of equipment for more electrical aircraft. In 2013 15th European Conference on Power Electronics and Applications (EPE) (pp. 1-10). IEEE.

[22] Voskuijl, M., Van Bogaert, J., & Rao, A. G. (2018). Analysis and design of hybrid electric regional turboprop aircraft. CEAS Aeronautical Journal, 9, 15-25.

[23] Corrigan, E. K. (2007). Survey of small unmanned aerial vehicle electric propulsion system.

[24] Sutton, G. P., & Biblarz, O. (2016). Rocket propulsion elements. John Wiley & Sons.

[25] Hill, P. G., & Peterson, C. R. (1992). Mechanics and thermodynamics of propulsion. Reading.

[26] Ramamurthi, K. (2010). Rocket propulsion. Macmillan.

[27] Mishra, D. P. (2017). Fundamentals of rocket propulsion. CRC Press.

[28] Silvestre, M. A., Morgado, J. P., & Pascoa, J. (2013). JBLADE: a propeller design and analysis code. In 2013 International powered lift conference (p. 4220).

[29] C. Cadou, T. Sookdeo, N. Moulton and T. Leach, "Performance Scaling and Measurement for Hydrocarbon Fueled Engines with Mass Less Than 1 kg," AIAA's 1st Technical Conference and Workshop on Unmanned Aerospace Vehicles, 20-23 May 2002.

[30] Ausserer, J., & Harmon, F. (2012, July). Integration, validation, and testing of a hybrid-electric propulsion system for a small remotely piloted aircraft. In 10th international energy conversion engineering conference (p. 4239).

International Journal of Engineering Research & Technology (IJERT)
ISSN: 2278-0181
Vol. 15 Issue 05 , May - 2026

[31] Menon, S., & Cadou, C. (2004, January). Scaling of losses in small IC aero engines with engine size. In 42nd AIAA Aerospace Sciences Meeting and Exhibit (p. 690).

[32] Moulton, N. L. (2007). Performance measurement and simulation of a small internal combustion engine. University of Maryland, College Park.

[33] N. Moulton, "Performance Measurement and Simulation of a Small Internal Combustion Engine," University of Maryland, 2007.

[34] Cadou, C., Moulton, N., Aluko, M., Sookdeo, T., & Leach, T. (2003, January). Performance measurement and scaling in small internal combustion engines. In 41st Aerospace Sciences Meeting and Exhibit (p. 671).

[35] Baranski, J., Fernelius, M., Hoke, J., Wilson, C., & Litke, P. (2011). Characterization of Propeller Performance and Engine Mission Matching for Small Remotely Piloted Aircraft. In 47th AIAA/ASME/SAE/ASEE Joint Propulsion Conference & Exhibit (p. 6058).

[36] Mattingly, J. D. (2006). *Elements of propulsion: gas turbines and rockets*. American Institute of Aeronautics and Astronautics.

[37] Mikkelson, D. C., Blaha, B. J., Mitchell, G. A., & Wikete, J. E. (1977, January). Design and performance of energy efficient propellers for Mach 0.8 cruise. In *1977 Natl. Business Aircraft Meeting and Exposition* (No. SAE-PAPER-770458).

[38] Weick, F. E. (1928). *Full scale tests of wood propellers on a VE-7 Airplane in the propeller research tunnel*. US Government Printing Office.

[39] Fink, J. J. (2004). *Aeromobile regenerative supercirculation test stand (ARSTS)* (Master's thesis, Ohio University).

[40] Sleeman, W. C., & Forsyth, D. R. (1977). *Low-speed wind-tunnel investigation of a swept-wing model having distributed upper-surface blowing near the wing leading edge or at the flap knee*. National Aeronautics and Space Administration.

[41] Shovlin, M. D. (1987). *Large-Scale Static Investigation of Circulation-Control-Wing Concepts Applied to Upper-Surface-Blowing Aircraft* (Vol. 2684). National Aeronautics and Space Administration, Scientific and Technical Information Branch.

[42] Wolowicz, C. H., Brown Jr, J. S., & Gilbert, W. P. (1979). *Similitude requirements and scaling relationships as applied to model testing* (No. H-1022).

[43] Kerho, M. (2015). Turboelectric distributed propulsion test bed aircraft, NASA learn phase II final report, contract# NNX14AF44A. *Rolling Hills Research Corporation, El Segundo*.

[44] Patterson, M. D., German, B. J., & Moore, M. D. (2012, September). Performance analysis and design of on-demand electric aircraft concepts. In *12th AIAA Aviation Technology, Integration, and Operations (ATIO) Conference and 14th AIAA/ISSMO Multidisciplinary Analysis and Optimization Conference*.

[45] Hartman, Joshua A., and Aaron Marshall (2010). Gas Turbine Data Acquisition System Design. Wright State University.

[46] Kerho, M. F. (2015). Aero-propulsive coupling of an embedded, distributed propulsion system. In *33rd AIAA Applied Aerodynamics Conference* (p. 3162).

[47] Kerho, M., & Kramer, B. (2013). Turboelectric distributed propulsion test bed aircraft. *Rolling Hills Research Coporation, El Segundo, Tech. Rep*.

[48] Patterson, M. D., German, B. J., & Moore, M. D. (2012, September). Performance analysis and design of on-demand electric aircraft concepts. In *12th AIAA Aviation Technology, Integration, and Operations (ATIO) Conference and 14th AIAA/ISSMO Multidisciplinary Analysis and Optimization Conference*.

[49] Raine, R. R., Moyle, K. E. R. I., Otte, G., & Robertson, J. O. H. N. (2002). A cost-effective teaching and research dynamometer for small engines. *International Journal of Engineering Education*, *18*(1), 50-57.

[50] Holman, J. P. (2021). Experimental methods for engineers eighth edition.

[51] Martyr, A. J., & Plint, M. A. (2011). *Engine testing: theory and practice*. Elsevier.

[52] Ogawa, T., & Kawaguchi, Y. (2007, January). Performance Testing of 5cc Glow-Ignition Four-Stroke Engine. In *Heat Transfer Summer Conference* (Vol. 42762, pp. 807-814).

[53] Warwick, B. T., Mechefske, C. K., & Kim, I. Y. (2017, August). Computational modal analysis of a twin-engine rear fuselage mounted aircraft support frame. In *International Design Engineering Technical Conferences and Computers and Information in Engineering Conference* (Vol. 58226, p. V008T12A007). American Society of Mechanical Engineers.

[54] Adkine, A. S., Overikar, G. P., & Surwase, S. S. (2017). Modal analysis of engine supporting bracket using finite element analysis. *International Journal of Advanced Engineering Research and Science (IJAERS)*, *4*(3), 55-63.

[55] Zhu, J., Haghighi, K., Krutz, G. W., & Smith, M. G. (1989). Harmonic and Modal Analysis of a Diesel Engine Chassis Mount Bracket—A Finite Element Approach. *Applied engineering in agriculture*, *5*(4), 467-474.

[56] Carne, T. G., Griffith, D. T., & Casias, M. E. (2007). Support conditions for experimental modal analysis. *Sound and Vibration*, *41*(6), 10-16.

[57] Munsi, A. S. M. Y., Waddell, A. J., & Walker, C. A. (2002). Modal Analysis of a Lightweight STRUCTURE—INVESTIGATION of the Effects of the Supports on the Structural Dynamics. *Mechanical Systems and Signal Processing*, *16*(2-3), 273-284.

[58] Adkine, A. S., Overikar, G. P., & Surwase, S. S. (2016). Static and modal analysis of engine supporting bracket-a literature review. *optimization*, *3*(11).

[59] Wang, M., Han, Q., Wen, B., Zhang, H., & Guan, T. (2017). Modal characteristics and unbalance responses of fan rotor system with flexible support structures in aero-engine. *Proceedings of the Institution of Mechanical Engineers, Part G: Journal of Aerospace Engineering*, *231*(9), 1686-1705.

[60] Nandhakumar, S., Seenivasan, S., Saalih, A. M., & Saifudheen, M. (2021). Weight optimization and structural analysis of an electric bus chassis frame. *Materials Today: Proceedings*, *37*, 1824-1827.

International Journal of Engineering Research & Technology (IJERT)
ISSN: 2278-0181
Vol. 15 Issue 05 , May - 2026

[61] Lim, T. C., Singh, R., & Zakrajsek, J. J. (1989, February). Modal analysis of gear housing and mounts. In *International Modal Analysis Conference* (No. NAS 1.15: 101445).

[62] Adkine, A. S., Overikar, G. P., & Surwase, S. S. An Experimental Investigation and Modal Analysis of an Engine Supporting Bracket. *International Journal of Advanced Engineering Research and Science*, *4*(5), 237175.

[63] Dhillon, J. S., Rao, P., & Sawant, V. P. (2014). Design of engine mount bracket for a FSAE car using finite element analysis. *Int. Journal of Engineering Research and Applications*, *4*(9), 74-81.

[64] Magryta, P., & Pietrykowski, K. (2021, December). Simulation research of the strength of an engine mount in an aircraft piston diesel engine. In *Journal of Physics: Conference Series* (Vol. 2130, No. 1, p. 012017). IOP Publishing.

[65] Ramesh, S., Handal, R., Jensen, M. J., & Rusovici, R. (2020). Topology optimization and finite element analysis of a jet dragster engine mount. *Cogent Engineering*, *7*(1), 1723821.

[66] Ramachandran, T., & Padmanaban, K. P. (2012). Review on internal combustion engine vibrations and mountings. *International Journal of Engineering Sciences & Emerging Technologies*, *3*(1), 63-73.

[67] Kaul, S., Dhingra, A. K., & Hunter, T. G. (2007). Frame flexibility effects on engine mount optimization for vibration isolation in motorcycles.

[68] Shim, T., & Margolis, D. (2006). Controlled equilibrium mounts for aircraft engine isolation. *Control engineering practice*, *14*(7), 721-733.

[69] Kim, J. J., & Kim, H. Y. (1997). Shape design of an engine mount by a method of parametric shape optimization. *Proceedings of the Institution of Mechanical Engineers, Part D: Journal of Automobile Engineering*, *211*(2), 155-159.

[70] Lee, J. S., & Kim, S. C. (2007). Optimal design of engine mount rubber considering stiffness and fatigue strength. *Proceedings of the Institution of Mechanical Engineers, Part D: Journal of Automobile Engineering*, *221*(7), 823-835.

[71] Junhong, Z., & Jun, H. (2006). CAE process to simulate and optimise engine noise and vibration. *Mechanical Systems and signal processing*, *20*(6), 1400-1409.

[72] Zhang, X., & Yu, S. D. (2009). Torsional vibration of crankshaft in an engine–propeller nonlinear dynamical system. *Journal of Sound and Vibration*, *319*(1-2), 491-514.

[73] Yu, Y., Peelamedu, S. M., Naganathan, N. G., & Dukkipati, R. V. (2001). Automotive vehicle engine mounting systems: a survey. *J. Dyn. Sys., Meas., Control*, *123*(2), 186-194.

[74] Snyman, J. A., Heyns, P. S., & Vermeulen, P. J. (1995). Vibration isolation of a mounted engine through optimization. *Mechanism and Machine Theory*, *30*(1), 109-118.

[75] Hoffman, D. M. W., & Dowling, D. R. (1999). Limitations of rigid body descriptions for heavy-duty diesel engine vibration.

[76] Dowling, D. R. (1997). Modal Content of Heavy-Duty Diesel Engine Block Vibration.

[77] Suh, C. H., & Smith, C. G. (1997). *Dynamic simulation of engine-mount systems* (No. 971940). SAE Technical Paper.

[78] Conti, P., & Bretl, J. (1989). Mount stiffnesses and inertia properties from modal test data.

[79] Tanaka, T., & Iwahara, M. (1996). The optimization of engine vibration reduction by simulation analysis.

[80] Ashrafiuon, H., & Nataraj, C. (1991, September). Dynamic analysis of engine-mount systems. In *International Design Engineering Technical Conferences and Computers and Information in Engineering Conference* (Vol. 6258, pp. 191-196). American Society of Mechanical Engineers.

[81] Sebastian, C. S., Baby, S., & Tony, A. (2016). Design And Optimization of Engine Mount Bracket.

[82] Foumani, M. S., Khajepour, A., & Durali, M. (2003). Optimization of engine mount characteristics using experimental/numerical analysis. *Journal of Vibration and Control*, *9*(10), 1121-1139.

[83] Krstic, B., Rasuo, B., Trifkovic, D., Radisavljevic, I., Rajic, Z., & Dinulovic, M. (2013). An investigation of the repetitive failure in an aircraft engine cylinder head. *Engineering Failure Analysis*, *34*, 335-349.

[84] Iwaniuk, A., Wiśniowski, W., & Żółtak, J. (2016). Multi-disciplinary optimisation approach for a light turboprop aircraft-engine integration and improvement. *Aircraft Engineering and Aerospace Technology: An International Journal*, *88*(2), 348-355.

[85] Ali H. Mutib, Classifications of Aircraft Engines,

[86] ANSYS Mechanical APDL Element Reference

[87] ULPower installation checklist

[88] ULPower Interactive Installation Manual

[89] ULPower maintenance manual

[90] ULPower Operating Manual

[91] ULPower troubleshooting guide

[92] ULPower Technical Data

[93] ULPower Illustrated Parts Catalogue

International Journal of Engineering Research & Technology (IJERT)
ISSN: 2278-0181
Vol. 15 Issue 05 , May - 2026

Bibliography

{1} https://aerotoolbox.com/engine-intro/
{2} https://www.electricalelibrary.com/en/2020/06/16/stirling-engine-what-is-it-and-how-it-works/
{3} https://www.researchgate.net/figure/Schematic-View-of-a-Steam-Engine_fig1_319072880
{4} https://eaglepubs.erau.edu/introductiontoaerospaceflightvehicles/chapter/reciprocating-engine-propeller/
{5} https://ulpower.com/en/engines/ul350/ul350i
{6} https://pipistrelaircraft.eu/virus-sw-80-100-115-is/#&gid=1&pid=1
{7} https://apheritage.blogspot.com/2013/08/the-drdo-nishant.html
{8} https://en.wikipedia.org/wiki/DRDO_Rustom
{9} https://www.israeli-weapons.com/weapons/aircraft/uav/searcher2/Searcher2.html
{10} https://en.topwar.ru/69572-bespilotniki-v-postafganskuyu-epohu-chast-3-iz-3.html

ACKNOWLEDGEMENT

I would like to express my profound gratitude to all those who have provided unwavering support and guidance during the journey of completing this thesis.

First and foremost, my deepest appreciation goes to my industrial guide and thesis advisor, **Ms. Tanvi Prakash, AGM**, **Unmanned Systems, Larsen & Toubro Precision Engineering and Systems, Mumbai** for providing this opportunity to conduct my project work within their esteemed organization.

I also extend my deepest gratitude to my institutional guide, **Dr. Vikas M. Phalle**, **Associate Professor, Department of Mechanical Engineering and Programme Coordinator, Defence Technology, VJTI, Mumbai**, for his invaluable guidance.

I'd also want to express my sincere gratitude to **Dr. P. A. Rajiwade**, **Assistant Professor, VJTI, Mumbai** for the consistent support and mentorship he has provided during my M. Tech program, enriching my academic experience.

Finally, I would like to express my profound appreciation to my family and friends for their unwavering encouragement and moral support throughout my journey.

Sincerely,

Atharva Basarkar

Roll No. – 222210002